Design and development of energy efficient indoor LED lighting system with combined effect of daylight

Thesis submitted by

Moutusi Bag

Doctor of Philosophy (Engineering)

Electrical Engineering Department,
Faculty Council of Engineering & Technology
Jadavpur University
Kolkata, India

Year 2024

1. Prof. (Dr.) Saswati Mazumdar

Electrical Engineering Department

Jadavpur University

Kolkata – 700032

2. Prof. (Dr.) Kalyankumar Ray

Former Professor

Department of Instrumentation and Electronics Engineering

Jadavpur University

Kolkata – 700032

List of SCI Journals

1. M. Bag, S. Mazumdar, and K. Ray and *"A cost-effective illuminance sensor for daylight harvesting lighting control system"*, Light & Engineering 28 (2020) 103-110.

List of SCI Conferences

1. M. Bag, S. Mazumdar, and K. Ray, *"A self-oscillating flyback converter for dimmable LED lighting system"*, 2023 3rd IEEE Conference on Applied Signal Processing, November 24-25, 2023, Haldia, West Bengal, India.

List of Patents

Nil

List of Presentation in National / International / Conferences / Workshops

1. **M. Bag, S. Mazumdar, and K. Ray, *"A self-oscillating flyback converter for dimmable LED lighting system"*, 2023 3rd IEEE Conference on Applied Signal Processing, November 24-25, 2023, Haldia, West Bengal, India.**

PROFORMA – 1

"Statement of Originality"

I Moutusi Bag registered on 20th May 2016 do hereby declare that this thesis entitled **Design and development of energy efficient indoor LED lighting system with combined effect of daylight** contains literature survey and original research work done by the undersigned candidate as part of Doctoral studies.

All information in this thesis have been obtained and presented in accordance with existing academic rules and ethical conduct. I declare that, as required by these rules and conduct, I have fully cited and referred all materials and results that are not original to this work.

I also declare that I have checked this thesis as per the "Policy on Anti Plagiarism, Jadavpur University, 2019", and the level of similarity as checked by iThenticate software is 8 %.

Moutesi Bag.
Signature of Candidate:

Date: 07.05.2024

Certified by Supervisor(s):

(Signature with date, seal)

1. Saswati Mazumder 7.5.24

Professor
Electrical Engineering Department
JADAVPUR UNIVERSITY
Kolkata - 700 032

2. Kalyankumar Ray
Former Professor
Dept. of Instrumentation and Electronics Engg.
J.U.

PROFORMA - 2

CERTIFICATE FROM THE SUPERVISOR/S

This is to certify that the thesis entitled "Design and development of energy efficient indoor LED lighting system with combined effect of daylight" submitted by Smt Moutusi Bag, who got her name registered on 20th May 2016 for the award of Ph.D. (Engineering) degree of Jadavpur University is absolutely based upon her own work under the supervision of Prof. (Dr.) Saswati Mazumdar and Prof. (Dr.) Kalyan Kumar Ray and that neither her thesis nor any part of the thesis has been submitted for any degree/ diploma or any other academic award anywhere before.

1. Saswati Mazumdar 7.5.24
Prof.(Dr.) Saswati Mazumdar

Professor
Electrical Engineering Department
JADAVPUR UNIVERSITY
Kolkata - 700 032

2. Kalyankumar Ray
Prof.(Dr.) Kalyan Kumar Ray

ACKNOWLEDGEMENT

Foremost I would like to express my sincere, deep sense of gratitude and indebtedness to my thesis supervisors Prof. (Dr.) Saswati Mazumdar, Professor of Electrical Engineering Department, Jadavpur University and Prof. (Dr.) Kalyan Kumar Ray, Former Professor and Head of Instrumentation and Electronics Engineering Department, Jadavpur University, for the continuous support of my thesis work, for their patience, motivation, enthusiasm, invaluable guidance and supervision.

I would like to acknowledge my sincere thanks to HOD, Electrical Engineering Department, and Lab In-charge, Illumination Engineering Section, Electrical Engineering Department, for providing me the opportunity to carry out my project work in Illumination Engineering Laboratory of Jadavpur University.

I would like to acknowledge my sincere thanks to Prof. (Dr.) Biswanath Roy, Professor of Electrical Engineering Department, Dr. Suddhasatwa Chakraborty, Assistant Professor, Electrical Engineering Department, Dr. Parthasarathi Satvaya, Director of School of Illumination Science, Engineering and Design for encouragement they provided me in carrying out this thesis work.

I am also very much thankful to Mr. Samir Mandi and Mr. Gobinda Pal, Laboratory Instructors and staffs of Illumination Engineering Laboratory of Jadavpur University, for their indispensable co-operation during my thesis work especially in measurement and instrument handling.

Finally, this thesis would not have been possible without the confidence, endurance and support of my mother, Purabi Bag, and father, Ardhendu Kumar Bag. They are always been a source of inspiration and encouragement.

Date: 07.05.2024

Moutusi Bag Moutusi Bag.

JADAVPUR UNIVERSITY

Kolkata- 700032

Abstract

Even in a reasonably large facility, it is challenging to control energy waste due to insufficient light management and lighting distribution. It is also impracticable to rely on people to manually control the light in order to conserve energy. Occupancy sensors, often referred to as motion and/or infrared emissions detectors, are among the many technological innovations that have been produced recently to reduce excessive energy use. These sensors determine activity within a certain region. It's convenient because they switch on instantly when someone walks into a room. The most common flaw is that it fails to consider the natural light already existing in the room. Another energy-saving strategy is to manually adjust artificial light intensity with dimmers.

Numerous studies have confirmed the energy savings that come from daylight harvesting. The California Energy Commission's Public Interest Energy Study Program recommended researching on/off control, however they did not elaborate on over-illumination caused by sunshine. In recent years, the European Union has aggressively supported political campaigns focused on energy efficiency. An energetic management program could follow three basic paths: improving the lighting control system to reduce energy waste for empty spaces and during the day; purchasing new, energy-efficient equipment (lamps, control gears, etc.); and implementing improved lighting design strategies (localized task lighting system).

Light-emitting diodes, or LEDs, are being utilized more often for general lighting in residences, commercial buildings, and office spaces. LED lighting solutions provide easily and flexibly adjustable light output. This is especially useful for managing daylight-adaptable lighting because it contributes to a considerable reduction in the amount of electricity needed for lighting. These lighting control systems allow luminaire light output to be varied with daylight to meet illuminance requirements while conserving energy. When there is sufficient daylight, the luminaires are thus muted to maintain the appropriate level of illumination at the workspaces.

Light Emitting Diodes, or LEDs, has fundamentally altered the interior lighting industry. The use of LEDs to develop artificial lighting systems that closely resemble natural sunshine. LEDs are the main component of modern lighting solutions due to their extended lifespan, energy efficiency, and favourable environmental effects.

One way to reduce lighting-related energy expenses is through daylight harvesting. It utilizes the sunshine that is present. Visible light, which makes up 45% of the solar energy spectrum, may be harnessed to illuminate buildings for nine to eleven hours per day.

Keywords:

Daylight Harvesting, LED, Sensor, PWM LED Driver, Window Blinds, MPPT Boost Converter, Artificial Daylight.

Table of Contents

List of Figures

List of Tables

1. Introduction

Saving energy is now one of the most challenging issues throughout the world. Almost 19% of the electrical energy consumption in India is spent in lighting. The popular artificial light e.g. tungsten filament lamp is highly inefficient in converting electrical energy to light. Energy conservation can take many forms - high efficiency lighting in particular saves a huge amount of electricity charges and reduces capital cost of generating plants. Moreover depletion of fossil fuel and natural gas is reduced and CO_2 emission is also reduced considerably. This project presents a system for saving electrical energy by making use of daylight, whenever possible, and supplementing it by just the adequate amount of artificial light, meeting the standard illumination level.

Because of the inadequate light management and lighting distribution, energy waste is difficult to regulate, even in a fairly sized structure. Furthermore, depending on users to manually regulate the light in order to save energy is impractical. Many technological advancements have been made recently to cut down on excessive energy use, such as occupancy sensors (also known as motion and/or infrared emissions detectors) that identify activity within a certain area. When someone enters a room, they immediately turn on, which is convenient. The most frequent drawback is that it doesn't take into account the natural light that is already present in the space. Using dimmers, a manual technique of controlling artificial light intensity, is another approach to save energy. While some dimmers do this automatically, others do not react when another source of light, such as sunshine is present.

A daylight harvesting system can reduce lighting energy use by 20–40%. The sort of space where the control system is installed determines how much energy can be saved. You can use daylight harvesting anytime there is daylight. It functions well in areas where windows or skylights are available. Offices, public buildings, and schools are examples of such environments.

Dimmable LED lamps will be used in this project. LED lighting has the potential to help individuals and society at large in a number of ways. Low life cycle cost can be achieved by combining very high efficiency with an incredibly long lifespan for the LEDs' resources. LED lighting needs to have dimming capacity at least on par with conventional light sources in order to gain widespread acceptance.

LED lighting has seen a sharp increase in popularity in recent years due to advancements in LED brightness, efficiency, and color rendering index (CRI). With significant energy savings, luminaires utilizing high brightness white LEDs (HB-LEDs) can now match or surpass conventional light sources built on incandescent, fluorescent, CFL, and metal halide technology. LEDs are now available in warm yellowish white as well as the cool, bluish white light using those LEDs in different way of R (red), G (green), B (blue) control of LEDs, different types of white colour can be generated which can be matched with the daylight outside and create same colored artificial daylight source inside keeping the illumination level fixed.

The energy savings resulting from daylight harvesting have been documented in multiple research [1] [2].The Public Interest Energy study Program [3] of the California Energy Commission suggested conducting study on on/off control, however they provided no details regarding over illumination brought on by sunshine. The European Union has been actively supporting political campaigns aimed at energy efficiency in recent years [4]. Three fundamental paths could be taken by an energetic management program: enhancing the lighting control system to prevent energy waste for vacant spaces and during the day; acquiring new, more energy-

efficient machinery (lamps, control gears, etc.); and applying better lighting design techniques (localized task lighting system).

Light energy is the most significant and valuable type of energy in the energy industry. Human function depends heavily on light, which gives us the ability to see and do a variety of tasks. However, it's also significant since it has an impact on people's physical and mental health. Emotions in people and their sense of wellbeing can be affected by lighting. It is possible to extract light energy from two different kinds of energy sources. They fall into two categories: "Daylight," which is direct light energy from "The Sun," and "Artificial Light." The greatest source of light energy available to humans is daylight. Daylighting allows life to see the world and do tasks since so much light falls on the planet.

It is possible to convert energy from various (conventional and non-conventional) energy sources, such as fossil fuels, wind, nuclear, gas, and many more, into light energy, which provides the electricity needed for artificial lighting. These artificial lights are necessary for the nighttime operations. Compared to solar energy, very little light energy comes from other sources.

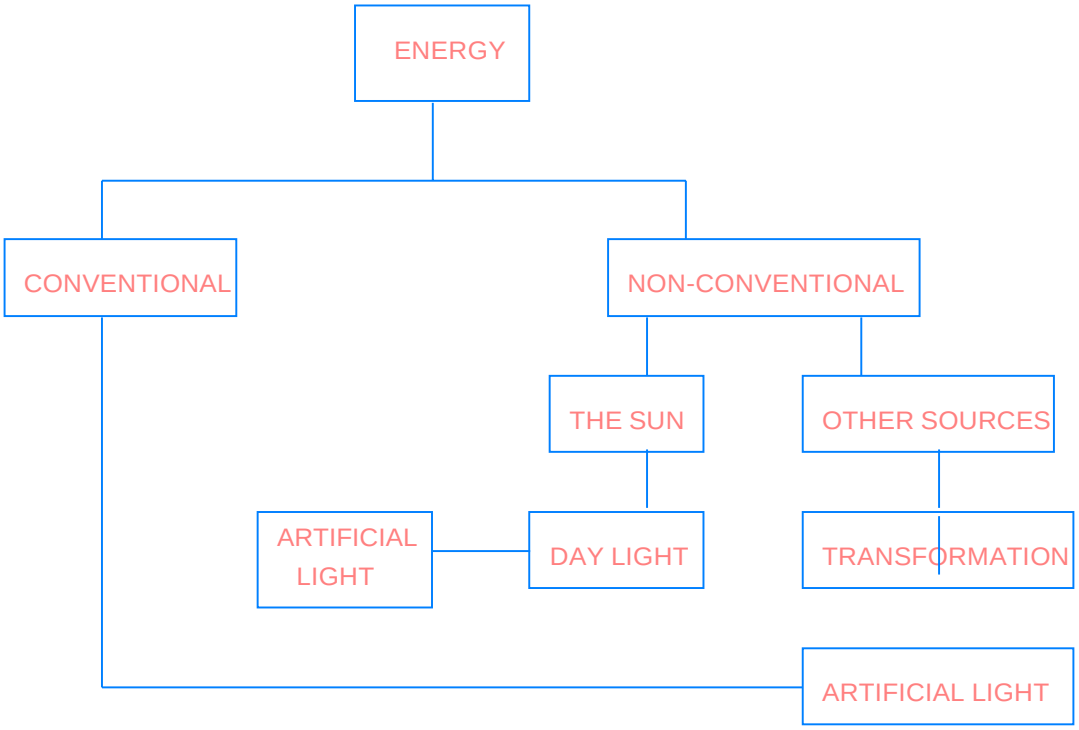

Fig 1 The energy classification diagram for light

Day by day, and season by season, the daylight varies. However, on an open surface, the typical amount of accessible light is between 10,000 and 1,60,000 LUX on overcast and bright days. Although it varies by region as well, the amount of direct light from the sun or daylight receives the greatest amount of energy overall. The energy classification diagram for light is displayed in Fig. 1.

In this system a closed loop illuminance control system has been developed using wall mounted sensors, dimmable luminaires with pulse width modulation (PWM) out processors and motorized blinds in the window

side. User can set the illuminance level as per their requirements by illuminance controller(IC) board. This IC consists ATmega 32A microcontroller and PWM out processors (ATmega8A) to maintain the desired illuminance level on the working plane. In order to achieve the target set-points of this daylight harvesting control system a cost-effective, two-wire, 4-20 mA industry standard illuminance transmitter has been proposed. It has various uses, such as controlling indoor lighting through daylight harvesting. The primary sensor is a light-dependent resistor made of cadmium sulfide (CdS), whose relative spectrum response is almost identical to that of the human eye. The transmitter's calibration method has been described, and the sensor's static and dynamic performance parameters have been ascertained through experimentation.
The fly back converter for use in interior LED lighting systems is suggested in this study as being dimmable, affordable, and energy efficient. With the use of a DC-DC converter and a traditional pulse width modulation (PWM) LED driver topology, this system also offers dimming capabilities. An experimental setting is used to test and assess the proposed notion. The LED driver produces a voltage of 60V when it is operating at 230V of ac input power and 50 Hz of line frequency. With PWM dimming at a frequency of 244 Hz, output current is controlled to 320 mA. Circuit efficiency is 83% at the rated light power. Based upon the set illuminance, the microcontroller will control the motorized vertical blinds to maintain the illuminance on the working plane.

Additionally, one of the walls will have an “Artificial Daylight (AD)”. System which will consist of a roof-mounted solar panel, a microcontroller based boost converter and LED panel. The system will not have any battery storage. The microcontroller unit will employ a maximum power point tracking (MPPT) algorithm so that maximum power available from the solar panel can be used for lighting. This concept can be utilized in spaces where a direct entrance of daylight through windows is not available.

The structure of this thesis is as follows:

The literature review on the current lighting control system is covered in Section 2.
Section 3 gives an overview of daylight harvesting for indoor illumination.
Section 4 illustrates the proposed daylight harvesting control system for interiors having windows.
Section 5 displays the experimental results used to assess the lighting control system's performance.
Conclusion and future scopes are provided in Section 6.

Summary

Nowadays, one of the most difficult problems in the globe is energy conservation. Lighting energy consumption can be lowered by 20–40% with a daylight harvesting system. By using daylight whenever possible and adding just enough artificial light to match the conventional lighting level, this initiative offers a method for saving electrical energy.

2. Literature survey on existing lighting control system

It is well known that adjusting artificial lighting when daylight becomes scarce can help save electricity. Photodetectors and state-of-the-art lighting systems are required to achieve such daylight management. Closed loop control systems are used to estimate luminary dimming settings in order to create the appropriate quantity of artificial light. The photodetector calculates the total amount of daylight and artificial light.

2.1 Daylight sensing lighting system

LEDs, or light-emitting diodes, are becoming increasingly used in homes, businesses, and offices for general illumination purposes. The light output of LED lighting systems may be readily and flexibly regulated. This is particularly appealing for controlling daylight adaptable lighting, as it helps to lower the significant amount of electricity used for illumination. With the use of these lighting control systems, luminaire light output can be adjusted to save energy while meeting illuminance needs by varying with daylight [5]–[8]. Thus, the luminaires are muted to maintain the desired level of illumination at the workplaces when there is a enough amount of daylight.

The achieved illuminance is tracked by external photodetectors, or sensors at the wall and ceiling, in modern lighting control systems. In office application, the goal is to achieve illuminance values specified according to lighting norms. The lighting controller adjusts the luminaires' dimming levels in an attempt to reach the specified set-points based on input obtained from photodetector measurements. Numerous control strategies with various goal functions have been taken into consideration.

These lighting control systems with photodetectors have the following shortcomings:

(i) Adding more photodetectors increases installation difficulty and costs.

(ii) A photodetector measures the light that is reflected back into its field of vision by luminaires, both artificial and daylight. Consequently, in order to achieve the luminaire dimming levels and preserve system stability and responsiveness to changes in illumination, rigorous closed-loop feedback control design is needed [5], [7].

(iii) Environmental changes may cause the surface beneath the photodetectors' reflectance levels to shift over time. Desk moves and the positioning of a bright object on a dark desk surface are two examples of these modifications. This causes both artificial light and natural light to be roughly (or not, depending on the reflectivity of the items) reflected back at the photodetector. This can also result in significant variations between the actual and intended illuminance levels [9], [10].

2.2 LED driver and dimming methods

A self-contained power supply with outputs tailored to the electrical properties of an LED or LEDs is known as an LED driver. Given that an LED lamp's I-V curve is voltage-sensitive. An rapid shift in current caused by a modest fluctuation in applied voltage has the potential to irreparably destroy an LED. Constant-voltage and

constant-current external LED drivers are the two primary varieties. varied types of drivers have varied electrical needs in order to run LEDs.

Constant-current drivers power LEDs that need a range of output voltages in addition to a constant output current. There will be a single output current that is indicated and labeled in amps or milliamps, in addition to a variety of voltages that change based on the LED's load (wattage).

Constant-voltage drivers power LEDs with a maximum output current that need a fixed output voltage. These LEDs already have internal constant-current drivers or straightforward resistors controlling the current inside the LED module.

Thus, it was advised against using the constant-voltage driver with LEDs. On the other hand, constant current driving is frequently found in commercial goods. For a freestanding solar LED lighting system, a DC/DC converter that can provide LEDs with continuous current is therefore required.

These days LED drivers should also be concerned with LED dimming because it can save electricity. Analog and digital dimming are the two types of dimming. Adjusting the LED array's forward current allows for analog dimming. The full driving current is used for full brightness; to achieve dimming, the current is linearly reduced until it reaches zero in the off position.

When using digital or pulse-width modulation (PWM) dimming, full amplitude current pulses are used to drive the LED array, and the perceived brightness is adjusted by varying the pulse width. The ability of the human eye to integrate the average quantity of light in the pulses is what allows for this type of fading. The eye only notices the overall average and not any pulsing at all if the pulse rate is high enough. For instance, pulses with equal ON and OFF times are used to drive the LEDs at 50% brightness. A pulse rate of roughly 200 Hz is usually sufficient to remove noticeable flickering.

Because there is no requirement for frequency creation, analog dimming is easy to implement. The gadget won't experience any inrush current. One drawback of analog dimming is that the LED's color may change between 0 and 100% dimming. On the other hand, PWM dimming results in no color shift and allows for linear duty cycle brightness variation. PWM dimming is typically more difficult to execute than analog dimming since it calls for the addition of a MOSFET switch and a PWM controller to the power supply.

LED dimming is achieved either by linearly varying the current passing through the LEDs or by using PWM (Pulse Width Modulation) with the nominal LED current acting as the amplitude. The primary distinction between the two dimming techniques is that the PWM technique applies a rectangular wave with a variable duty cycle to the LED, whilst the first technique applies a linear modification of the continuous current amplitude value. Fig. 2 displays the two waveforms that were employed for dimming. The average current provided to the LED in both scenarios is equal to 50% of the nominal current.

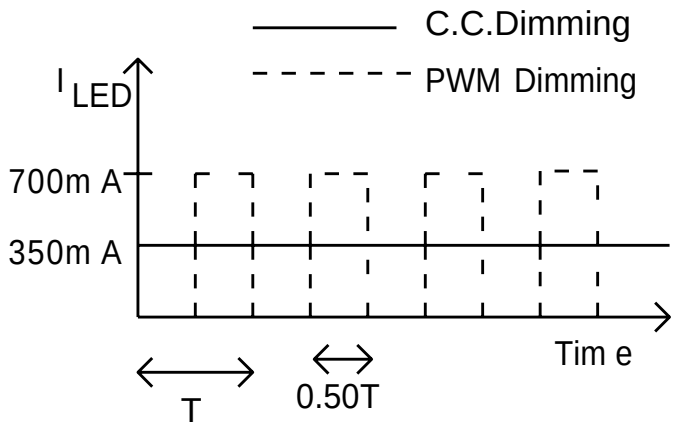

Fig. 2 Current waveforms in the LED for the two dimming techniques

As shown in [11], there is an offset in the point chromaticity that allows one to change the brightness of a white LED. The amplitude, peak wavelength, and form of the light spectrum are all altered by this displacement, which also modifies the distribution of the spectrum. Depending on whether PWM or dc variation dimming is being used, these modifications can take various forms. The results produced by demonstrate that when the intensity of the LED light is adjusted by PWM, the chromaticity deviation is less. Many LED manufacturers accepted this technique as standard, and most Power LEDs Catalogs started mentioning PWM modulation as a workable means to control the LED's luminous flux in recent years [12]. The wavelength of light emitted by the LED can be adjusted by varying the amount of current passing through it. PWM dimming is therefore more appropriate in this situation since rated current is always delivered to the LED, varying only in the percentage of time that current flows in each period (duty cycle). The results of a simulation used to inform the power source's design indicated that the inductor current reference behavior improved with decreasing PWM frequency. Additionally, the controller's reaction to variations in the reference signal improves. In actuality, though, these low frequencies will make the LEDs flash or flicker, which can be bothersome or possibly lead to neurological conditions.

2.3 Window blinds

The lighting system, which is often operated by manually and automatically, will be affected by blind use in buildings. While closing the blinds can make a room more comfortable, doing so may also require more artificial lighting. Consequently, it is important to take into account the possible effects of both manual and automatic blind operation on lighting when modeling energy usage [13]. For smart indoor lighting systems, generally two types of blinds are used.

1. Vertical blinds and,
2. Horizontal blinds

The blinds have used in this system which is known as Vertical blinds. It is controlled by a motor. Two modes have been operated i.e., Closing the blinds and opening the blinds. For manual mode, the position of the blinds can be shift by the use of switches. For automatic mode, it can be control by the microcontroller. Vertical and venetian blinds have been shown in Fig.2.1.

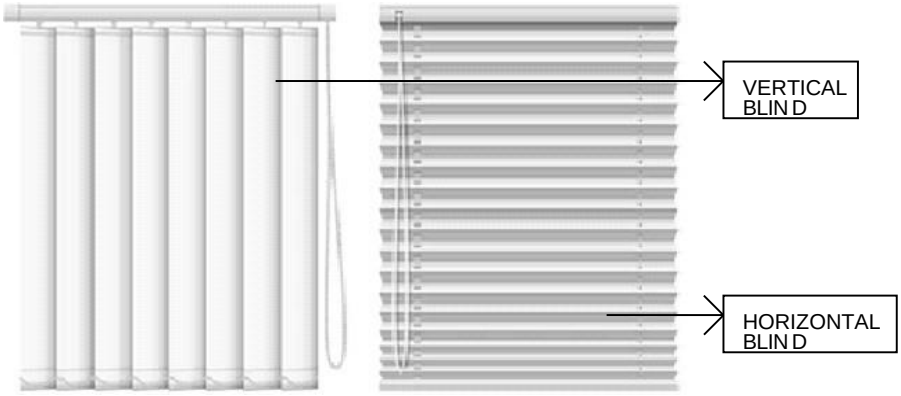

Fig. 2.1 The image of vertical and horizontal blinds

2.4 Maximum power point tracking for artificial skylight

The product of voltage and current yields the power output from a solar cell array. The voltage is at its highest when the circuit is open, yet the current is at zero. Thus, there is no output power at all. Once more, the net voltage is zero yet the maximum current flows through the wire when the array is sort circuited using a non-resistive wire. Thus, the power drops to zero once more. Therefore, there must be a circumstance in which voltage and current are both present. There is a point when the power is at its highest and the voltage and current are both adequate between these two extremes. Fig. 2.2 illustrates this state. This is referred to as the array's maximum power point. It fluctuates according to temperature and changes in the amount of solar radiation that strikes the PV solar array. To operate the array under the maximum power point scenario, a suitable load is needed. These days, there are many different ways to maximize a photovoltaic cell's power point. Among them are the following: dP/dV or dP/dI Feedback control; Hill-Climbing Method; Incremental Conductance Method; Fractional current sweep, fuzzy logic control, neural networks, RCC, fractional open circuit voltage, fractional short circuit current, load voltage or load current maximization, etc.

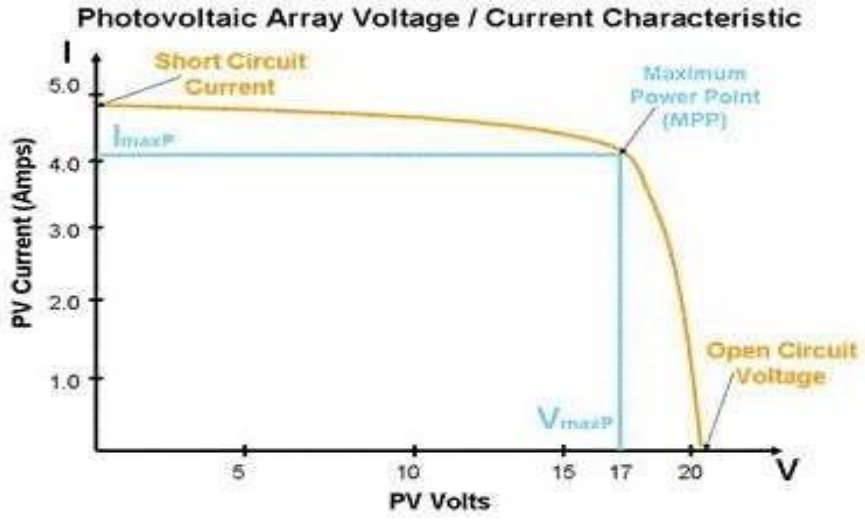

Fig. 2.2 I-V characteristics of Solar PV module

To track the maximum power point in all environmental situations, an effective maximum power point tracking (MPPT) technique is therefore required. Curve-Fitting, Hill Climbing/P&O, Incremental Conductance, Fractional Open-Circuit Voltage, Fractional Short-Circuit Current, Fuzzy Logic Control, Neural Network, etc. are a few of the commonly utilized MPPT approaches. In addition, 19 additional number approaches are discussed along with their advantages and disadvantages.

2.4.1 MPPT techniques

The many MPPT methods have been covered in the sections that follow, in an arbitrary order.

A. Hill Climbing/P&O

As you ascend a hill, P&O in the PV module's operating voltage and the duty ratio of the power converter are both disrupted. Variations in the duty cycle of the boost converter, which the PV module is attached to, result in changes in the PV module's current, which in turn cause variations in the PV module's voltage.

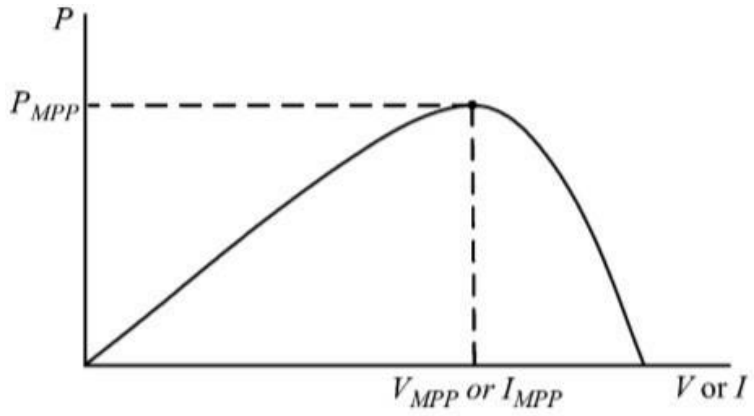

Fig 2.3 (a) Characteristics curve of the PV module

According to Fig. 2.3(a), when the voltage is acting on the left side of the MPP, it raises (decreases) power, and when it is operating on the right side of the MPP, it decreases (increases) power. In order to reach MPP, the perturbation should be reversed if there is a power decrease and the perturbation should be maintained constant if there is a power increase. Given that lengthy sampling happens just once each switching cycle, Table 2 demonstrates that the approach is similarly effective when instantaneous PV module voltage and current are employed.

Table 2. Summary of Hill Climbing and P&O algorithm

Perturbation	Change in Power	Next Perturbation
Positive	Positive	Positive
Positive	Negative	Negative
Negative	Positive	Negative
Negative	Negative	Positive

Until the MPP is attained, the operation is frequently repeated. Following that, the system oscillates about the MPP. The size of the perturbation can be decreased to lessen this oscillation. However, the MPPT process is slowed down by smaller perturbation sizes. Fuzzy logic control is utilized to maximize the next perturbation's magnitude, and a variable perturbation size that decreases toward the MPP serves as the solution to this contradicting phenomena. It is also possible to employ a two-step algorithm, with the first stage involving faster tracking and the second stage involving finer tracking. However, by estimating a starting operating point near the MPP using a nonlinear equation, the first stage can be omitted.

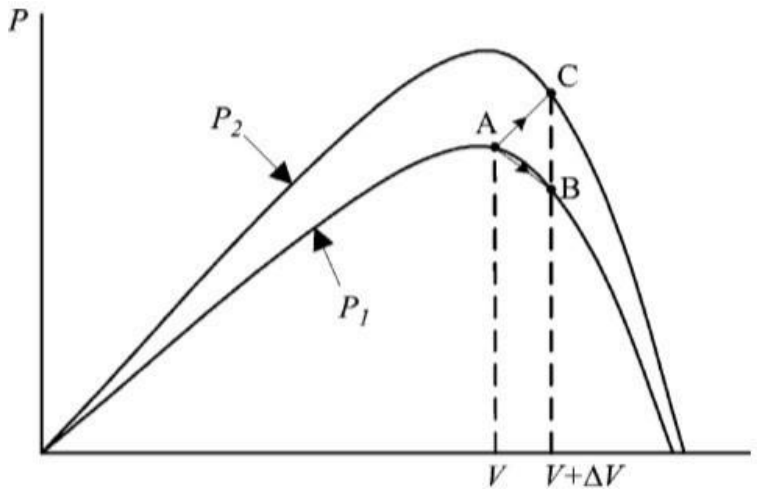

Fig 2.3 (b) Divergence of Hill Climbing/P&O from MPP

This method can fail if a rapidly changing atmospheric conditionhappens. If the irradiance is shifted from curve P1 to curve P2 as in fig. 2.3 (b) within the sampling period, the process moves from A to C and afalse MPP will occur. A three-point weight comparison P&O approach is suggested as a solution to lessen the issue. It compares the current point to two previous ones before determining the perturbation sign.

Typically, two sensors are needed to detect the voltage and current that are used to convert power, although the architecture of the power converter may just require a voltage sensor and the PV module current is estimated from PV module voltage and eliminates the current sensor. A microcontroller is more suitable than a discrete analog methodology in this type of MPPT.

B. Incremental Conductance

The PV module power curve's slope, which is zero at the MPP, positive on the left side of the MPP, and negative on the right side, is the foundation of the incremental conductance approach. This information is provided below. The algorithm is described in fig 2.4

$$dP/dV = 0 \text{ ,at MPP}$$

$$dP/dV > 0, \text{ left of MPP}$$

$$dP/dV < 0, \text{ right of MPP} \quad (2)$$

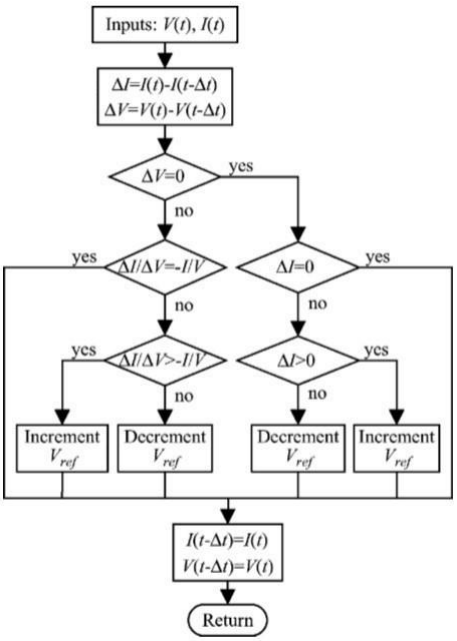

Fig 2.4 Algorithm of the Increment conductance method

Since

$$\frac{dP}{dV} = \frac{d(IV)}{dV} = I + V\frac{dI}{dV} \sim I + V\frac{dI}{dV} \tag{2.1}$$

(2) can rewrite as

$$\Delta I/\Delta V = -I/V, \text{ at the MPP}$$

$$\Delta I/\Delta V > -I/V, \text{ left of the MPP}$$

$$\Delta I/\Delta V < -I/V, \quad \text{right of the MPP} \tag{2.2}$$

This means that the MPP can be monitored by comparing the incremental conductance (ΔI/ΔV) to the instantaneous conductance (I/V), as illustrated in the flowchart of Fig 2.4. The reference voltage, or Vref, is the minimum voltage at which the PV module must function. When the MPP is reached, the operation is sustained until a change in ΔI is noticed, indicating a change in the atmospheric condition and the MPP. At reference, VMPP is equal to Vref. To follow the new MPP, the algorithm modifies the Vref either higher or lower.

The MPP is tracked at a rate that depends on the increment size. A larger increment can be used to accomplish fast-tracking, although the system may oscillate rather than operate at the maxima. A solution to this is any other proposed method that brings the operating point near the MPP in the first stage and then the incrementalconductance method determines the MPP by fine-tuning. Initially, theoperating point is set to an operating point to match the load and then the MPPT is done.

A less evident yet equally efficient method of executing the IncCond methodology involves creating an error signal by utilizing the instantaneous and incremental conductance's.

$$e = \frac{I}{V} + \frac{dI}{dV} \tag{2.3}$$

we know that "**e"** becomes zero at the MPP. A simple proportional integral (PI) controller can be used to drive it to zero.

This method requires two sensors and can be controlled by DSP ora microcontroller which can keep all the previous values and make the correct decision.

C. Dividends for Open-Circuit Voltage

Under different temperature conditions, the almost linear relationship between VMPP and VOC gave rise to a fractional VOC technique as

$$V_{MPP} \approx k_1 V_O \tag{2.4}$$

k_1 is a proportionality constant in this case. The PV module's properties determine the k1, which must be ascertained prior to determining the V_{MPP} at various temperatures and insolation levels. According to reports, the factor k1 ranges from 0.71 to 0.78. After k1 has been established, V_{MPP} can be calculated using V_{OC}, which must be frequently measured by briefly stopping the power converter. It could lead to some power loss. To prevent this, pilot cells are used to obtain V_{OC}. Pilot cells are carefully chosen that represents the characteristics of the same PV module that is underuse. It was stated that about 75% of the voltage produced by the p-n junction diodes is V_{OC}. Thus, the controversial V_{OC} and V_{MPP} checking is eliminated. After approximating the V_{MPP}, the power converter's close loop control can be utilized to automatically achieve the necessary voltage.

This is one of the cheapest processes for MPPT but nowadays as partial shedding is under consideration, it leads to invalidation of k_1. So, this process is not so effective in partial shedding condition. This process does not require a microcontroller or DSP.

D. Fractional short circuit current

The fractional I_{SC} method is dependent on the fact that, the relationship between a PV module's ISC and IMPP is linear.

$$I_{MPP} \approx k_2 I_{SC} \tag{2.5}$$

Where the value of the proportionality constant, k_2, has been determined to be between 0.78 and 0.92. It is difficult to measure I_{SC} when it is operating. To measure the ISC using a current sensor, a second switch must be attached to the power converter in order to periodically short by the PV module. The solar array in a boost converter can be shorted using the converter's switch.

Because the MPP is never exactly matched, the power output is also decreased when determining the ISC. The k_2 needs to be recorded in the changed atmospheric condition and in case of multiple maxima the PV

module needs periodic sweep from open-circuit voltage to short- circuit current to update k_2. This process can be controlled by DSP but a loop of current feedback can also be used instead.

E. Control using fuzzy logic

The fuzzy logic control scheme has been started for MPPT with a microcontroller in the last decade and it is one of the popular ones. Its benefits include handling nonlinearity, coping with imperfect inputs, and not requiring an exact mathematical model.

Fuzzification, rule-based table lookup, and defuzzification are its three phases. Fuzzification is the process of converting numerical input variables, as shown in table 2.1, into linguistic variables based on membership functions. Five fuzzy levels are employed in this instance: ZE (zero), PS (positive small), NB (negative big), NS (negative small), and PB (positive big). If greater accuracy is required, seven fuzzy levels can also be applied.

Table 2 .1 fuzzy rule-based table

E \ ΔE	NB	NS	ZE	PS	PB
NB	ZE	ZE	NB	NB	NB
NS	ZE	ZE	NS	NS	NS
ZE	NS	ZE	ZE	ZE	PS
PS	PS	PS	PS	ZE	ZE
PB	PB	PB	PB	ZE	ZE

Typically, the inputs of a fuzzy logic system consist of error E and a variation in error ΔE. The method by which E and ΔE are calculated is up to the user. Since the MPP is where dP/dV disappears, applying the approximation

$$E(n) = \frac{P(n)-P(n-1)}{V(n)-V(n-1)} \tag{2.6}$$

And

$$\Delta E(n) = E(n) - E(n-1) \tag{2.7}$$

After computing and translating E and ΔE into a language variable, the fuzzy logic control output which often varies in the duty ratio ΔD of the power converter—can be found using a rule-based table such as table 2.1.

The linguistic factors related to ΔD for the different E and ΔE pairs depend on the user's skill level and the power converter being used.
The fuzzy logic controller output is transformed from a linguistic variable to a numerical variable during the defuzzification stage. This gives the MPP an analog signal to operate the power converter.

Although MPPT fuzzy logic controllers function effectively in a variety of atmospheric situations, their efficacy is mostly dependent on the user's or control engineer's ability to select the appropriate error computation and apply a rule-based table. To get optimal performance to MPPT, an adaptive fuzzy logic control must continuously tune the membership function and rule basis table.

F. Neural Network

Along with the fuzzy logic control, another technic for MPPT came upand named Neural Network which is also adopted by the microcontroller unit for processing. As seen in Fig. 2.5, input, hidden, and output layers are the three layers that are typically found in neural networks. Each layer's node count is entirely user-dependent and subject to large fluctuations. The input variables can be any combination of the following: temperature, irradiance, V_{OC}, or I_{SC}, as well as atmospheric data. One or more reference signals, such as the duty cycle needed to drive a power converter to run at MPP, make up the output. The hidden layer's algorithm and the neural network's training quality determine how near the operating point is to the MPP. There is weight in the links connecting the nodes. Weighting W_{ij} is the label applied to the link between nodes i and j. W_{ij} must be carefully ascertained during the training phase, in which the PV module is tested over a predetermined period of time and the patterns between input and output are documented, in order to precisely calculate the MPP.

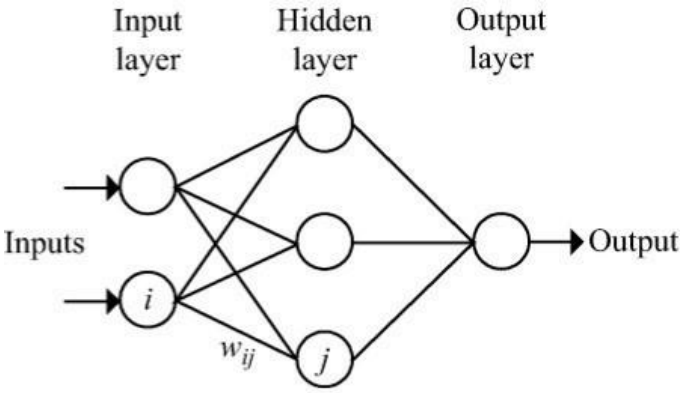

Fig 2.5 A neural network structure

The characteristics of every PV module is different. Therefore, a neural network must be specially trained for the particular PV module that is not being used. Since the PV module's characteristics change over time, the neural network must also be trained on a regular basis to ensure accuracy MPPT.

G. Ripple correlation control (RCC)

A power converter's switching process causes a voltage and current ripple on a photovoltaic module when it is linked to one. Therefore, ripples can potentially affect the power of the PV modules. Ripple is used by ripple correlation control (RCC) to regulate the MPPT. To drive the power gradient to zero and reach MPP, RCC correlates the time derivative of the time-varying PV module power, p', with the time derivative of the time-varying PV array current, i', or voltage, v'.

If v' or i' is increasing and p' is increasing, then the operating point lies below the MPP and if v' or i' is increasing and p' is decreasing, then the operating point lies above the MPP. Combining these observations, we see that p'v' or p'i' are positive on the left side of the MPP, negativeon the right side of the MPP, and zero at the MPP.

In the event that the power converter is a boost converter, the duty ratio lowers the PV module voltage while increasing the inductor current, which is equal to the PV module current. Consequently, the control input for duty ratio is

$$d(t) = -k_3 \int \dot{p}\dot{v}\, dt$$

or

$$d(t) = k_3 \int \dot{p}\dot{i}\, dt \qquad (2.8)$$

where k_3 is a positive constant. Controlling the duty ratio in this process assures a contentious MPP tracking and making the RCC a true MPP tracker.

H. Current Sweep

The current sweep method obtains and updates the PV module's I-V characteristics at predetermined intervals by using a sweep waveform for the module's current. The characteristics curve can then be used to compute the VMPP within the same intervals.

The sweep's selected function is exactly proportionate to its derivative as

$$f(t) = k4 \frac{df(t)}{dt} \qquad (2.9)$$

Where k4 is a proportionality constant. The PV module power is given by

$$p(t) = v(t)i(t) = v(t)f(t) \qquad (2.10)$$

At the MPP

$$\frac{dp(t)}{dt} = \left[v(t)\frac{df(t)}{dt} + f(t)\frac{dv(t)}{dt}\right] = 0$$

(2.11)

Substituting (2.9) in (2.11) we get,

$$\frac{dp(t)}{dt} - \left[v(t) + k4\frac{dv(t)}{dt}\right]\frac{df(t)}{dt} - 0$$

(2.12)

The differential equation in (2.9) has the following solution

$$f(\iota) = C\,\exp[\iota/k4]$$

(2.13)

C is chosen to be equal to the maximum PV module current I_{max} and k4 to be negative, resulting in a decreasing exponential function with time constant $\tau = -k4$. The eq. (2.13) leads to

$$f(t)=I_{max}\,\exp[-t/\tau] \qquad (2.14)$$

The current in eq. (2.14) can be easily obtained by using some current discharging through a capacitor. Since the derivative of eq.(2.13) is non zero, eq. (2.11) can be divided throughout by df(t)/dt and, with f(t)=i(t), eq.(2.12) simplifies to.

$$\frac{dp(t)}{di(t)} = v(\iota) + k4\frac{dv(t)}{dt} = 0 \qquad (2.15)$$

It is possible to confirm whether or not the MPP has been reached by applying eq. (xvi) once the V_{MPP} has been calculated using the current sweep. The general method of implementing the current sweep is analog computation. The current sweep loses some power and takes roughly 50 ms every turn. This MPPT method is only practical if the tracking unit's power consumption is less than the increase in power it can provide to the PV system as a whole.

I. DDC – Control of Link Capacitor Droop

This MPPT system is intended to operate with a photovoltaic system linked in parallel to an alternating current system line. An optimal boost converter's duty ratio is

$$d = 1 - \frac{V}{V_{link}} \tag{2.16}$$

Where V is the voltage across the PV module and V_{link} is the voltage across the dc link. If the V_{link} is kept constant, and the current going to the inverter increases, it results in an increased power coming out of the converter, and consequently, the power from the PV module increases also. It goes on until the module's maximum power output is achieved. Should that not be the case, V_{link} begins to sag. Just prior to the point, PV runs at MPP and the inverter's Ipeak (current control command) is at its highest level. In order to keep V_{link} from drooping, the ac system line current is fed back, and "d" is adjusted to maximize I_{peak} and achieve MPPT.
With this approach, the response of the inverter's dc-voltage control loop directly determines the response, negating the need to compute the power of the PV modules. Using decision-making logic units and an analog op-amp, this technique is simple to create. Figure 2.6 displays a typical diagram of the DC-Link Capacitor Droop Control Topology.

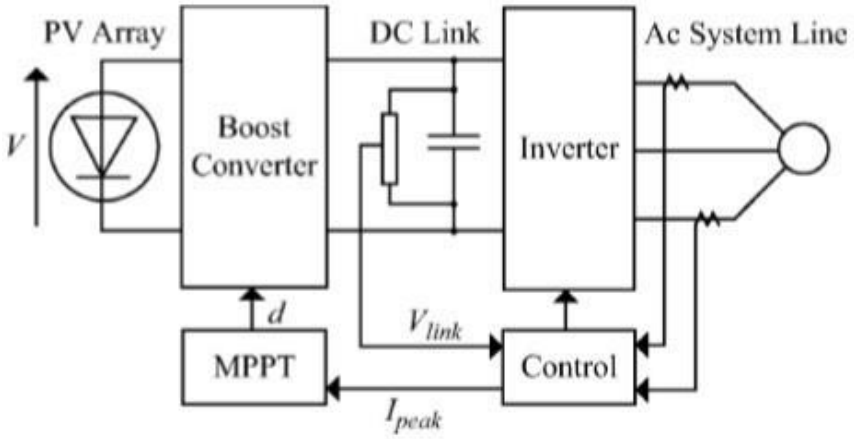

Fig. 2.6 DC-Link Capacitor Droop Control Topology

J. Load Current or Load Voltage Maximization

In this method, when the PV module is connected to a power converter, maximizing the PV module power also maximizes the power output ofthe load of the converter. Conversely, it works as vice-versa, assuming a lossless converter.

The majority of the loads can be resistive, voltage source, current source, or any combination of these. To get the greatest output power for a voltage source type load, the load current I_{out} should be maximized. The load voltage V_{out} for a load that is current source type needs to be maximized. You can use either I_{out} or V_{out} for any other load. As long as the load does not show signs of negative impedance, it is also true for non-linear loads. Consequently, one sensor is sufficient to optimize the load power for nearly all load types by maximizing either the load voltage or the load current. The power converter is controlled by positive feedback to maximize the load current and operate the PV module in close proximity to the MPP. Because this MPPT approach is predicated on the premise that the power converter is lossless, which is not true in real life, operation precisely at the MPP is rarely attained.

K. dP/dV or dP/dI Feedback Control

With the use of a microcontroller, it is easy to handle complex computation, and a very obvious way to perform MPPT is to compute the slope of the PV power curve (dP/dV or dP/dI) and feedback to the power converter with some control topology to drive it to zero.

A linearization method can be used to determine dP/dV. After computation of dP/dV, the sign(+ or -) is stored for the few cycles, and based on these signs, the duty ratio of the power converter is changed i.e. incremented or decremented to reach the MPP. The dynamic step size can be used to improve the transient response. The transient response is then enhanced by integrating the dP/dI with an adjustable gain. Until the MPP is reached, the PV module's voltage is gradually increased or decreased, and dP/dV is compared using a marginal error signal.

L. Other Methods

Some other methods are not as much popular as those are discussedpreviously but those can also be used for MPPT. Some of those are Array Reconfiguration, Linear Current Control, IMPP & VMPP Computation, State-based MPPT, OCC MPPT, BFV, LRCM, Slide control, etc. These are not popular but MPPT can be done suitably with these methods also.

The user may find it difficult to determine which of the numerous MPPT methods for PV systems best meets their application requirements. The next subsections of table 2.2 emphasize the key elements of the MPPT approaches that need to be taken into account.

Table 2.2 Major Characteristics Of Various MPPT Techniques

MPPT Technique	PV Array Dependent?	True MPPT?	Analog or Digital?	Periodic Tuning?	Convergence Speed	Implementation Complexity	Sensed Parameters
Hill-climbing/P&O	No	Yes	Both	No	Varies	Low	Voltage, Current
IncCond	No	Yes	Digital	No	Varies	Medium	Voltage, Current
Fractional V_{OC}	Yes	No	Both	Yes	Medium	Low	Voltage
Fractional I_{SC}	Yes	No	Both	Yes	Medium	Medium	Current
Fuzzy Logic Control	Yes	Yes	Digital	Yes	Fast	High	Varies
Neural Network	Yes	Yes	Digital	Yes	Fast	High	Varies
RCC	No	Yes	Analog	No	Fast	Low	Voltage, Current
Current Sweep	Yes	Yes	Digital	Yes	Slow	High	Voltage, Current
DC Link Capacitor Droop Control	No	No	Both	No	Medium	Low	Voltage
Load *I* or *V* Maximization	No	No	Analog	No	Fast	Low	Voltage, Current
dP/*dV* or *dP*/*dI* Feedback Control	No	Yes	Digital	No	Fast	Medium	Voltage, Current
Array Reconfiguration	Yes	No	Digital	Yes	Slow	High	Voltage, Current
Linear Current Control	Yes	No	Digital	Yes	Fast	Medium	Irradiance
I_{MPP} & V_{MPP} Computation	Yes	Yes	Digital	Yes	N/A	Medium	Irradiance, Temperature
State-based MPPT	Yes	Yes	Both	Yes	Fast	High	Voltage, Current
OCC MPPT	Yes	No	Both	Yes	Fast	Medium	Current
BFV	Yes	No	Both	Yes	N/A	Low	None
LRCM	Yes	No	Digital	No	N/A	High	Voltage, Current
Slide Control	No	Yes	Digital	No	Fast	Medium	Voltage, Current

2.4.2 Problem overview

The problem considered by the MPPT technique is to automatically find the V_{MPP} or I_{MPP} at which the module should operate to obtain maximum power output P_{MPP} under a given temperature and irradiance. In some cases, mainly under partial shedding, there could be multiple maxima but there is still a true maximum always. The MPP varies with temperature and irradiance in the majority of cases, although some are particularly more helpful in situations where the temperature is roughly constant. Most of the cases automatically respond to changes but some of them are open-loop and need periodic fine-tuning. The module is typically connected to a power converter that can vary the current from the PV module and extracts the power.

2.5 A Survey of solar photovoltaic system

Three major components make up a standalone photovoltaic system: an electrical load, such as an LED array for lighting, a controller circuit, and a solar PV module. Occasionally, a charge controller is used to store the charge from the solar PV module in a battery, which then provides the required power to the lighting fixture or other electrical appliances when there is no daylight. The lighting unit or other appliances are powered by the electronic circuit, which draws electricity from the PV module.

The photovoltaic phenomenon, which forms the scientific foundation of solar cells, was discovered by Sir Albert Einstein, who was awarded the Nobel Prize in Physics in 1921. Semiconductor materials are used to

make solar cells. Semiconductor materials are in between insulators and conductors because they can conduct electricity under specific circumstances. Germanium and silicon are the two most widely used semiconductor materials. Doping is the technique of combining it with other elements to increase its conductivity.

2.5.1 Solar cell physics

Semiconductors of the p-type and n-type together to form a photovoltaic cell. Extra electrons are present in an n-type semiconductor, while extra free holes are present in a p-type semiconductor. A n-type electron will diffuse to a p-type crystal and recombine with free holes, whereas p-type holes will diffuse to an n-type crystal and recombine with electrons when two p and n-type crystals are forced together. Two types of charges are left on the n-side and p-side respectively by the diffusion of electrons and free holes. A potential difference across the p-n junction is produced as a result of the charge distribution, which also generates an electrical field. Soon after, a potential difference with an energy of ΔE develops at the interface, large enough to merely halt additional charge carrier diffusions. The system reaches equilibrium when the contact potential leads the p-side's energy level to rise and the n-side's energy level to fall, lining up the Fermi levels of the two sides.

When photon energy ($h\upsilon$) from solar radiation surpasses the energy gap (E_g) and reaches a p-n junction, the electrons in the valence bond gain sufficient energy from the photon to go to the conduction band, where they form an electron-hole pair. Pairs are separated by the junction, where holes travel up the potential hill on the p-side and electrons travel down the potential hill on the n-side. The potential hill's height is decreased by this action. When the junction is ultimately reached, a new equilibrium condition and potential difference emerge. Open-circuit voltage (Voc), which is a function of the solar panel's incident radiation intensity, is the name given to this potential difference. The cell-generated electron-hole pair is now forced to split and cross the complete potential hill if the two contacts are connected by an external wire with very little resistance. The electron travels to the p-side and the holes to the n-side via the wire before recombining. We refer to this flow as Isc, or short circuit current.

To do useful work, the produced electron-hole pairs are introduced into an external circuit. For current to flow through the external resistance, there must be a sufficient potential difference, V. The difference in Fermi levels on either side of the junction must provide the necessary potential difference with an energy equivalent of eV. This reduces the potential hill across the junction to (ΔE -eV), where ΔE is the complete potential hill's short circuit current. The junction is no longer as effective at separating the generated electron-hole pair as it was in the short circuit scenario because the potential hill has decreased. This causes a current leak at the junction Ij, a decrease in the load current I supplied to the load, and the inability of part of the charges to cross the junction in the intended direction.

A. Junction current

Junction current (Ij) is the net current flow from the p-side to the n-side caused by all charge carriers (electron and hole). Because the junction tends to slope downhill, the minority carriers—electron—can cross it readily, but the majority carriers—holes—cannot cross it easily until their energies are higher than the barriers. Equation (i) can be used to express the junction current:

$$I_j = I_0[\exp(eV/kT)-1] \quad (2.17)$$

Where, I_0 = Saturation current density, k = Boltzmann constant, and T is the absolute temperature in kelvin.

B. Design of a solar cell

Crystalline silicon, the best semiconductor currently available for this purpose, is used to make solar cells. It is doped with boron, an acceptor impurity. The cell can be shaped into a square, round, or semi-circular shape with a cross-sectional area of up to 100 mm. Its thickness is around one-third of a millimeter. At roughly 850° C, phosphorus, another donor impurity, diffuses in the semiconductor wafer to create the p-n junction just a few micrometers below the surface. The rear contact spans the entire back surface, while the front contact resembles a grid of thin fingers. On the front surface, an antireflective coating is typically applied.

C. Choice of materials

Choosing a semiconductor material is determined by the quantity of photons absorbed that have energy above the bandgap. An increase in the bandgap results in an increase in the saturation current density I0, which in turn raises the output voltage.

Energy gaps in semiconductors between 1.1 and 2.3 eV are necessary for solar cell utility. These materials include: a) Indium Phosphide (InP = 1.27 eV); b) Gallium Arsenide (GaAs = 1.35 eV); c) Aluminum Antimonide (AlSb = 1.49 eV); d) Cadmium Telluride (CdTe = 1.5 eV); e) Zinc Telluride (ZnTe = 2.1 eV); f) Aluminum Arsenide (AlAs = 2.16 eV); and g) Gallium Phosphide (GaP = 2.24 eV). The solar cell can also be made using mixed semiconductors, which are created by mixing several semiconductors in this energy gap range in varying quantities.

D. Properties required in semiconductor for a typical solar cell

The particular semiconductor material that is used in a solar cell determines certain specialized features. While these attributes differ throughout materials, the fundamental ideas remain the same. Among the characteristics are:

a. Light Absorption:

Different semiconductor materials absorb light (photons) at different rates. A micron's thickness may absorb almost 90% of light for some of them, whereas it takes a micron for others to do the same. Thus, the selection of absorption-dependent materials is based on the intended use.

b. Absorption Length:

Absorption length is the distance a photon travels within a semiconductor material prior reaching 63% of its absorption. It describes the degree to which the substance absorbs the photon. A solar cell's thickness is designed based on this parameter.

c. Quantum efficiency:

This represents a solar cell's ability to convert photon energy into another kind of energy, such as electricity, using semiconductor material. The fraction of the carrier that contributes to the electric current is measured.

d. Effect of Temperature:

As temperature rises, there is a discernible decrease in open-circuit voltage (Voc). The open-circuit voltage of each silicon cell decreases by 2.3 mV for every degree that the temperature rises. One way to express the impact of temperature is using equation (ii):

$$V_{oc}(T)(mV) = V_{oc}(25°C)(mV) - \Delta T \times K_t(mV) \quad (2.18)$$

Where, **ΔT** is the temperature difference and $\mathbf{V_{oc}(25°C)\ (mV)}$ is the open-circuitvoltage at 25° C and $\mathbf{K_t}$ is a constant, that varies with the location.

2.5.2 Advancement in photovoltaic

Cost affects a photovoltaic cell's efficiency. Choosing between crystalline and thin-film materials ultimately comes down to preference for greater efficiency and less manufacturing costs. Although thin-film devices are more expensive, crystalline devices are more efficient. Research is still being done to create more efficient and acceptable materials. These days, thin-film technology is becoming more and more popular due to its efficiency and thin material, which makes it portable.

2.6 LEDs for natural day-light creation

The world of interior lighting has completely changed with the launch of Light Emitting Diodes, or LEDs. In this section, we look at using LEDs to create artificial lighting systems that mimic the characteristics of daylight as nearly as possible. Modern lighting solutions are based mostly on LEDs because of their long lifespan, energy efficiency, and environmental advantages.

A. Color Rendering Index (CRI) of LEDs

We explore the idea of Color Rendering Index (CRI) after realizing how crucial color accuracy is in lighting. When trying to replicate the natural colors found in daylight, this measure is essential for attaining high-quality color reproduction under artificial illumination. This section delves into the ways in which LED technology has been developed to get optimal CRI values, hence facilitating the construction of lighting conditions that closely resemble natural sunlight. Daylight has the CRI value of 100 and the CRI of the normal LEDs is near about more than 80. Early LED lighting faced challenges in achieving high CRI values, as early LEDs had limited spectral coverage and often produced light with uneven spectral distributions. Historically, some LEDs

struggled to accurately render certain colors, particularly reds and skin tones, leading to lower CRI scores and less desirable color quality. Advancements in LED technology have addressed many of the challenges associated with color rendering. Modern LEDs can achieve higher CRI values through improved phosphor coatings, better color mixing techniques, and enhanced spectral tuning. Specialized LEDs, such as phosphor-converted white LEDs and RGB LEDs, offer greater flexibility in achieving specific color temperatures and rendering vivid colors.

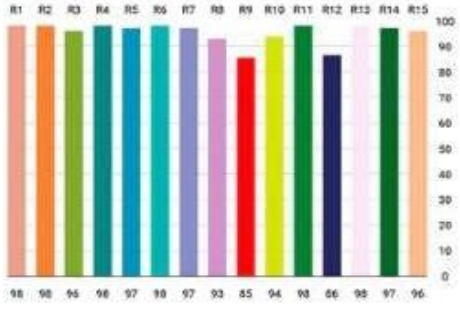

High Color Quality LEDs CRI

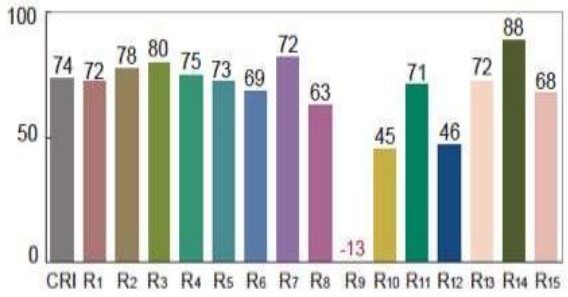

Conventional LEDs CR

B. Spectral Characteristics of LEDs

A detailed analysis of the spectrum characteristics of LEDs is given, with a focus on how emission spectra can be altered to replicate the intricate characteristics of actual sunshine. This presentation highlights any new advancements or discoveries in LED technology that enhance the ability to faithfully reproduce the spectral properties of natural daylight.

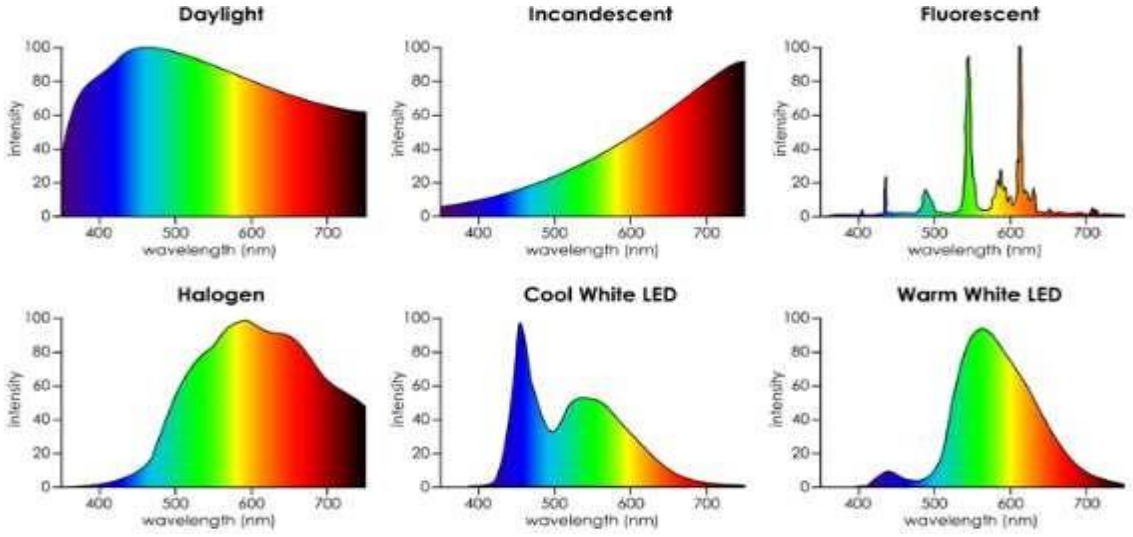

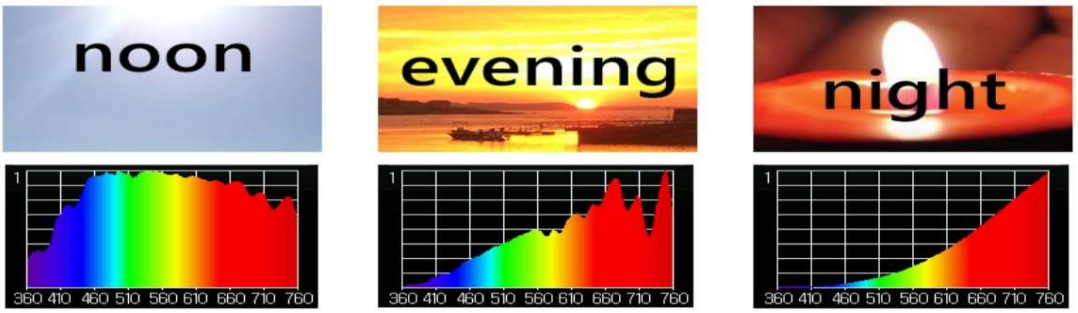

C. Circadian Lighting and LEDs

The subject this article examines how lighting affects human circadian rhythms and well-being and how LEDs can be used to create lighting conditions that promote health. A discussion of pertinent research and discoveries highlighting how LED lighting affects human comfort in general and sleep patterns in particular highlights the potential advantages of LED-based interior lighting systems. Secretion of some hormones like melatonin, serotonin depends upon the daylight which controls our sleeping cycle, mood and human productivity. If we can use daylight like color quality LEDs then the hormone secretion will not be hampered.

D. Tunable CCT White LEDs

We present the idea of adjustable white LEDs and investigate how dynamic color temperature changes can be made to replicate different daylight scenarios all day long. The talk covers the theoretical underpinnings as well as the useful design considerations of using adjustable white LEDs in interior lighting systems.

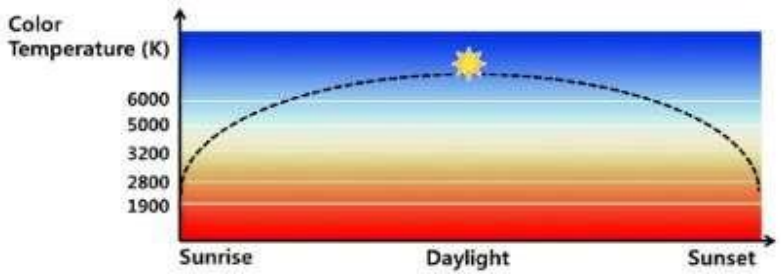

The LED of high color quality that is having CRI and CRI R9 is near about 100, the continuous and balanced spectrum and CCT near about 5000K-5500K but practically it reaches upto more than 6000K that closely matches the daylight. That daylight like color quality can be acheived by proper mixing of colors that may be two color or three colors and also may be four colors. But in our laboratory we have got the maximum CRI value near about more than 96 by mixing of four colors of LEDs that is Warm White, Cool White, Green and Blue color. Here for indoor illumination the LED that has been used has CRI more than 96, CRI R9 more than 95 and CCT 6200K and has a continuous spectrum just like the quality of daylight which has been developed in our lab. The information of this section has been taken from the M.E. thesis of Mr. Kafiur Rahman that is entitled as “Design and Development of Daylight like high color quality LED Light Source for Critical Task Performance” in the year of 2023.

3. Overview of daylight harvesting for indoor illumination

In order to save energy, daylight harvesting systems employ natural light to balance the amount of artificial lighting required to effectively light a place. This is accomplished by using lighting control systems that have the ability to dim or switch electric lighting in response to changes in the amount of daylight.

3.1 Daylight Harvesting

According to the Cambridge Dictionary, the word "harvesting", apart from its traditional meaning, also means "the process of collecting a natural resource to use it effectively." This leads to the use of terms like sunlight harvesting or daylight harvesting when sunlight is used along with artificial light sources to reduce the amount of energy consumption for lighting. Two main types of approach can be used for harvesting daylight (a) Direct approach, (b) Indirect approach. Fig. 3 shows the two different approaches for daylight harvesting.

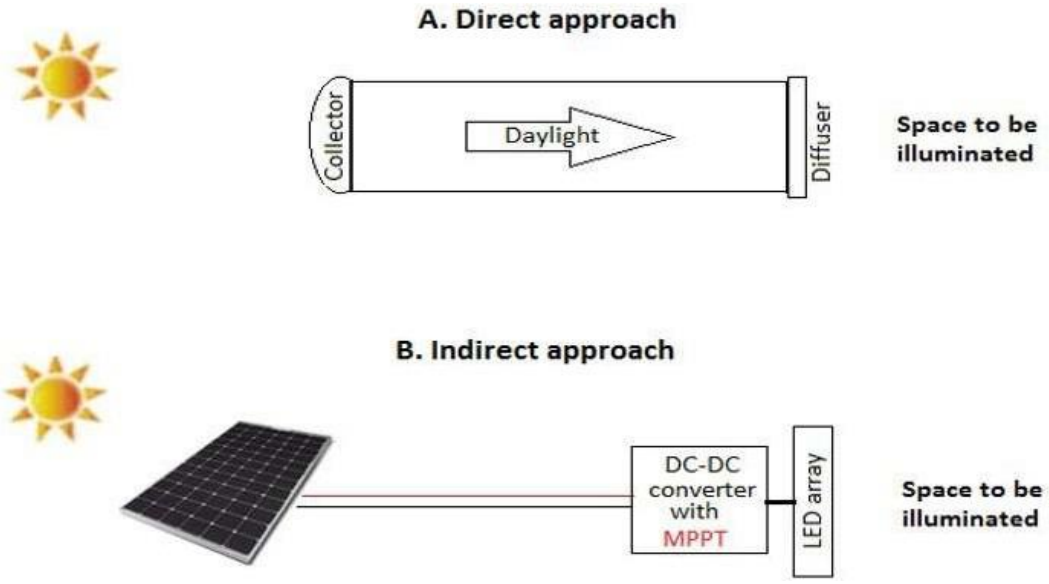

Fig. 3 Daylighting approaches

3.1.1 Direct Approach

In the direct approach, the light comes directly to the earth from the sun. In vacant space under the sky , the light falls directly on the surface. But in the indoor rooms , the sunlight can not reach directly. So, there are some process by which the daylight can reach the interior of a room. Fig. 3.1 shows various methods for the direct daylight harvesting approach.

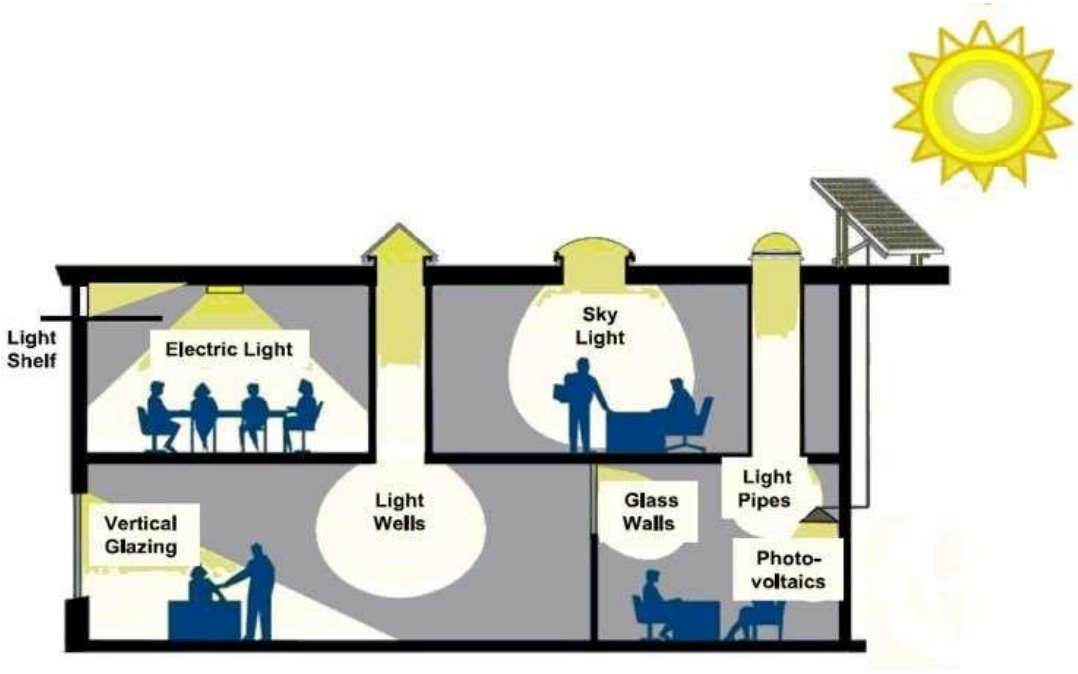

Fig. 3.1 Various type of daylight harvesting methods

I. Gladged window and light tray

It is the most common type of direct of direct approach. Mostly every household has windows and the light comes to the floor or walls amount directly from the Sun and illuminates the room surface. Fig. 3.2 shows the daylight coming from the window. Direct light can create a huge amount of glare which may be very obtrusive for a viewer. So, every window must have a diffuser glass that may control the glare and also the direction of light and heat passing through it. Many parameters control daylight through a window. Those are:

Transmittance –

The percentage of radiation that can flow through a glazed window is referred to as transmittance. Some glasses transmit all the wavelength and some transmit selected wavelength. Polarized glass transmits only a specific light wavelength and the output color from the window is a specific one.

Fig. 3.2. Direct sunlight coming from window to the surface

Reflectance –

Just like light reflects from the surface of the water, some light always reflects from the glass surface and looks similar to the mirror. The percentage of light reflects from the glass is called reflecting of the glazing.

Absorptance –

The energy that does not transmit or reflected from the glass surface is absorbed by the glass.The percentage of energy absorbed by the glass is called the absorptance of the glass.

U-factor-

when the outside and inside of a window have different temperatures. The rate of a window, heat is lost or gained through the window. The rate of heat transfer through a window is called the U-factor or Insulating factor.

Solar Heat Gain Coefficient-

Heat can be obtained through the window by direct or indirect sun radiation, regardless of the outside temperature. The Solar Heat Gain Coefficient (SHGC), also known as the Shading Coefficient (SC), is the capacity to regulate this heat gain.

Visible Transmittance-

It is the quantity of light that comes through the window that is visible. For uncoated transparent glass, visible transmittance ranges from 90% to less than 10%, depending on how reflective the glass is.

Ratio of light to solar gain-

It is the proportion of solar heat transmission via a window to visible light transmission. It has a wide range of values from as high as 1.87 to as low as 0.27. Nowadays a low-solar-gain low-E coating is most efficient for a glazed window in reducing the all over heat without compromising the amount of light transmission.

II. LIGHT PIPE

Light Pipe is an optical device that transfers the light from a source to a surface by using optics inside it. The light pipe consists of highly reflecting glass inside it which reflects the light from a source to destination. It has a glass protected aperture outside the building to capture the daylight and a diffuser at the end side to reduce the glare. Fig. 3.3 shows a typical design of the daylight harvesting light pipe. There are two types of light pipes available. One is “hollow” type and another is “the light with reflective surface”.

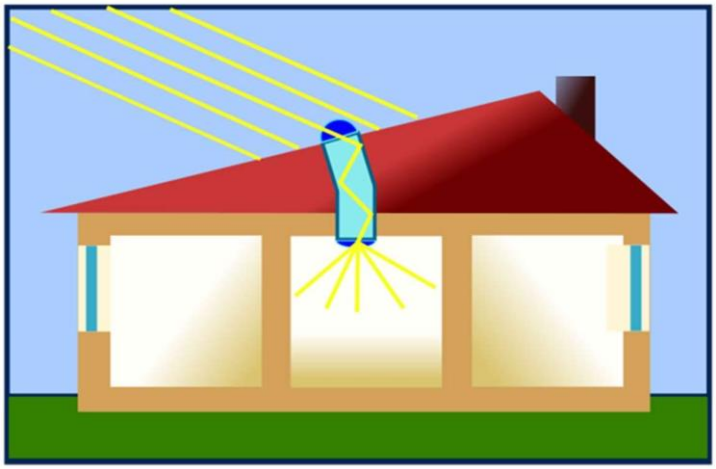

Fig 3.3 Daylight integration using a light pipe

It is generally used in the rooms where direct sunlight does not reach easily but the distance of the pipe is not so long . It can not be used in a room that does not have an opening for the sky.

3.1.2 Indirect Approach

The indirect approach depends on the use of the solar cell. A solar cell is a device that generates electricity while absorbing light. It transforms photon energy into electrical energy, and this electrical energy, and this electrical energy may be used to power the artificial light. The indirect approach depends on some components. The solar cell, the electronics part, and the artificial light unit like incandescent light or gas discharge light or LED light. The electricity generated from the solar panel is very little compared to other conventional sources. The most useful lighting type for solar-based light is LED. LED is most efficient type of artificial light available in the market today. The electronics extract power from the solar cell and feed the lighting unit. The extract power from the PV cell may be divided into two parts. One part may go directly to the

solar lighting unit or the other electrical appliances like fan, TV, or mobile and laptop charger. Another part may go to the battery. The battery is a storage device which stores charges in the form of a chemical reaction in the daytime and supplies current in the absence of the daylight. The battery stores the energy from the PV cell using some electronics circuit called “battery charging circuit”. It supplies the lighting unit or the other electrical appliances in the absence of daylight shown in Fig. 3.4

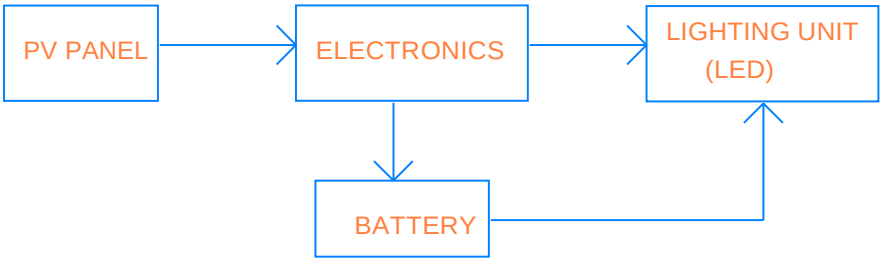

Fig. 3.4 Solar powered lighting system with battery

Another approach is like the previous one but does not include the battery, shown in Fig. 3.5. It directly feeds the lighting unit without any storage devices. So it cannot work at night time but it will be useful in the daytime for the buildings where daylight does not reach the inside rooms. This approach could save a huge amount of energy from other conventional sources.

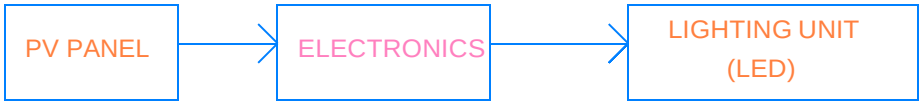

Fig. 3.5 Solar powered lighting system without battery

In an indirect approach, the most important parameter is the maximum power fetching from the PV cell because the IV characteristics of the PV module are not linear. This can be done by using a method named “Maximum power point tracking” or in short “MPPT”. There are various techniques to do so but the main phenomena depend on the I-V characteristics of the PV module.

3.1.2.1 Photosensors

In both open-loop and closed-loop daylight harvesting systems, the light level, also known as luminance or brightness, is detected by a light level sensor, also known as a photosensor. Electric lighting is controlled by photosensors in response to the amount of daylight present in the area. The photosensor in an open-loop system can be placed within the building facing a window or skylight, or outside on the building's wall or roof. It just measures the quantity of daylight that is available.

The photo sensor in a closed-loop system measures the entire photometric amount of light in the room from both artificial and daylight sources. To measure the amount of light on a work surface, for instance, a closed-loop photo sensor in an office can be mounted on the ceiling facing the desktops. This is because it would be impossible to place the sensor on the desktop itself. The signal from the photo sensor needs to be precisely calibrated in both the open- and closed-loop versions in order to accurately reflect how changes in outside daylight affect the amount of light in areas designated as "important function."

3.1.2.2 Dimming and the control module

A lighting control system module, an automatic light switching device in the electric lighting system, interprets the signal from the photosensor and can dim or turn off fixtures as needed to lower the amount of electric lighting. Artificial lighting can be continuously adjusted to match the amount of daylight available if the electric lighting is dimmable. An electric light fixture or bulb must operate constantly until daylight can provide the appropriate quantity of light for the area if the electric lighting is only turned on or off. A number of non-adjacent light fixtures are examples of non-dimming variations; they include alternating units in a ceiling "grid layout" or daylight source neighboring fixtures next to windows or skylights that are connected for module on-off switching. An extra type of on-off switching that enables many lamps in a single light fixture to be turned on and off independently of one another is termed step switching (sometimes known as "bi-level switching"). This often allows for one or two steps between the maximum output and zero.

Dimming systems typically have higher costs than turning systems off. When sunshine can only partially fulfil the needs of the space, they have the ability to limit electric light output, which could result in even greater energy savings. But dimming systems could also need a bit extra energy to run on a basic level. The people using the area won't notice variations in electric illumination caused by daylight harvesting if a dimming system is tuned properly, but they will definitely notice changes caused by on-off or step switching.

3.1.2.3 Energy saving

The energy savings from daylight harvesting have been documented in numerous research. Energy savings of between (20-40)% are typical for electric lights. The savings are mostly dependent on the type of space in which the light harvesting management system is installed and how it is utilized. Obviously, savings are only achievable in locations with plenty of natural light, as these would have eliminated the need for electric illumination. Therefore, the best locations for daylight harvesting are those with access to skylights, light tube groups, glass block walls, conventional or clerestory windows, and other passive daylighting sources from sunlight, as well as places where electric lighting is typically left on for lengthy periods of time. These environments have included offices, atria, indoor public multistory plazas and shopping center courts, and schools.

Trying to boost energy savings by enlarging windows is overly straightforward. Over-illumination of the daylight may irritate residents, prompting them to close blinds or employ other window coverings, which could jeopardize the daylight harvesting system. Venetian blinds that are only partially opened might reduce energy savings by half.

Inadequate system design, calibration, or commissioning may prevent impressive energy savings projections from being realized in real-world scenarios. Residents have the ability to interfere with systems that provide overall light levels that are deemed too low, or that distractingly dim or switch on electric lighting. (For instance, covering a sensor with tape will result in continuous, maximum-output electric lights.)

The exorbitant costs and subpar performance of daylight harvesting technology have prevented widespread use. On the other hand, research indicates that owners can see an average yearly energy savings of 40% when they utilize daylight harvesting equipment.

3.1.2.4 LED Driver

3.1.2.4.1 Flyback converter

The ringing choke converter (RCC), also known as the self-oscillating flyback converter, is a low-component count circuit that is resilient and has been extensively utilized in low-power off-line applications. The total cost of the circuit is typically less than that of a traditional PWM flyback converter, which uses a commercially available integrated control, because the circuit's control can be built with a relatively small number of discrete components without sacrificing performance.

Fig. 3.6 shows the block diagram of the fly back converter. The complete operation of this circuit is explained in three different interval.

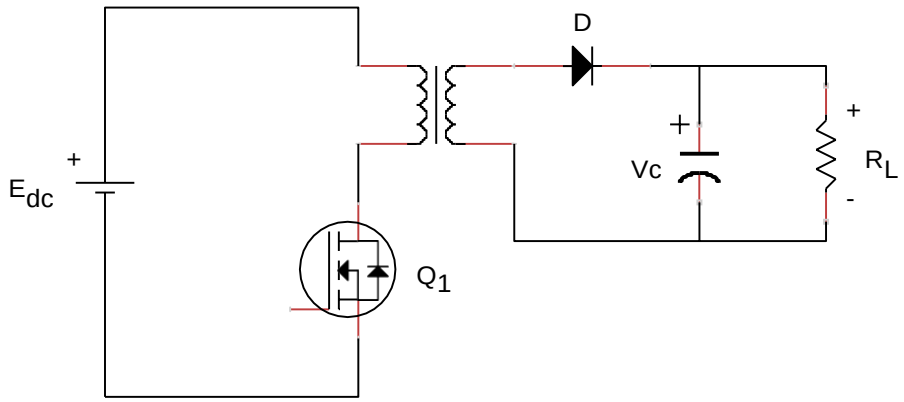

Fig. 3.6 Basic circuit diagram of Fly-back converter

A. Interval 1: The input supply is connected to the transformer's primary winding when switch Q_1 (MOSFET) is turned on. At this point, the induced voltage to the secondary causes the diode D, which is linked in series with the secondary winding, to become reverse biased. Thus, when switch Q_1 is turned on, current can flow through the primary winding, but the reverse biased diode prevents current from flowing through the secondary winding.

Under this interval, the primary current increases linearly as the input supply voltage crosses the primary winding inductance. The expression for the rise in current through the primary winding can be found in the following mathematical relation:

$$E_{DC} = L_p * \frac{d}{dt} i_p$$

where i_p is the instantaneous current flowing through the primary winding, L_P is the primary winding's inductance, and E_{DC} is the input dc voltage.

The energy stored in the flyback inductor-transformer's magnetic field at the conclusion of switch-conduction is equal to Lp I2p / 2, where Ip is the primary current's magnitude at the end of the conduction period. Due to the output capacitor's previously stored charge, the load connected to it receives continuous current flow even when the secondary winding is not conducting in this mode. Assuming a large capacitor, the secondary winding voltage is nearly constant during period 1 and is equal to $Vs = E_{dc} N_2 / N_1$.

B. Interval 2: After conducting for a while, switch Q_1 is turned off to initiate this mode of operation. Due to the disruption of the primary winding current route, the voltage polarities across the winding reverse in accordance with the rules of magnetic induction. The diode in the secondary circuit becomes forward biased when the voltage polarities are reversed.

As soon as switch Q_1 is turned off, the secondary winding current for the hypothetical circuit under consideration climbs sharply from zero to $Ip * N_1 / N_2$. The numbers N_1 and N_2 indicate how many turns there are in the primary and secondary windings, respectively. The output capacitor is charged by the secondary winding current. The output capacitor is often big enough that, over the course of multiple switching cycles, the capacitor voltage increases to its steady state value without noticeably changing in a single cycle.

C. Interval 3: At this point, the diode connected in series with the winding stops conducting and the secondary emf and current both drop to zero as the magnetic field energy has fully transferred to the output. Nonetheless, the output capacitor keeps the load's voltage constant. Switch Q_1 is turned on to finish Interval 3, at which point the circuit returns to Interval 1 and the procedure is repeated.

3.1.2.4.2 Boost converter

An electronic switch is periodically opened and closed by the boost converter, a switching converter. Because the output voltage is higher than the input, it is referred to as a boost converter.

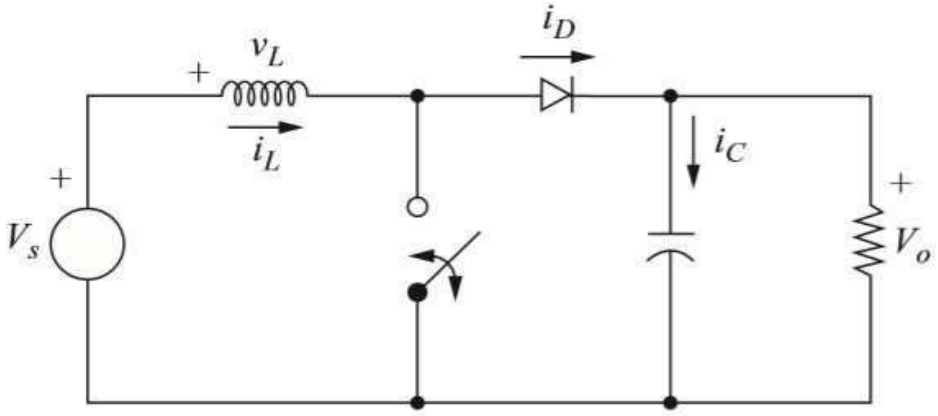

Fig 3.7 Schematic diagram of the Boost converter

Fig 3.7 shows the schematic diagram of a typical boost converter. There are two modes of operation.
(i) is the condition when the switch is closed. (ii) thecondition when the switch is open.

A. Analysis for the condition when the switch is closed

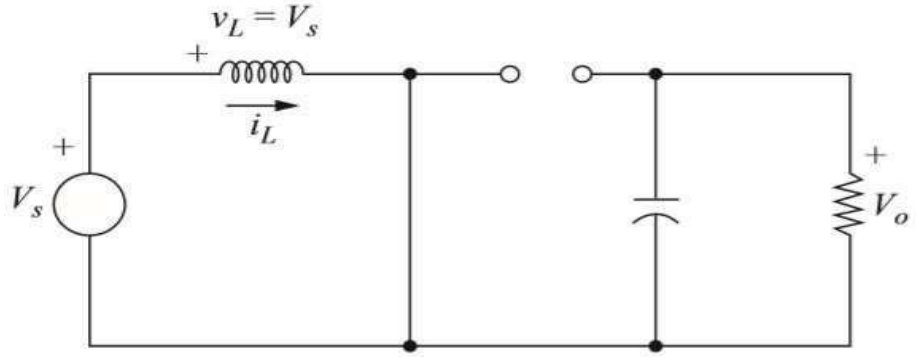

Fig 3.8 Mode of operation when the switch is closed

When the switch is closed, the diode is reversed biased. According to Kirchhoff's voltage law (the closed path contains the input dc source, an inductor, and a closed switch)

$$v_L = V_s = L\frac{di_L}{dt} \qquad \text{or} \qquad \frac{di_L}{dt} = \frac{V_s}{L} \tag{3}$$

In the inductor, the rate of change of current is constant, so the current increases linearly while the switch is closed. Then the change in inductor current is computed from Eq.(3.1) as,

$$\frac{\Delta i_L}{\Delta t} = \frac{\Delta i_L}{DT} = \frac{V_s}{L} \tag{3.1}$$

Solving Eq.(3.1) for Δi_L when the switch closed

$$(\Delta i_L)_{\text{closed}} = \frac{V_s DT}{L} \tag{3.2}$$

B. Analysis for the condition when the switch is open

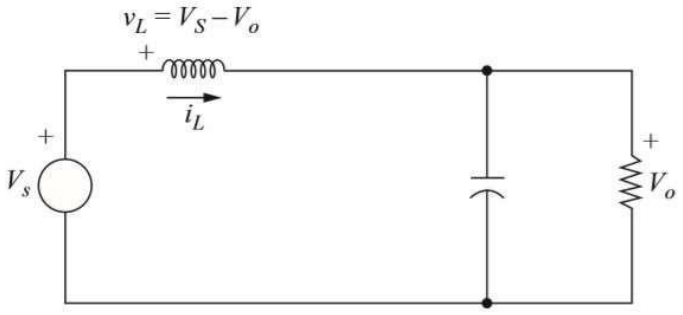

Fig.3.9 Mode of operation when the switch is open

The diode becomes forward biased and creates a conduit for the inductor current to travel through the load when the switch is opened because the inductor current cannot change immediately. Given a constant output voltage V0, the voltage across the inductor is

$$v_L = V_s - V_o = L\frac{di_L}{dt}$$

$$\frac{di_L}{dt} = \frac{V_s - V_o}{L} \tag{3.3}$$

$$\frac{\Delta i_L}{\Delta t} = \frac{\Delta i_L}{(1-D)T} = \frac{V_s - V_o}{L} \tag{3.4}$$

Solving Eq.(3.4) for Δi_L, when the switch is open,

$$(\Delta i_L)_{\text{open}} = \frac{(V_s - V_o)(1-D)T}{L} \tag{3.5}$$

For steady-state operation, the net change in the inductor current must bezero.

So,

$$(\Delta i_L)_{\text{closed}} + (\Delta i_L)_{\text{open}} = 0$$

$$\frac{V_s DT}{L} + \frac{(V_s - V_o)(1-D)T}{L} = 0 \tag{3.6}$$

Solving Eq. (3.6) for V_o,

$$V_s(D + 1 - D) - V_o(1-D) = 0$$

$$\boxed{V_o = \frac{V_s}{1-D}} \tag{3.7}$$

Additionally, the average inductor voltage needs to be zero for periodic operation. The average inductor voltage during a single switching time can be expressed as:

$$V_L = V_s D + (V_s - V_o)(1 - D) = 0$$

(3.8)

"D" is the duty ratio, which is defined by (T_{on} / T_{total}). Equation (3.7) demonstrates that in the event that the switch is always open and the "D" is zero, the input and output voltages are equal. The denominator of Eq. (3.7) decreases with increasing duty ratio, increasing output voltage. If the switch is always closed (D = 1), the voltage should theoretically be infinite, but this is not really achievable. As a result, the output voltage of the boost converter is either higher than or equal to the input voltage. As with a buck converter, the output voltage, however, cannot be lower than the input voltage. Fig 3.10 shows the voltage and current graphs across the inductor with respect to time.

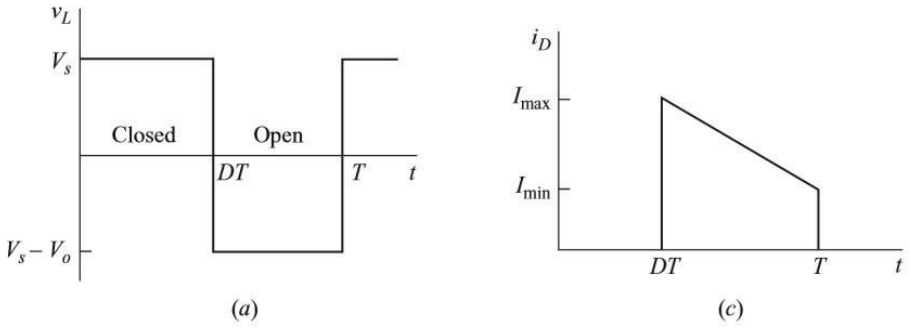

Fig 3.10 Inductor (a) inductor voltage (b) inductor current

Summary

Daylight harvesting systems use natural light to regulate the amount of artificial lighting needed to adequately light a space, saving energy. The signal from the photo sensor is interpreted by a lighting control system module, an automatic light switching mechanism in the electric lighting system, which can then dim or turn off fixtures as necessary to reduce the quantity of electric lighting. If the electric lighting is dimmable, artificial lighting can be continuously adjusted to match the quantity of daylight available.

4. Proposed daylight harvesting control system

As the number of buildings and rooms within them has increased significantly over time, it has become more challenging to minimize energy waste because of ineffective light control and distribution. Furthermore, depending on users to manually regulate the light in order to save energy is impractical. In order to control the excessive energy usage, a lot of technologies and sensors have developed recently. One example is occupancy sensors, which identify activity within a specific area. By automatically turning on lights when someone enters a room, they offer convenience. By shutting off lights quickly after the final person leaves the room, they lower the energy consumption of lighting. One of its drawbacks is that it ignores any additional light sources that may be present in the space. Additionally, the internal sensor's trigger relies on the user's position. While very useful, motion detectors are insufficient. Dimmers are another manual technique to manage the amount of artificial light in a room. While some dimmers accomplish this automatically, others do not adjust to the presence of another light source in the space.

The energy savings from daylight harvesting have been documented in numerous research. The Public Interest Energy study Program of the California Energy Commission [14] suggested conducting study on on/off control, however they neglected to account for the over-illumination brought on by daylight. While using an on/off switch is less expensive, a continuous dimmer will save a significant amount of energy at a fair price. Systems that capture daylight can save 20–40% on electric lighting [15]. The sort of space where the control system is installed determines how much energy can be saved. When there is daylight available, daylight harvesting can be used whenever possible; it functions best in areas with windows or skylights. These spaces include public buildings, schools, and offices. By making windows larger, energy savings can be achieved at the expense of over-illumination, which may annoy residents and force them to utilize manual venetian blinds or other shade mechanisms.

It is vital to comprehend the type of light source that is offered in order to create an efficient energy-saving technique. Direct or indirect sunlight (ambient light or light reflected from surfaces of objects) can be considered natural light. One way to create artificial light sources is to provide a normal light bulb with an electrical power source. The position of the light source, the light's angle of incidence, the placement of the photo sensors, and their alignment and calibration are additional crucial variables. Lastly, a light source's hue can have a big impact on a sensor's reading [16].

In this system a new low-cost system is proposed where both the light sources and the necessary illuminance sensors are wired, it is a scheme which is very much cost effective even for rooms of size not exceeding $300m^2$. Wireless sensors for this purpose may be considered at a later stage.

For the purpose of concept–proving we have chosen a laboratory space (length 6.2m *breadth 4.1m) with two windows on the northern side. The space will have six dimmable LED luminaires, four wall mounted and two ceiling mounted sensors that measure the work plane illuminance in an indirect way. Additionally, one of the walls will have an “Artificial Daylight (AD)”.

But here we have done the experiment using one luminaire and one wall mounted sensor with one window. Window blinds are used in this system. These are effective at reducing summer heat gain and reduction of glare, while providing good daylight and energy efficient system.

An Artificial Daylight will consist of a roof-mounted solar panel, a microcontroller- (MC) based LED driver and LED panel. The system will not have any battery storage. The MC unit will employ a maximum power point tracking (MPPT) algorithm so that maximum power available from the solar panel can be used for

lighting. It is foreseen that this concept can be utilized in spaces where a direct entrance of daylight through windows is not available.

Because it is modular, the suggested system can be extended to cover enormous buildings. The appropriate management of artificial light and the utilization of daylight can result in the desired level of illumination. It is the controller's job to figure out how to get the necessary amount of light while using the least amount of energy.

I. Main System Components

The system is composed of a one wall mounted indirect illuminance sensor; internal artificial light source i.e. one dimmable LED luminaries, a microcomputer controlled illuminance controller (MIC), and the main control computer system (MCC) with human machine interface. The communication between MIC and MCC via a standard USB interface. The illuminance sensor uses Light Dependent Resistors (LDRs) to measure daylight illumination and the room's brightness. The LDRs should be positioned in the luminance meter so that it captures light from the job surface while avoiding direct light from light sources.

II. System Operation

A simplified block diagram of the proposed system is shown below in Fig. 4

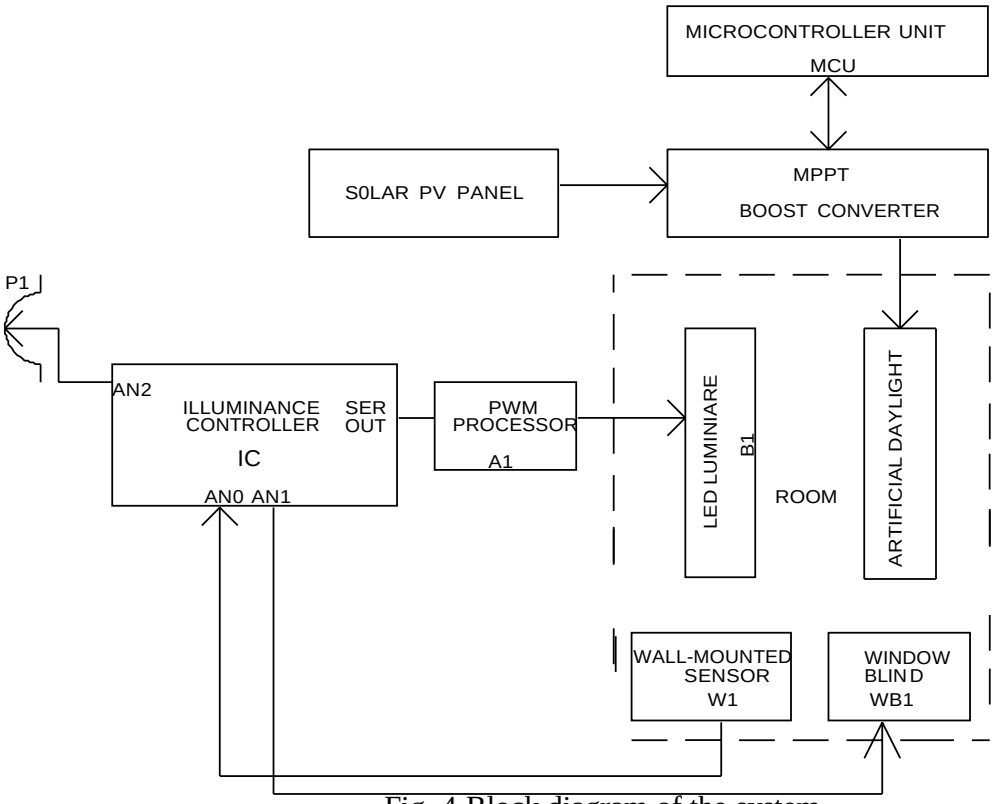

Fig. 4 Block diagram of the system

Legends:

PI : Illuminance level setting POT
W1: Wall-mounted sensor
WB1: Window Blind
A1: Serial-in, PWM-out processor
B1: PWM-dimmable LED luminaire
AN0……AN2 – Analog to Digital Converter (ADC) Channels
Illuminance Controller (IC)
Micontroller Unit (MCU)
MPPT Boost Converter
Artificial Daylight

All of the incoming environmental variables, such as the amount of light coming from the daylight outside the room, the amount of light coming from the lamp inside the room, and ultimately the user input, are collected by the controller and indirect illuminance sensor. The controller is in charge of analysing all inputs and coming up with the best way to light the space while using the least amount of energy.

The IC handles the data from the luminance meter and sets the light output of the LED luminaries, which are PWM-dimmable.

The sensor and luminaire are working in our laboratory is shown in the below Fig. 4.1

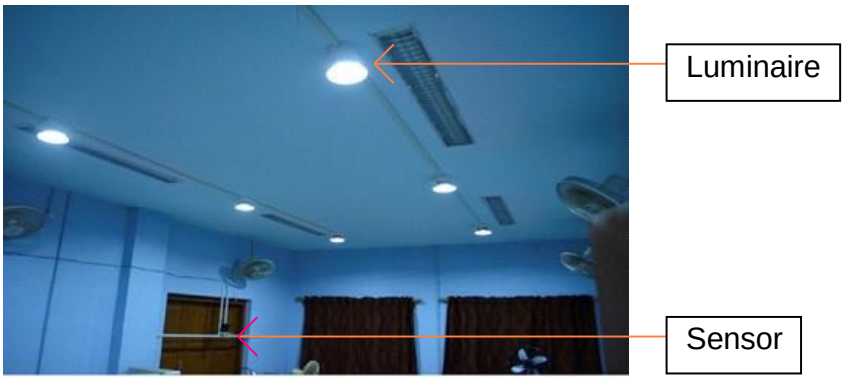

Fig. 4.1 The laboratory showing sensor and luminaire

(a) (b)

Fig. 4.2 (a**)** A luminaire in on state, (b) A luminaire in off state

4.1 Development of indirect illuminance sensors

4.1.1 General Background

When measuring frequently occurring process variables like temperature, pressure, flow, level, etc., two-wire sensors have become increasingly popular [17–20]. Their simplicity of installation, low cost of wiring, and lack of an additional power supply are the main factors contributing to their appeal. When developing a daylight-harvesting lighting scheme, a highly energy-efficient lighting system that combines artificial daylight with dimmable light emitting diode (LED) luminaires—it became apparent that a two-wire sensor was required for measuring illuminance [21–25], [26–27]. It was vital to build a sensor with a good performance/cost ratio because commercially available sensors for the purpose were either difficult to find or expensive. It may be necessary to use a lot of sensors (usually 1 to 4 per thousand m2) in order to maintain a uniformity of illumination. Because of this, the price of the sensor and the wire are crucial design considerations.

4.2.2 LDR as an Illuminance Sensor

Initially, we focused on developing an inexpensive indirect illuminance measurement system for daylight harvesting applications, with a silicon PIN photodiode (SIPD) serving as the main sensor element. This bias resulted from the evident fact that the short-circuit photo current was very linear as a function of the incident illuminance [28]. Nevertheless, as the sensor was being developed, a number of drawbacks became clear. First, a bipolar power supply with two supply wires (separate from ground) was needed for the amplifier in order to amplify the photocurrent to a practical current or voltage level. Using an on-board positive-to-negative voltage converter was the alternative strategy, which increased supply current requirements, costs, and complexity. If the supply current was greater than 4 mA, an industry-standard, 2-wire, 4–20 mA signal output could not be produced. This implied that despite all of the drawbacks of a voltage-type sensor, one must continue to be content with an output of 0–10V or 0–5V [29]. Four cables, or a minimum of three, would have been needed to link such a sensor to a distant instrument or controller.

The second reason that prevented a SIPD from being very useful for our purposes was a significant discrepancy between its spectral response and the human eye's. Figure 4.3 displays the relative spectral response characteristic of a typical SIPD. The wavelength range that the average human eye responds to is 360 nm to 720 nm, with a peak reaction occurring at 555 nm. Between 425 and 675 nm is where the 10% of the peak reaction happens. The 10% peak response of a SIPD, as illustrated in Fig. 4.3, reaches far into the infrared spectrum, up to roughly 1080 nm, making it highly sensitive for wavelengths beyond the visible range. A SIPD produces a higher output for an infrared light source (such as a daylight or incandescent lamp) when used in conjunction with an appropriate infrared-stop optical filter than for an infrared light source (such as a white LED or fluorescent lamp), even though both produce the same amount of visible light. The research in this area was discontinued because the necessary infrared-cut filters were costly and difficult to get. It has been announced that TEMT6200FX01 [30] is a photodiode with an integrated optical filter that has a spectral response that almost matches that of the human eye. We decided not to use it in this study due to concerns about cost and availability.

At 555 nm, the human eye's highest spectral response for photopic vision occurs. Figure 4 displays the relative spectral responses (RSR) of a Si PIN photodiode and a CdS LDR. The spectral peak of the RSR of typical CdS LDRs [31–32] is located at 525 nm. Moreover, the RSR drops to just 0.04 at 800 nm, which is above the visual range. An RSR of 0.87 for a PIN diode sensor, on the other hand, is completely unacceptable.

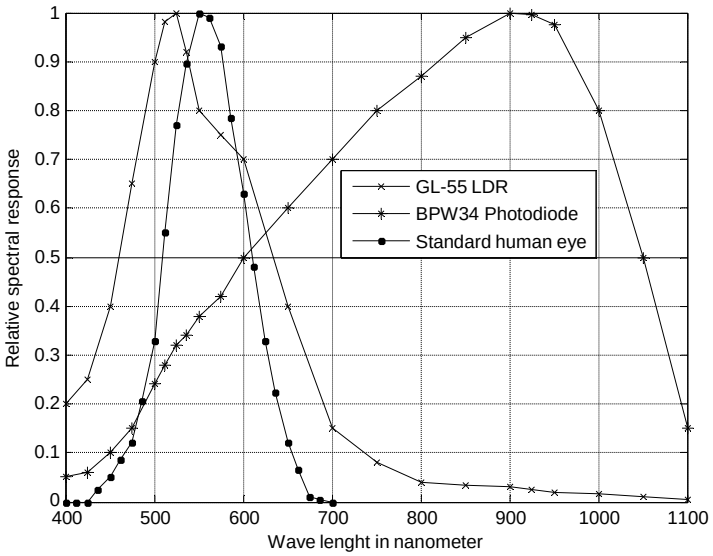

Fig. 4.3 Comparative spectrum response properties of an LDR, an ordinary human eye, and a conventional Si PIN BPW 34 photodiode.

The basic equation that represents the variation of the terminal resistance R (E) as a function of the incident illuminance E is given by [32]

$$R(E)\, E^{\gamma} = K \tag{4}$$

where K is a constant and γ is a constant called the LDR's illuminance index.
Considering two illuminances E_1 and E_2 the following can be obtained

$$R(E_1) / R(E_2) = (E_2 / E_1)^{\gamma} \tag{4.1}$$

Manufacturers specify the value of γ on the basis of two measurements at E_1 = 10 lx and E_2 = 100 lx. Thus we get

$$R(10) / R(100) = 10^{\gamma}$$

or, equivalently,

$$\gamma = \log \frac{R(10)}{R(100)} \qquad (4.2)$$

In section III an experimental method for evaluation of an approximate value of γ has been described.

4.2.3 Principle of Operation of the Sensor

4.2.3.1 Block Diagram Description

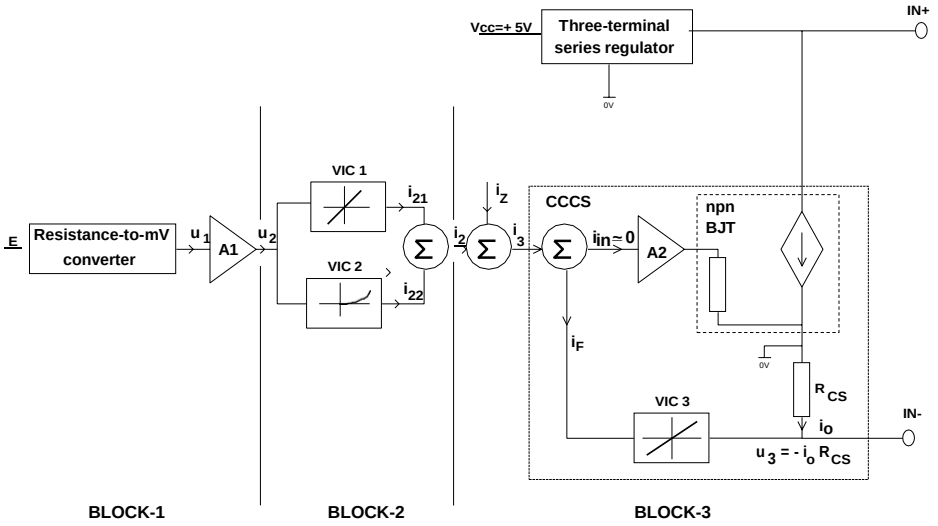

Fig. 4.4 Simplified block diagram of the sensor

Fig. 4.4 illustrates the cascade combination of three blocks, which helps explain the concept of operation. The incident illuminance E is converted by the first block into a low level voltage u_1, which has a full scale value of 90 mV on average. Using an amplifier A1, this voltage is increased to a greater level u_2. Approximately 1V is the normal full scale value of u_2. Additionally, a fixed offset is provided to the output to enhance the transmitter's linearity for low values of E.

Using two 2-terminal components designated as VIC1 and VIC2, the second block produces two currents, i_{21} and i_{22}. In reality, VIC1 is a variable linear resistor. As mentioned in Section II-B, VIC2, on the other hand, is a non-linear resistor. The VICs are selected so that the linear relationship between the illuminance E and the sum i_2 of the two component currents, i_{21} and i_{22}, is achieved.

The current i_3 is generated in the third block by adding the values of i_2 and adjustable current iz. After that, the current i_3 is sent to a Current Controlled Current Sink (CCCS), amplifying the current i_3 that is pulled between the transmitter terminals IN+ and IN-. An op-amp and a medium-power NPN bipolar junction transistor (BJT) are used in this block. This section concludes with a thorough explanation.

An expression for the output current i_o may be considered now. Clearly i_o is given by

$$i_o = G_i (i_2 + i_z) \quad (4.3)$$

where G_i is the gain of the CCCS.

Since i_2 is proportional to E, equation (4.3) is modified to

$$i_o = K_1 E + K_2 \quad (4.4)$$

where K_1 is a constant and $K_2 = G_i i_z$ is also a constant. For an ideal transmitter K_2 caters for the "live-zero" component of the output current which is commonly 4 mA.

4.3.3.2 Realization of the Circuit for the Functional Blocks

Fig. 4.5 displays the circuit diagram for the first block. Through the variable resistor R_1, the photocurrent of the LDR, which is dependent upon the incident illuminance E, flows and generates the amplifier's input voltage, u_1 [33]. When the LDR is at its full scale value of E, the resistor R_1 should have a value that is tiny in relation to its resistance. At full scale, the value of u1 is maintained within 90 mV for a supply voltage of Vcc = 5V. By doing this, the terminal voltage across the LDR is guaranteed to remain almost constant.

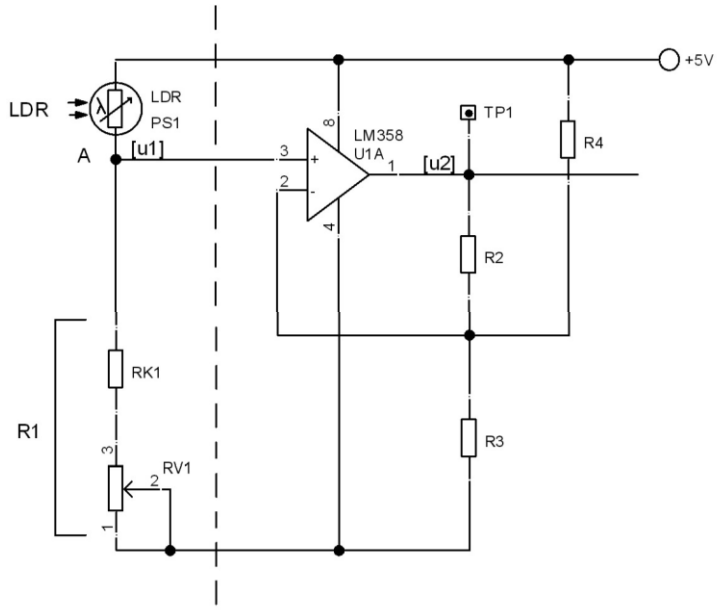

Fig. 4.5 Illuminance to voltage converter and linear amplifier

In [33] and [34], the amplifier is designed to operate on half of a standard LM358 operational amplifier in a non-inverting arrangement. When resistor R_4 is not present, the amplifier's gain, $Gv = u_2 / u_1$, is determined by

$$G_v = 1 + R_2 / R_3 \tag{4.5}$$

However, with R_4 in circuit the expression for u_2 is modified to

$$u_2 = (1 + R_2 / R_3)\, u_1 - (R_2/R_4)\, V_{cc}$$

The above expression reduces to

$$u_2 = G_v\, u_1 + u_{20} \tag{4.6}$$

where $u_{20} = -(R_2/R_4)\, V_{cc}$

To obtain a Gv of 11, we employed values of R_2 and R_3 in our investigation that were 10 K and 1 K, respectively. For all transmitters, a fixed output offset of -5mV was obtained with a fixed value of R4 equal to 1MΩ. The variable portion of R_1, RV1, was changed so that the output value, u_2, became 440mV at 40% of E_{FS}, or the full scale value of E.

As a function of E, Fig. 4.6 displays the fluctuation of u_2 for a typical LDR with $\gamma = 0.81$ and R (100) = 7.1 KΩ. Here, the nonlinear nature of the function can be seen. At 40% of span, the highest variation of roughly 72 mV occurs. On the E-u_2 graph, the slope represents a monotone decreasing function of E. The latter finding is true regardless of R(100) and γ values.

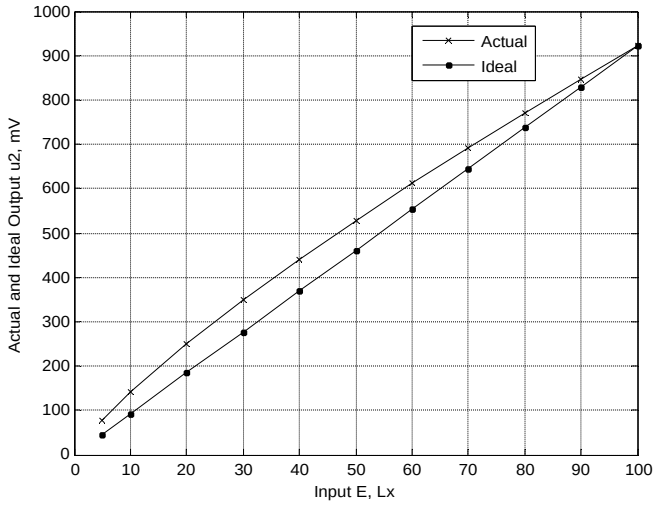

Fig. 4.6 Amplifier 1 output as a function of incident illuminance E.

Fig. 4.7 displays the second block's circuit realization. Because of factors outlined in the following section, the ground terminal depicted on the right side of this diagram achieves a potential relatively near to ground. Consequently, the current in the upper branch i_{21} is provided by

$$i_{21} = u_2 / R_5 \qquad (4.7)$$

where R_5 is a variable resistance made up of a series combination of RV5 and RK5 series resistances. RV5 can therefore be used to change the value of i_{21} that corresponds to any u_2. By virtue of Eqn. (4.7), a plot of i_{21} as a function of E has the same form as that in Fig. 4.6. Since $\frac{du2}{dE}$ is a monotone decreasing function of E and $i_{21} = u_2/R_5$, the same nature is found in the i_{21}-E function. A complementary non-linearity, whose slope is monotone increasing in nature, is produced by the voltage to current converter VIC2. The latter complementary function should have the property that, over the working range, the total i_2 of the component currents i_{21} and i_{22} becomes a linear function of E.

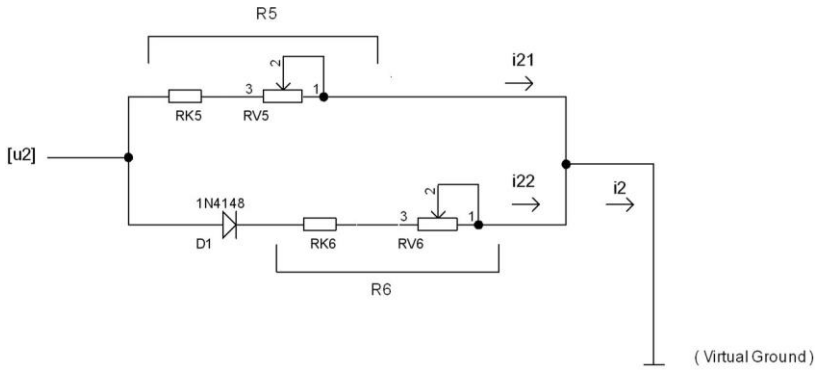

Fig. 4.7 Amplifier output to linear and non-linear current converter.

Assuming D_1 to be an ideal diode with a fixed threshold voltage V_F and a negligible dynamic resistance, i_{22} is given by

$$i_{22} = 0 \qquad \text{for } u_2 < V_F$$

$$i_{22} = (u_2 - V_F) / R_6 \qquad \text{for } u2 \geq V_F \qquad (4.8)$$

where R_6 consists of a fixed part of RK6 and a variable part of RV6 in series.

Plotting the u_2-i_{22} features provided by equation (4.9) is simple. When the voltage hits V_F, it will have a zero slope; at higher voltages, it will have a slope of $1/R_6$. When an actual small-signal diode, such as 1N4148, is utilized, no such sudden shift in slope is seen. Fig. 4.8 displays the u_2-i_{22} graphs for three distinct values of R6, namely 8.2 KΩ, 10KΩ, and 12 KΩ, in series with the 1N4148. The current i_{22} is found to decrease with an increase in R_6 for a fixed u_2, and the graph's slope grows monotonically with an increase in R_6 for a fixed u_2.

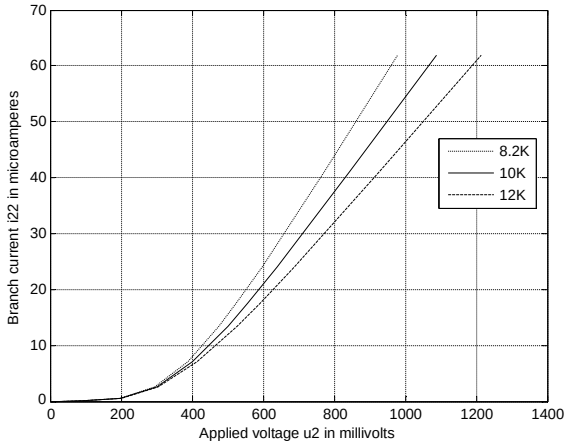

Fig. 4.8 i_{22} as function of u_2 for various values of R6.

We now consider the third block's circuit realization. Fig. 4.9 displays the output stage of the sensor, which functions as a current-controlled current sink [35]. The output terminals I+ and I- are connected to the positive side of an 8-24V loop supply, while the latter is connected to the ground side of the same supply through the use of a current sensing resistor Rcs, which is not depicted in the image. The sensor's current output is measured using the drop across Rcs. Thin lines in the same picture indicate the output current Io's route. The flow of Io causes a voltage u_3 to be produced across R_{14}.

$$u_3 = -i_o R_{14} \tag{4.9}$$

This consequently produces a current i_F, in the shown direction, given by

$$i_F = u_3 / R_{13} \tag{4.10}$$

Combination of Eqns. (4.9) and (4.10) yields

$$I_O = i_F G_I \tag{4.11}$$

where G_I is the current gain factor given by

$$G_I = R_{13} / R_{14} \tag{4.12}$$

The required expression of the output current as a function of the currents i_2 and i_Z can be otained by considering the Kirchoff's current equation at node B which is

$$I_2 + i_Z = i_F,$$

since the input current I_{in} at the non-inverting inut of the opamp U1 can be neglected in comparison to the other terms. Substitution of i_F from eqn (13) and the fact that

$$i_Z = V_{cc} / R_7 \tag{4.13}$$

therefore, yields that

$$i_O = G_I (i_2 + V_{cc} / R_7) \tag{4.14}$$

According to Equation (16), at zero illuminance (E = 0), the output current assumes a value of Vcc / R_7 and can be changed to its nominal value of 4 mA by adjusting RV7, the variable component of R_7. This is because both i_{21} and i_{22} have zero values. This will constitute a step in the sensor's calibration process, as will be seen later.

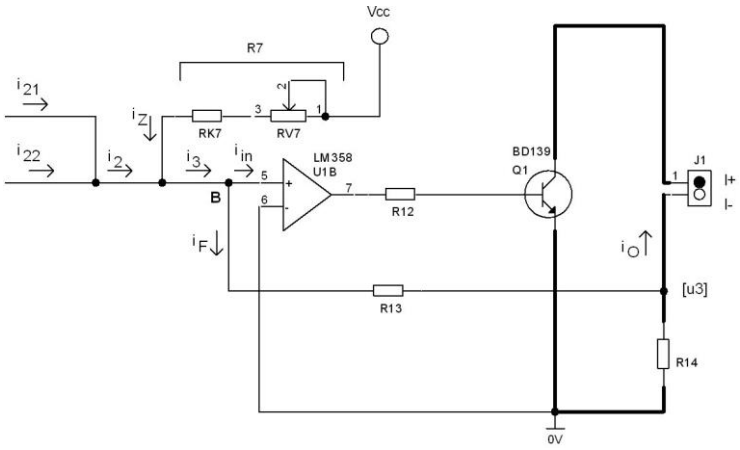

Fig. 4.9 Current summer and output current converter.

The laboratory developed wall mounted sensor is given below in Fig. 4.10

Fig. 4.10 Photograph of the typical wall mounted sensor

4.1.3 APPROXIMATE DETERMINATION OF γ AND SELECTION OF A SUITABLE LDR

Under the condition that the voltage u_1 is very small compared to Vcc. The values of u_1 at 10 lx and 100 lx are given by

$$u_1(10) \sim= \frac{Vcc}{R(10)} R1 \tag{4.15}$$

$$u_1(100) \sim= \frac{Vcc}{R(100)} R1 \tag{4.16}$$

where the symbol '~=' indicates 'approximately equal to'.

Division of equation (4.16) by equation (4.15) yields

$$u_1(100) / u_1(10) \sim= R(10) / R(100) \tag{4.17}$$

In the absence of the output offset voltage u_{20}, which can be ensured by omitting R_4 in Fig. 4.5, the left hand side of equation (4.17) can be replaced by $u_2(100) / u_2(10)$ since u_1 and u_2 are related by a constant gain factor Gv. Thus,

$$u_2(100) / u_2(10) \sim= R(10) / R(100) \tag{4.18}$$

A combination of equation (4.18) with equation (4.2) therefore produces

$$\gamma \sim= \log [u_2(100) / u_2(10)] \tag{4.19}$$

We can determine approximate γ in a straightforward manner using equation (4.19). Based on our experience, the resulting sensor can provide a linearity of better than 1% if the estimated value of γ is within the range of (0.7, 0.85). Therefore, an LDR that had a measured γ outside of the range was disqualified.

4.1.4 CALIBRATION OF THE SENSOR

To calibrate the sensor head, it was placed close to a calibrated luxmeter contained in a light-tight cage. A white LED light source was positioned above the sensor, and the LED current values were selected to enable the creation of 40 lx and 100 lx illuminances by turning on two switches that had the correct markings. The sensor experiences zero illumination when both switches are turned off. A milliampere is used to link the sensor's IN+ and IN-terminals to a 12-V dc power source. The sensor is then calibrated by carrying out the subsequent actions.

1. Establish a 0 lx condition. Raise the value of RV7 Fig.(4.9) to iO = 4mA.

2. Maintain RV6 at its highest setting.

3. Set E to 100 lx and modify RV5 Fig.(4.7) so that iO reaches 18 mA, or 90% of its full scale value.

4. Set iO to (4+0.4*16), or 10.4 mA, and modify RV6 Fig. (4.7) with E = 40 lx.

5. Set iO to 20 mA by adjusting RV5 Fig.(4.7) and setting E = 100 lx.

Until the sensor is calibrated at both 40 lx and 100 lx, repeat steps (4) and (5).

The next section describes the sensor's performance across the full 0–100 lx range.

4.1.5 Hardware Variants of the Sensor

Two distinct hardware versions of the sensor were constructed using the LDR sensor and the related circuit. The first one mounts to the wall, while the second is designed to be put to the ceiling. Fig. 4.8 displays a picture of the wall-mounted variant. The sensor head is positioned below the 25 mm diameter by 30 mm long cylinder that is displayed. The cylinder and the horizontal, matte-white platform form a 45° angle. The light incident on the sensor is produced by the incident light on the platform, which is the outcome of various light sources in a room. The output variable from many sensors can be integrated in a standard lighting control system to calculate the illuminances at multiple places of interest in the room.

A more straightforward version of the sensor is designed to be mounted on the ceiling. A cylinder measuring 20 mm in diameter by 20 mm in length, with its open end toward the ground, is behind the LDR. A conical zone with a total viewing angle of roughly 53° is the outcome. The illumination of the work plane within the viewing zone determines the sensor's output.

4.1.6 Applications

The sensor covered in this work can be applied in situations where indirect placement (on a wall or ceiling), two-wire connectivity, and low cost are the main requirements[36]. Additionally, the system's bill-of-materials cost is extremely low when compared to commercially available sensors because self-low cost components have been used. The last requirement comes from the fact that in most situations, the sensor required cannot be placed directly on the work plane.

This kind of sensor is employed in our study in an integrated feedback lighting system that combines artificial controllable LED lights with natural daylight. The daylight harvesting control approach results in a significant reduction of electrical energy consumption and consistent illumination at predetermined points-of-control (POC) on the work plane [37][38]. The current design includes four wall-mounted sensors and six ceiling-mounted LED luminaires in a 6.2 m × 4.1 m room with windows on one side. The illuminances resulting from the combined effects of artificial light and natural sunshine are to be maintained at set-point levels at six POCs. At the POCs, the four sensors' available illuminance data are transformed into the six illuminances using an appropriate matrix transformation.

4.2 Development and study of LED driver

Light-emitting diodes (LEDs) are very widely used for general indoor lighting applications in offices, industries and homes. Due to their compact size, high efficiency, extended lifespan, and lack of mercury in their manufacturing, LEDs have a number of advantages over conventional lighting sources [39]–[40]. The popularity of LEDs has increased in various applications due to significant improvements in power capacity and cost reduction [41]–[42]. As a result, the need for an appropriate driver circuit has grown proportionately [43]–[48]. One factor to consider while constructing LED drivers is energy economy. Driver solutions should also have dimming capabilities for both interior and exterior lighting since it has become into a crucial and essential feature. Since a luminaire's energy consumption is intended to be decreased by dimming, high energy efficiency is preferable at low dimming levels to further boost these energy savings. A common way to adjust an LED's brightness level is by modifying the forward current of the LED by amplitude modulation or pulse width modulation (PWM) control [49].

Self-oscillating flyback converters, also known as ringing choke converters (RCCs), are a reliable, low-component count circuit that have been extensively utilized in low-power offline applications [50]. They are one of the most widely used cost-effective LED drivers to date. The circuit's overall cost is typically lower than that of a traditional PWM flyback converter that uses an integrated circuit that is readily available on the market because the control of the device can be implemented with a relatively small number of discrete components without sacrificing performance.

In this study an offline driver has been developed with all the features described above additionally, since off the self- low cost components have been used, the bill-of-materials cost of the system is very low.

4.2.1 Configuration of the circuit

The considerable benefit of not requiring secondary inductors makes the flyback converter topology a popular choice for drivers of low voltage (less than 150W) LEDs. Fig. 4.11 depicts the set-up of the suggested driver with an LED light made of many LEDs connected in series and P controller-based current control.

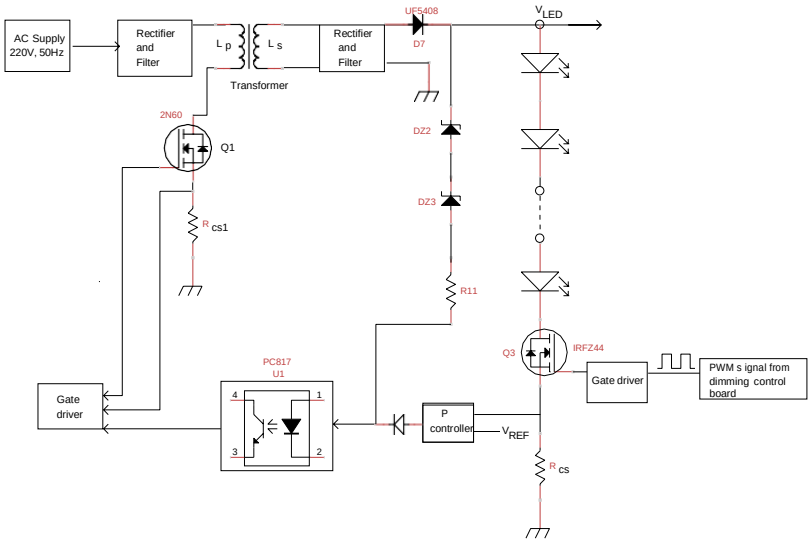

Fig. 4.11. Layout of a typical PWM-based LED driver with dimming capabilities and a DC-DC converter for P controller-based current control.

Through the use of a rectifier and filter, the input voltage source (220V, 50Hz AC supply) is converted to DC. Next, a high frequency switch and a transformer are used to convert the DC voltage to the required level of DC so that the LED can be driven. The switch duty ratio of a fast switching device Q_1, such as a MOSFET,

which is the ratio of ON time to switching time-period, is immediately dynamically regulated to maintain the required output voltage. The transformer is used for improved input-output voltage and current matching, voltage isolation, and current matching. The transformer's primary and secondary windings are made to be closely coupled and connected by essentially the same magnetic flux.
As a result, when switch Q_1 is turned ON, current can flow through the transformer's primary side (L_p), but the secondary winding (Ls) is blocked because of the inverted diode (D_7). Regenerative action causes Q_1 to abruptly shut off, energizing the transformer's secondary side (Ls). o measure the primary current Ip, utilize a low value resistance RCS1 that links the MOSFET source and ground terminals. When there is no feedback, the MOSFET Q_1's gate-source voltage drops when the peak value of the primary current Ip * RCS1 surpasses the NPN transistor Q_2's base-emitter threshold voltage. Based on the primary current, the gate driving circuit will quickly turn the MOSFET ON and OFF. The transformer's secondary coil is isolated from the primary coil by use of optocoupler U_1.

A LED bulb is driven by the desired level of dc voltage V_{LED} in such an arrangement. The P controller in this driver implements the current control mode. Thus, the lamp current can be regulated by varying the PWM signal, which is generated from Dimming Control Board (DCB). A semiconductor switch Q_3 is a N channel power MOSFET IRFZ44. In the GATE driver circuit a NPN transistor Q_4 (BC547) is used to provide the necessary GATE current to turn ON and turn OFF Q_3 which is shown in below Fig. 4.12.(b).

4.2.2 Circuit Function

The driver circuit's flyback converter can be used in boundary conduction mode (BCM), discontinuous conduction mode (DCM), or continuous-conduction mode (CCM). The proposed circuit is created to be used with BCM in order to reduce switching loss and effectively regulate the LED current using a P controller. Three steps can be identified in the power conversion process.

The fundamental idea behind BCM is that the controller functions exactly where CCM and DCM meet. In other words, the switch opens for a brief period of time before turning off and storing just enough change to restock the board. Once all of the energy has been converted to output, the switch will flip on once more.

The three operation phases' detailed circuits and current flows are depicted in Figures 4.12 and 4.13 The circuit of the right of A and B is used to achieve the control of the converter RCC so that both current control and voltage limiting control can be achieved is shown in Fig. 4.12. In a typical cycle of PWM for dimming, during turns ON of MOSFET Q_3 (IRFZ44), the current control loop will be activated to protect the MOSFET Q_1.

In Figure 4.12(b), the drain terminal of MOSFET Q_3 is high when the DCB signal is high because Q_3's GATE terminal is grounded through Q_4 (BC547). Conversely, when the DCB signal is low, Q_3's GATE terminal is high, meaning that LED luminaires will be ON during low DCB signal.

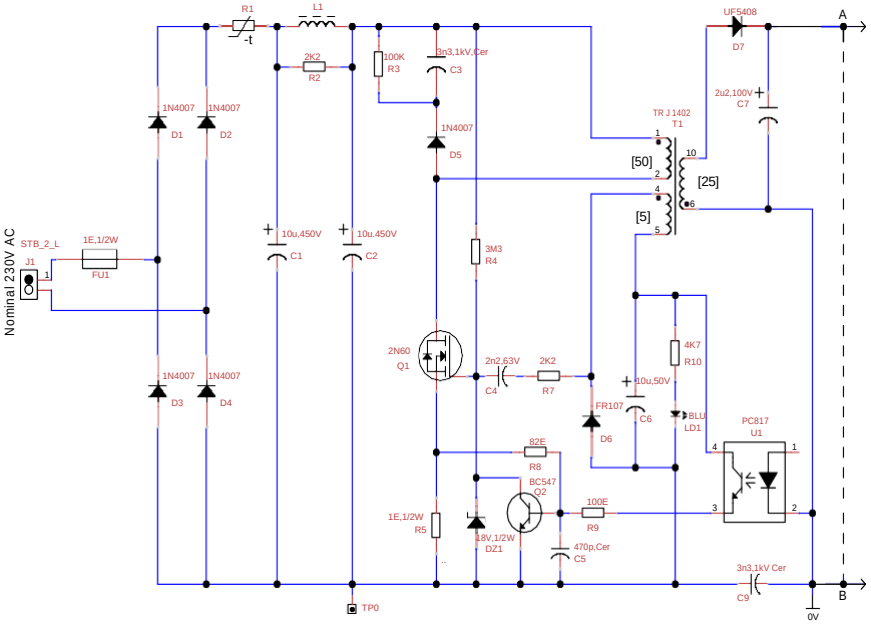

(a)

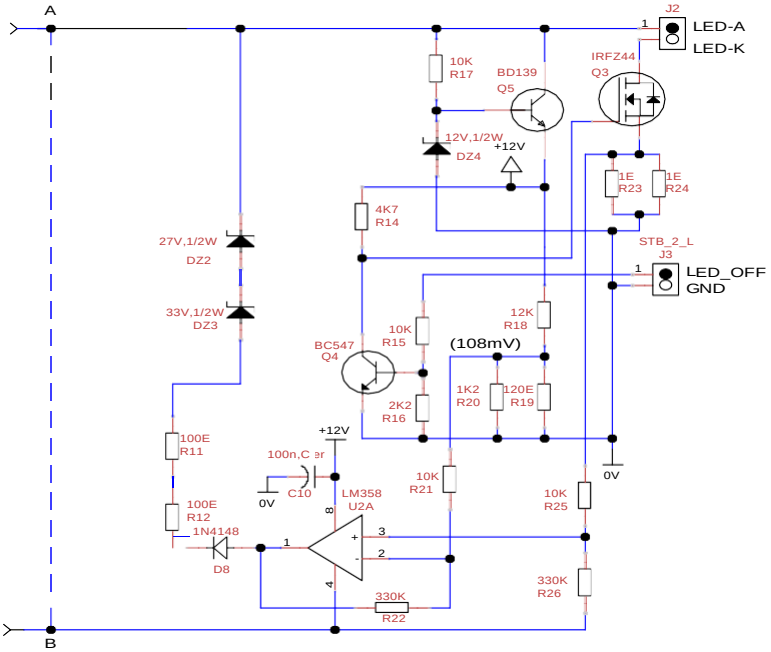

(b)

Fig. 4.12. Detailed circuit diagram of the proposed LED driver (a) Flyback converter part (b) P controller based current control

Detailed principle operation of this type of converter is given in [50]. For a simplified analysis a typical period of operation T can be broken up into three intervals. The hypothesized waveforms on significant components are shown in Fig. 4.13

A. Interval 1: 0 < t < t_1

Interval1begins when the MOSFET Q_1 is turned ON. The secondary winding and diode D_7 are linked in series at this point, and the induced voltage causes the diode to become reverse biased. The primary winding is prepared to carry current when the switch is closed, but the reverse biased diode prevents current from flowing through the secondary winding. As seen below, the primary current grows linearly as the input supply voltage is applied across the primary winding inductance.

$$E_{dc} = L_p * \frac{dip}{dt}$$

That is $$\frac{dip}{dt} = E_{dc} / L_p \qquad (4.20)$$

where E_{dc} is the input dc voltage, L_p is the primary winding's inductance, and ip is the current flowing through the primary winding at that moment. Since the right hand side of (1) is a constant the peak value of current IP at the end of the ON time t1 is determined from (4.20) by substituting $\frac{dip}{dt} = I_P / t_1$

$$I_P = E_{dc}\, t_1 / L_p \qquad (4.21)$$

At the end of the ON interval, W_P the energy stored in the magnetic field of the flyback transformer is

$$W_P = \tfrac{1}{2} L_p I_p^2 \qquad (4.22)$$

An alternative expression for W_P in terms of the ON time t_1 can be obtained by substituting (4.21) in (4.22) as

$$W_P = \tfrac{1}{2} E^2_{dc}\, t_1^2 / L_P \qquad (4.23)$$

Equation (4.22) indicates that the value of the peak energy stored can be controlled by exercising control over the peak primary current I_P. Additionally, since I_P appears in a squared form in (4.23) a 20% increase of I_P gives rise to a 44% increase in W_P.

Equation (4.23) also indicates that for a constant dc supply voltage W_P is proportional to square of the ON time.

Due to the previously stored charge in the output capacitor, the load connected to it continues to receive current even when the secondary winding is not conducting. During period 1, the secondary winding voltage is essentially constant and equal to

$$v_{sec} = E_{dc} * N_2 / N_1 \quad (4.24)$$

where N_1 and N_2 denote the number of turns in the primary and secondary windings respectively.

In this interval, diode D_7 is reversed biased and the transformer primary current i_D increases linearly as shown in Fig. 4.10 (a). This continues till time t_1 up to which Q_1 is ON. The peak value of the primary current I_{Dp} is given in terms of the supply DC voltage E, primary inductance L_p, and the duration t_1 as

$$I_{Dp} = E*t_1/L_p \ . \quad (4.25)$$

Assuming a negligible base current in Q_2 and applying KCL law at node A of Fig. 4.10 (a)

$$(V_{BE} – I_{Dp}R_5) / R_8 = i_2 \quad (4.26)$$

$$=> I_{Dp} = (V_{BE} – i_2R_8) / R_5 \quad (4.27)$$

For an optocoupler, the transistor output current i_2 is nearly proportional to the input infrared emitter diode current i_1 :

$$i_2 /i_1 = \alpha$$

where, α is the Current Transfer Ratio (CTR) of the optocoupler

substituting the above in equation (4.31) we get

$$I_{Dp} = (V_{BE} – i_1\alpha R_8) / R_5 \quad (4.28)$$

The stored energy has a peak value given by

$$W_p = E^2 t_1^2/(2L_p) \quad (4.29)$$

From (9) and (14) we get

$$V^2_oT / R_L\eta = ½ * (E^2 t_1^2/L_P)$$

$$V^2_o = ½ * (E^2 t_1^2/L_P)* (R_L\eta / T) \quad (4.30)$$

When the feedback is not applied, the peak value of the primary current Ip * RCS1 in this interval surpasses the base-emitter threshold voltage of an NPN transistor Q_2, which lowers the gate-source voltage of the MOSFET

Q_1. Regenerative action causes Q_1 to abruptly shut off, converting the primary stored energy—½ Lp Ip2—into the secondary. The value of Ip * RCS1 is altered in the presence of voltage or current feedback, modifying the necessary secondary voltage or current. The feedback signal or primary current will cause the MOSFET driving circuit to quickly turn ON and OFF the MOSFET Q_1.

B. Interval 2: $t_1 < t < t_2$

During this interval switch Q_1 is turned off after conducting some period. Then the secondary winding current abruptly rises from zero to $I_P * N_1 * N_2$ and changes the output capacitor. The output capacitor is large enough that no ripple occurs in its voltage.

Then the output power

$$P_O = V^2_o / R_L \quad (4.31)$$

Where R_L is secondary load resistance and V_o is secondary load voltage

Output energy over a cycle

$$W_s = (V^2_o / R_L) * T \quad (4.32)$$

Assuming an efficiency of η

$$W_p = W_s / \eta \quad (4.33)$$

From (4.22) and (4.31) we get

$$W_p = V^2_o T / R_L \eta \quad (4.34)$$

As Q_1 is switched off, the diode D_7 is forward-biased. At this mode stored energy of the primary coil is transferred to the secondary coil of the transformer. The lamp's power is then continued at DC-controlled voltage. The second interval is over when the secondary current reaches zero.

C. Interval 3: $t_2 < t < T$

When all of the energy from the magnetic field has been transferred to the output, the secondary winding's emf and current will have reached zero, and the diode D_7 in series with the winding will have ceased to function. However, the output capacitor keeps providing the load with constant voltage. During this stage, both Q_1 and D_7 are turned OFF. As explained later the value of the gate-source voltage of Q_1 starts to increase from a very low value to its threshold V_{TH} and to a higher subsequent value so that Q_1 rapidly goes to the ON state in a time very short compared to either interval 1 (0-t_1) or interval 2 ($t_1 – t_2$). It should be mentioned that when Q_1 is turned OFF, the output current charges the huge filter capacitor C_7.

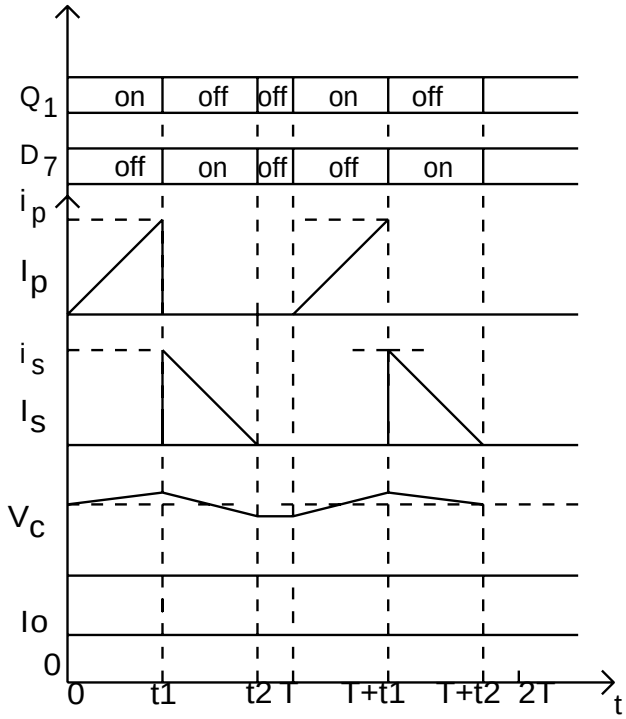

Fig. 4.13.Theoretical waveforms for the suggested LED driver

D. Current control mode with P

An LED's brightness is directly correlated with the current passing through it. When the load exceeds the maximum permitted current or the output terminal or LED shorts, the control loop controller will activate.

This article modifies the feedback control system by utilizing a P controller, which is necessary to carefully regulate the LED current. The reference voltage and driving current I_{LED} are compared using an operational amplifier (OP-AMP) LM358, which is utilized.

E. Mode of voltage regulation

The comparator will have a low output while it is in voltage control mode. D_8, an optocoupler diode, and two zener diodes, DZ2 and DZ3, respectively, control the LED terminal voltage. Under no circumstances may the output voltage at the LED terminal exceed the supply voltage of the LED.

4.2.3 Dimming Control

Both PWM (Pulse Width Modulation) and linear current adjustment can be used to dim LEDs. PWM uses the nominal LED current as the amplitude. The main difference between the two dimming approaches is that

the first one requires a linear adjustment of the value of the continuous current amplitude, whereas PWM techniques require an LED current in the shape of a rectangular wave with a variable duty cycle. The switch Q_3 is used to turn on and off the LED luminaire in accordance with the duty ratio as illustrated in Fig. 4.12 (b). The current that will be supplied by LED driver to LED lamp can be expressed by this equation

$$I = I_{LED} * T_{ON} / (T_{ON} + T_{OFF}) \quad (4.35)$$

The maximum permissible current through an LED is equal to its ILED, which may be computed using equation (4.35). The turn-on and turn-off times are, respectively, TON and TOFF. Since duty cycle may be adjusted between 0 and 100%, the LED's light output can likewise be adjusted between 0 and 100%.

The average current of an LED is roughly proportional to its brightness. PWM is employed in the suggested LED driver to manage dimming. Low-frequency PWM control can be used to dim an LED lamp to prevent color shift [51]–[53]. The PWM dimming frequency is generated from the dimming control board must be higher than 100 Hz to avoid flickering as described by [54] is shown in Fig. 4.11.

The dimming control board (DCB) consists of ATmega 8A microcontroller which is a low-power CMOS 8-bit microcontroller based on the AVR RISC architecture. The ATmega 8A provides the following features like, 8Kbyte of In-system programmable flash memory with read-write capability, PWM signal generator channel, 23 general purpose I/O lines, 32 general purpose working register, three flexible Timer/Counter with compare modes speed 0-4 MHz, 512 bytes of EEPROM etc [55]. PWM signal is generated by enabling Timer 2 of ATmega 8A. DIP switch in DCB board is used for switch setting to change the duty cycle of PWM signal.

The program for PWM generation is written in Atmel Studio 6.2 software (from Atmel corporation) [56] and the HEX file is loaded into the ATmega 8A microcontroller using USBASP programmer.

RegisterTCCR2 of Timer 2 of ATmega 8A is used for frequency selection. OCR2 register is used to set the duty cycle of the generated wave by comparing OCR2 and TCNT2 register value.

Frequency of the generated wave can be calculated by using equation (4.35)

$$F_{\text{generated wave}} = \frac{\text{Foscillation}}{256 * N} \quad (4.36)$$

N is the prescaler value that may be (1/8/64/256/1024), the value of the prescaler chosen 64, oscillator frequency is equal to 4 MHz. So, Fgenerated wave willbe 244.14 Hz.

Duty cycle of PWM signal can be varied by OCR2 register of ATmega 8A through DIP switch setting (00-0F). So the duty cycle of the generated wave can be calculated by the equation (17)

$$\text{Duty cycle (D)} = \frac{0CR2+}{256} \quad (4.37)$$

Where OCR2 = (Switch value * 15) – 1

From (4.36) and (4.37) we get

$$\text{Duty cycle (D)} = \frac{\text{Switch value} * 15}{256} \quad (4.38)$$

The pin connection of the dimming control board is shown in Fig. 4.14

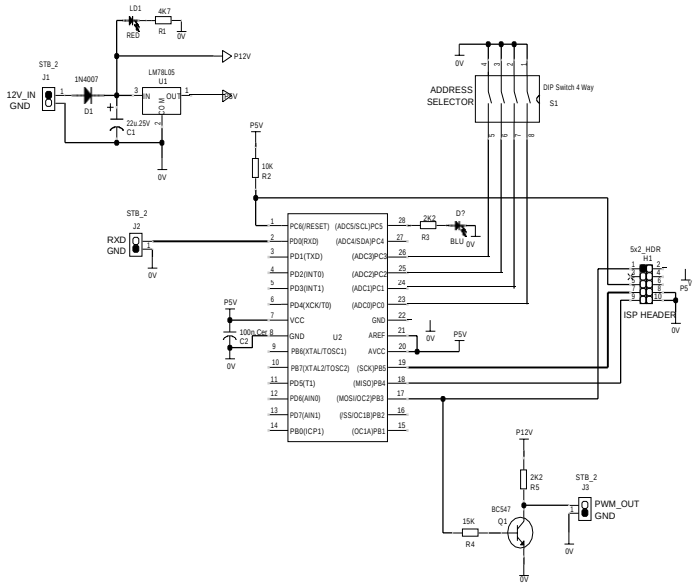

Fig. 4.14. Pin connection of Dimming Control Board

4.2.4 Experimental Prototype of the LED Driver

In Fig. 4.15. a laboratory prototype of the suggested LED driver is implemented and evaluated for an 18W LED luminaire supplied from an ac input voltage of 230V, at a line frequency of 50 Hz. [56]-[62]. Table 1 is a list of the circuit parameters. The primary side magnetizing inductance of the prototype LED driver significantly contributes to the power transfer process. The magnetizing inductance is adjusted to 370 μH. To obtain the proper size of magnetic components, the switching frequency is set at 147 KHz. To achieve a low voltage ripple, the output capacitance is set at 2.2 μF. The two-line, parallel LED strings with 18 LEDs each make up the LED module. 150 mA and 0.5W are the specifications for each LED. For PWM dimming, a BCM and a flyback converter are meant to operate at a frequency of 244 Hz By altering the PWM's duty ratio between 0.05 and 1, it is feasible to control the LED current from 0 mA to its maximum rated current of 320 mA. The LED bulb in this situation is powered by the rated current.

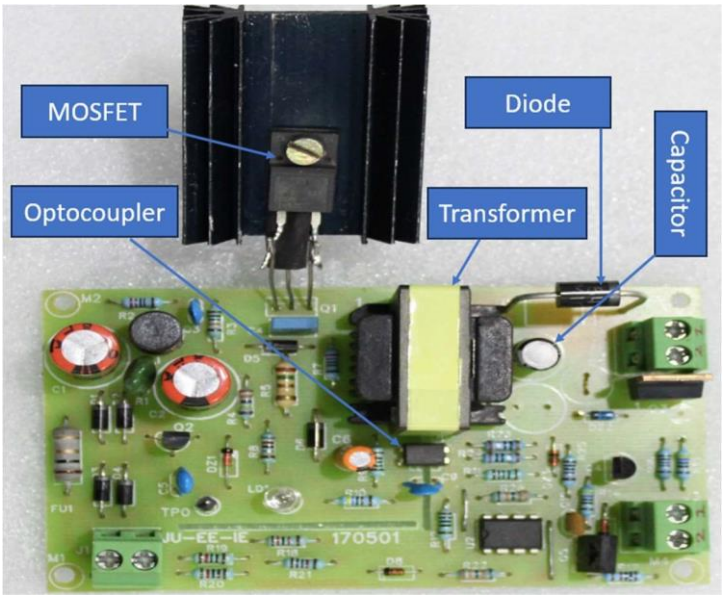

Fig. 4.15. Experimental prototype of the LED driver

TABLE 4. CIRCUIT PARAMETERS OF THE DRIVER CIRCUIT

Parameters	**Values**
Nominal input voltage, V_{in}	230V, 50Hz AC
Nominal output voltage, V_{out}t	60 V
Primary inductions, L_1	370µH
Output Capacitance	2.2µF
LED rated current, I_{LED}	320mA
Switching frequency at D=1, f	147 kHz
Duty ratio, D	0.1-1.0
PWM Dimming, f_{dim}	244Hz
Current sense resistor	0.5 Ω
LED type	5730 SMD LED,

The experimental system for the suggested driver is depicted in Fig. 4.16 in a photograph

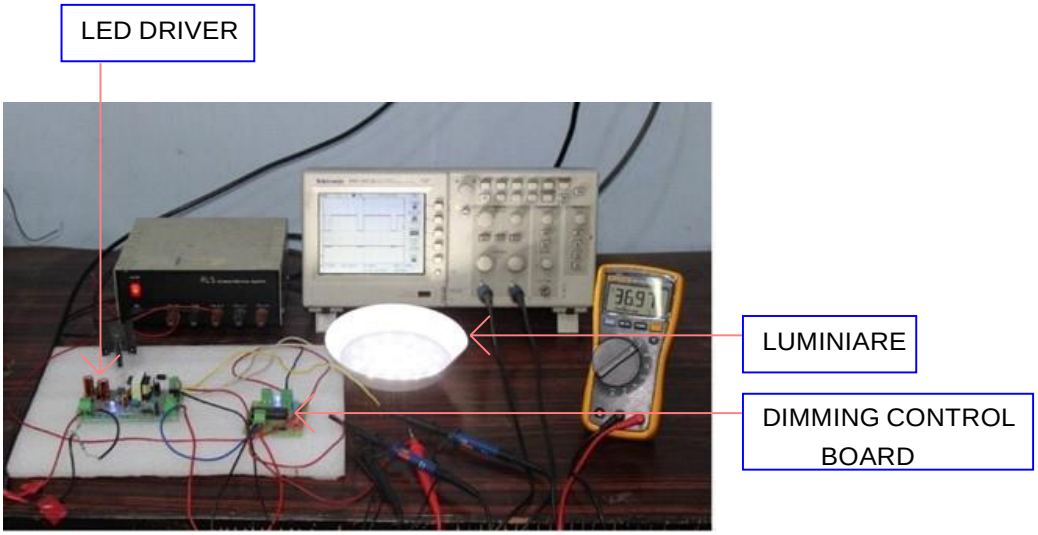

Fig. 4.16 The laboratory developed experimental set up of a luminaire with driver and dimming control board

4.3 Development of illuminance controller board

4.3.1 Introduction

On a single metal-oxide-semiconductor (MOS) integrated circuit (IC) chip, the microcontroller is a tiny CPU. A microcontroller has memory, programmable input/output peripherals, and one or more CPU cores. These are intended for use in embedded software.

Microcontrollers are utilized in automatic control devices, including power tools, office equipment, appliances, medical equipment, remote controls, car engines, and other embedded systems. Because it consumes less space and money for a product than a design that requires a separate CPU, memory, and input/output devices, it is extensively utilized. These days, mixed-signal microcontrollers are widespread. utilizing a digital device to integrate analog components which are ideal for the microcontroller that are required to operate the non-digital electronic system.

For reduced power consumption, certain microcontrollers can operate at frequencies as low as 4kHz and employ a four-bit word. They can continue to function as they wait for something to happen, like an interruption. These are ideally suited for long-lasting battery operation because their power consumption is measured in nanowatts.

These days, high-frequency microcontrollers with operating frequencies of 2-3GHz are also accessible. These chips are employed by automation systems and other multitasking systems.

Here, an ATMega32A microcontroller chip is being used. It is an 8-bit device with improved RISC architecture that is low powered and CMOS based. 32 KB of flash, 2 KB of SRAM, and 1 KB of EEPROM memory are spread across 40 pins. The device can process close to one million instructions per second by completing an instruction in a single clock cycle, which enables the system designer to balance processing speed and power consumption.

4.3.2 The Illuminance Controller (IC) Development Board

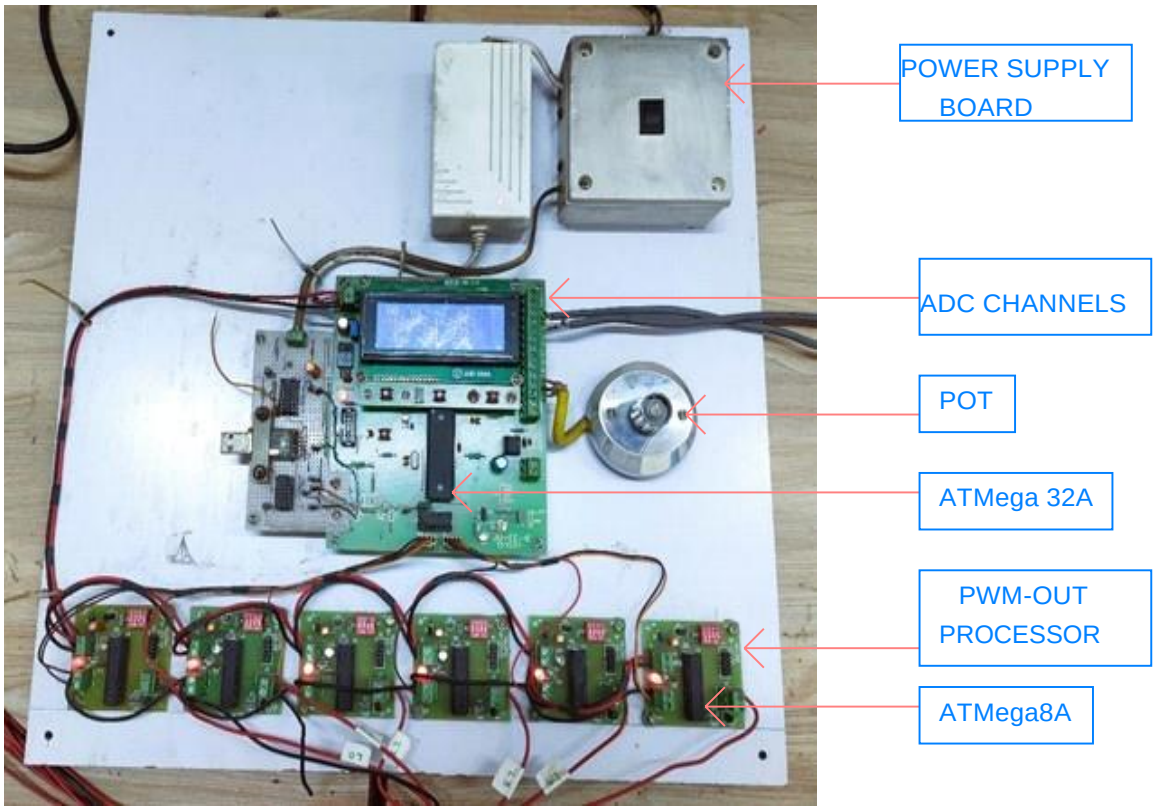

Fig. 4.17 Laboratory developed Illuminance Controller Board

The illuminance controller board which is shown in above Fig. 4.17, is developed by six PWM out-processor for six luminaires with dimmable drivers and several analog to digital converter (ADC) channels for six wall mounted sensors, two celling mounted sensors and two window blinds, according to our laboratory space. But we have done the experiment using one wall mounted, one PWM dimmable luminaire and one window blind.

4.4 DEVELOPMENT OF WINDOW BLINDS

We have developed the motorized window blinds in our laboratory which is known as Vertical blinds. The condition of blinds closing and opening have shown in Fig.4.18(a) and Fig.4.18(b).

Fig. 4.18 (a): Blinds at closing condition

Fig.4.18 (b) Blinds at opening condition

4.4.1 Hardware implementation of the window blinds

The main hardware components of the proposed system are power supply for microcontroller unit, Photo Detector, Servo motor, Liquid Crystal Display, amplifier circuit, controller circuit, and motor rotation controlling circuit. The block diagram of the closed loop system has been shown in Fig.4.19.

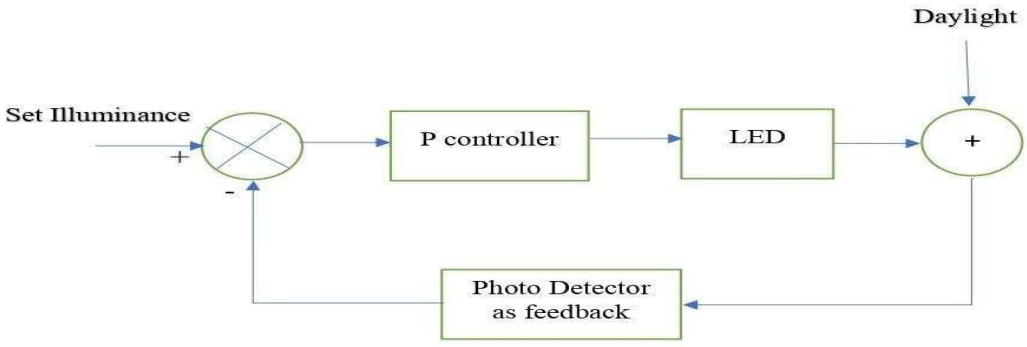

Fig.4.19 The block diagram of the system

4.4.1.1 The block diagram of the controller board

The block diagram of the controller circuit is shown in Fig.4.20.

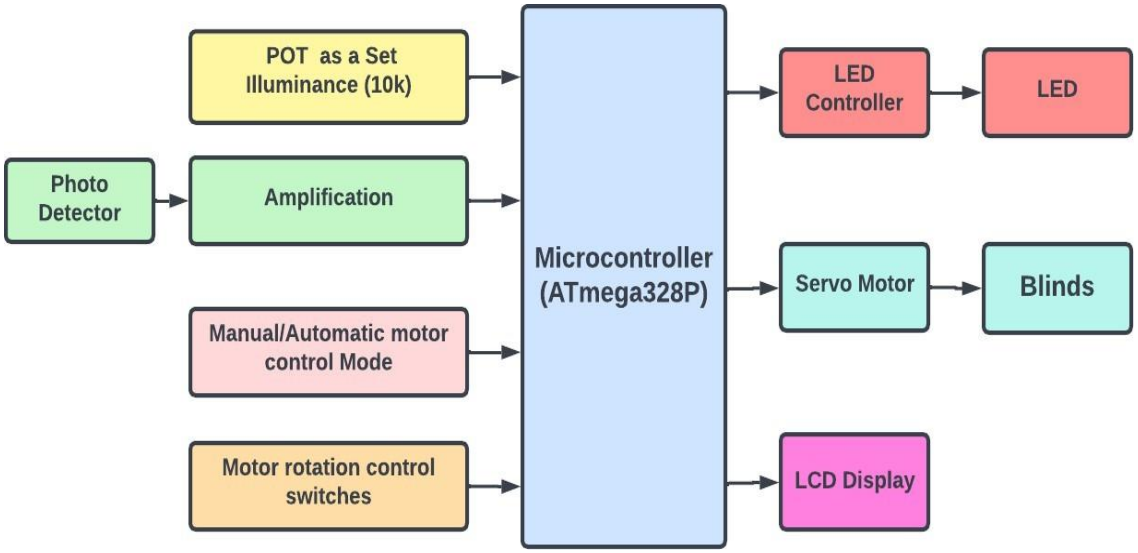

Fig.4.20 The block diagram of the controller circuit

A. Photo detectors and amplification of the signals

An amplifier circuit can be used to change the Analog value that the Photo Detector reads on the working surface. For the purpose of altering the signal, an operational amplifier, or Op-amp, is therefore required. The signal is amplified by means of the TL082 Op-amp. The TL082 is a monolithic integrated circuit that combines high voltage JFET and bipolar transistors in a well-matched dual operational amplifier design. It operates at high speed. Low input bias and offset current, low offset voltage temperature coefficient, and high slew rates are characteristics of this device. The photo detector's (PD) output is connected to the input of the Op-amp. The 8-bit microcontroller's pin 24 is linked to the signal that has been amplified. The Amplification circuit of this system is shown in Fig.4.21 and the amplifier board is given in Fig. 4.22

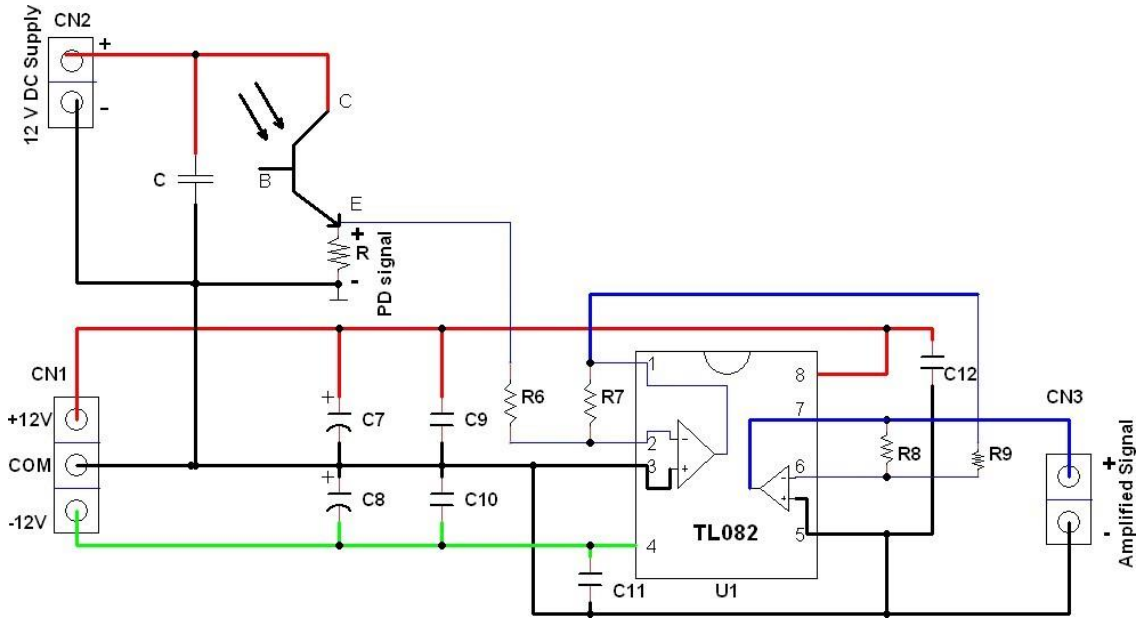

Fig.4.21 Amplification circuit diagram

C7 and C8 in this circuit serve as a 100 µF electrolytic capacitor. The values of the ceramic disc capacitors, C, C9, C10, C11, and C12, are 0.1 µF, in that order. R, R6, R7, R8, and R9 have the following values, in order: 5.6 kΩ 10 kΩ, 82 kΩ, 82 kΩ, and 10 kΩ. A 12 volt DC power supply is connected to channel 1 (CN1) in order to turn on the circuit. The control circuit is run by the amplified signal.

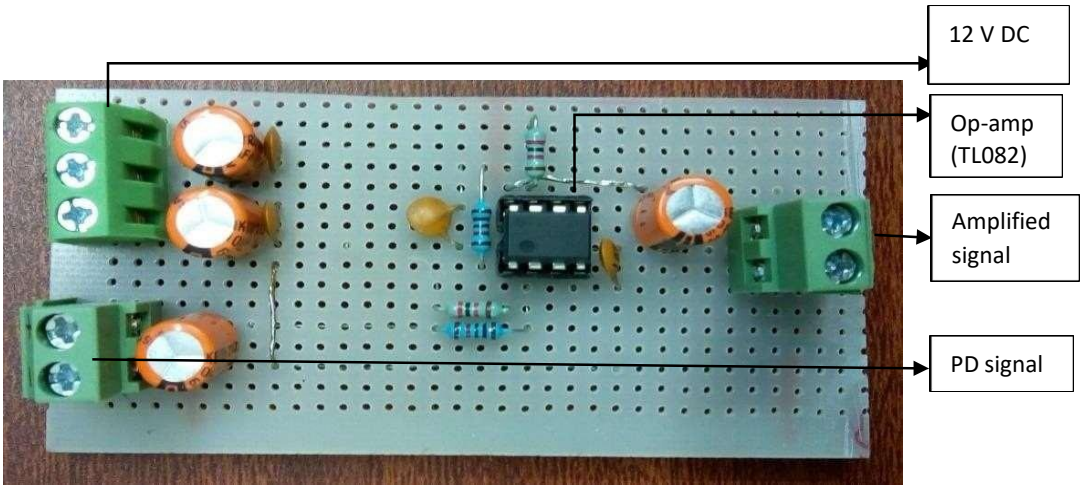

Fig.4.22 Amplifier board

The non-amplified signal is linked to a two-pin connector in the diagram above, and the signal has been altered by the Op-amp. The circuit's output has produced an amplified signal, which has been collected. A microcontroller digital pin will be used to generate a PWM signal from this signal.

B. LED controller circuit

A driver circuit is necessary for each LED light source. There are two main types of LED driver circuits: constant-voltage and constant-current. The LED driver serves as a protective buffer in addition to managing electrical current. An LED driver of the constant-voltage and constant-current kind is utilized in this experiment. The microcontroller's PWM pins provide a 5 V TTL control signal, which is insufficient to drive the MOSFET and cause it to function as an ON switch in the saturation area. The MOSFET driver IR2011PBF IC, which converts the TTL level signal to a 12 V power signal sufficient to operate the MOSFET in saturation area, has been utilized to achieve satisfactory conduction of the switching MOSFET. Fig. 4.23 displays the schematic diagram of the LED controller circuit. The switching MOSFET Q conducts when the PWM control signal pulse is HIGH and is driven to saturation, where it functions as an ON switch. As a result, the LED sources turn ON. LED sources are switched off when the switching MOSFET is open-circuited and stays in the cut-off zone, functioning as an OFF switch, when the pulse of the PWM control signal is LOW. The PWM signal's duty cycle affects the average illuminance.

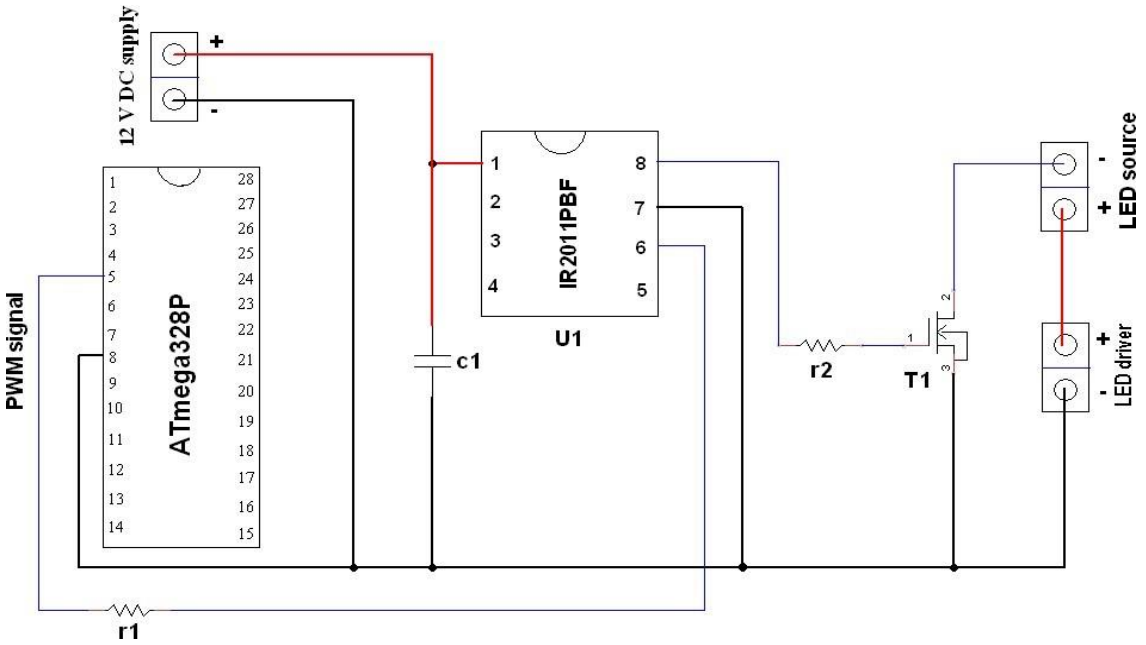

Fig.4.23 LED controller circuit

The capacitance c1 in this circuit has a value of 0.1µF, and the values of r1 and r2 are 10 Ω. The MOSFET's gate, drain, and source terminals are indicated by the numbers 1, 2, and 3, respectively. The pin 6 of the IC U1 is connected to the microcontroller's digital PWM pin.

4.4.1.2 The microcontroller unit and LCD display

The user's requirements have the ability to modify the illuminance value. A POT serves as a potentiometer (10k) in this system, and it can be made to have a variable resistance by simply turning the knob on top of its head. It features three terminals, with pin 22 of the 8-bit microcontroller attached to the middle of the terminals. A power source and ground are connected to a terminal that has red and black wires connected to it. The Set Illuminance (Es) has been adjusted from 0 lx to 300 lx using the potentiometer.

Liquid crystal displays, or LCDs for short, use liquid crystals' light-modulating properties. Flat panel, video, and electrical visible displays are among the options offered. Fig. 4.24 displays the Set Illuminance value, Measured Illuminance value, error, etc.

Fig.4.24 A diagram of LCD display

The circuit diagram of POT and LCD with the microcontroller has shown in Fig.4.25.

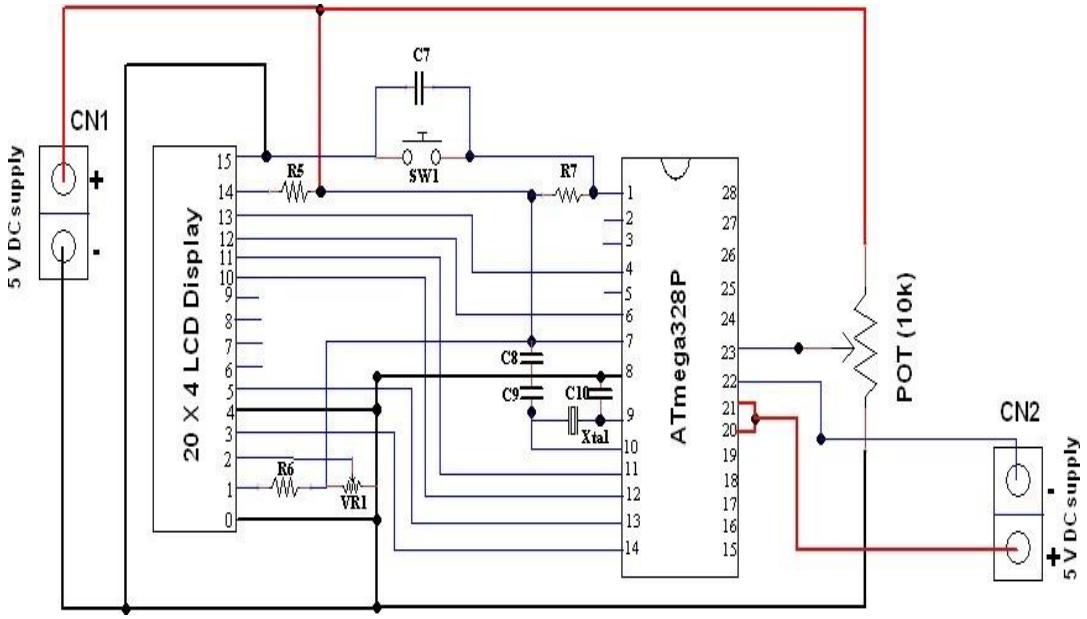

Fig.4.25 The circuit diagram of POT and LCD with microcontroller

4.4.1.3 Operation of manual or automatic control of blinds using switches

The push button switch is a type of commonly used control switch appliance that is often used to turn on and off the control circuit. It is used to manually provide control signals to electromagnetic starters, contactors, relays, and other components in electrical automatic control circuits. Basic functions including start, stop, rotation in both directions, speed change, and interlock can all be performed with a push button switch. In this experiment, the servo motor's rotation has been controlled by three push buttons: STOP, Clockwise, and Counterclockwise. Fig. 4.26 displays the push button switch's connecting diagram.

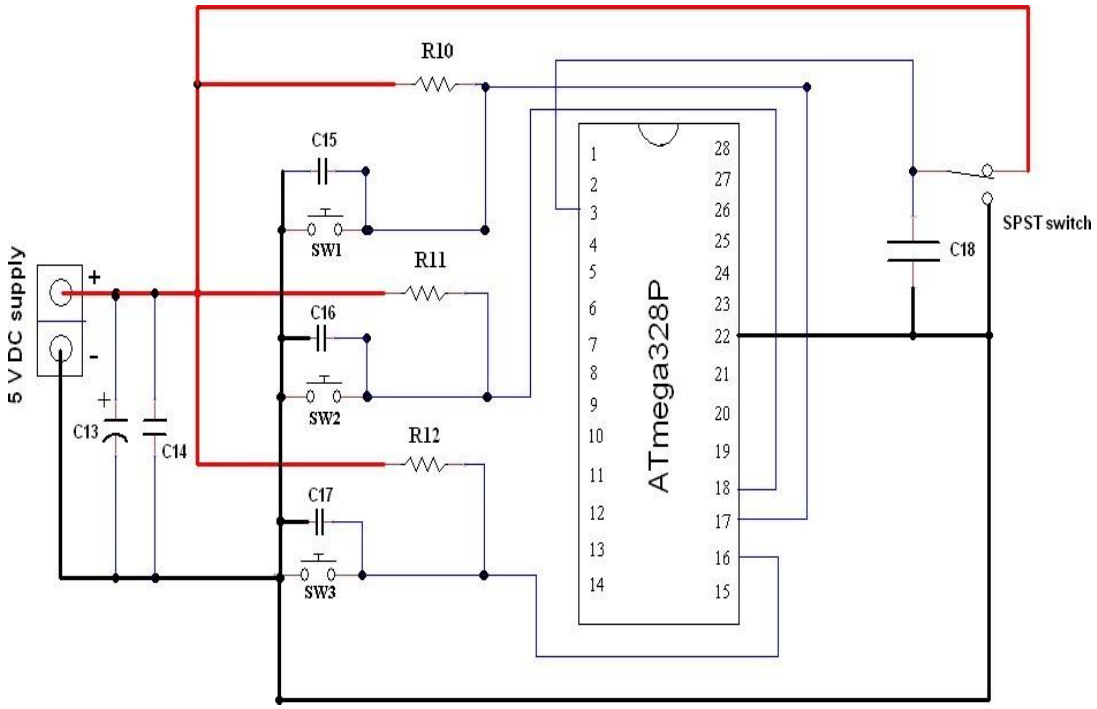

Fig.4.26 Connection diagram of push button switches

Capacitance values for C13, C14, C15, C16, C17, and C18 are 100µF, 0.01µF, 0.01µF, 0.01µF, and 0.01µF, respectively. Resistance values for R10, R11, and R12 are 10 kΩ.

The pin connections of the push button switches SW1, SW2, and SW3 to the microcontroller are Pin17, Pin18, and Pin16, respectively. These switches are designated as STOP, Clockwise, and Counter clockwise, respectively. The switches can be manually adjusted for Set Illuminance. Table 4.1 has been used to follow the operation of switches.

Table 4.1: Operation of switches

Mode of blinds	**SW1**	**SW2**	**SW3**
Opening	HIGH	HIGH	LOW
Closing	LOW	HIGH	HIGH
Stop	HIGH	LOW	HIGH

A toggle switch is fitted into the push button circuit. It can be altered by switching from manual to automatic mode of operation, or vice versa. When in automatic mode, adjusting the desired illuminance can cause the blinds to move. For instance, when the Measured Illuminance (Em) is less than the Set Illuminance (Es), the blinds are fully open. The light turns on and the intensity is raised to the Set Illuminance if the intended illuminance is not reached. The blinds are fully closed when the Measured Illuminance (Em) is greater than the Set Illuminance (Es). The light intensity decreases up to the Set Illuminance if the desired illuminance is not reached. The circuit diagram of this switches is shown in Fig.4.27.

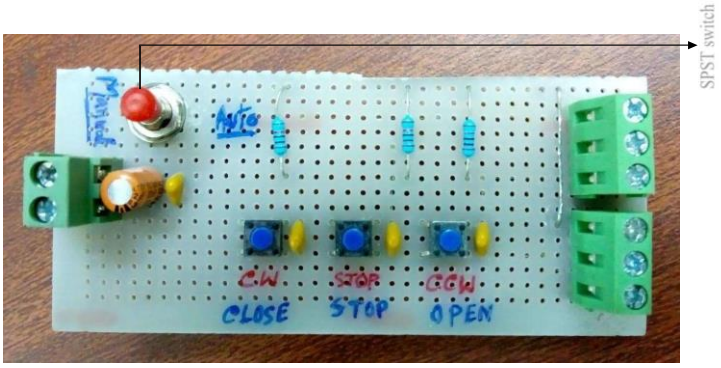

Fig.4.27 Circuit board of the switches

The complete circuit diagram of the system is shown in Fig.4.28.

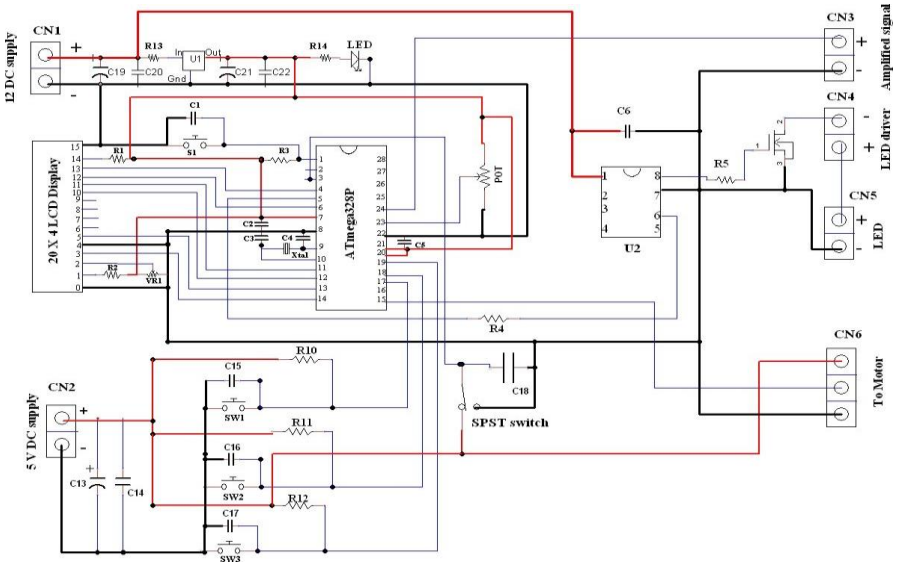

Fig.4.28 The Complete circuit diagram of the proposed system

The channels CN1 and CN2 are connected to a 12 V and a 5 V DC power source in this diagram. Channel CN3 has been connected to the amplified signal's output. The channels of CN4 and CN5 are connected to the LED driver and LED. Additionally, the servo motor is connected via channel CN6. Pin 3 of the microcontroller is the connection point to the SPST switch. The switch is necessary to alter the system's operating mode. By correctly connecting each circuit to the microcontroller, all of the circuits are displayed in a single schematic.

The configuration of the controller circuit board is shown in Fig.4.29. Four circuits have been developed to build the system.

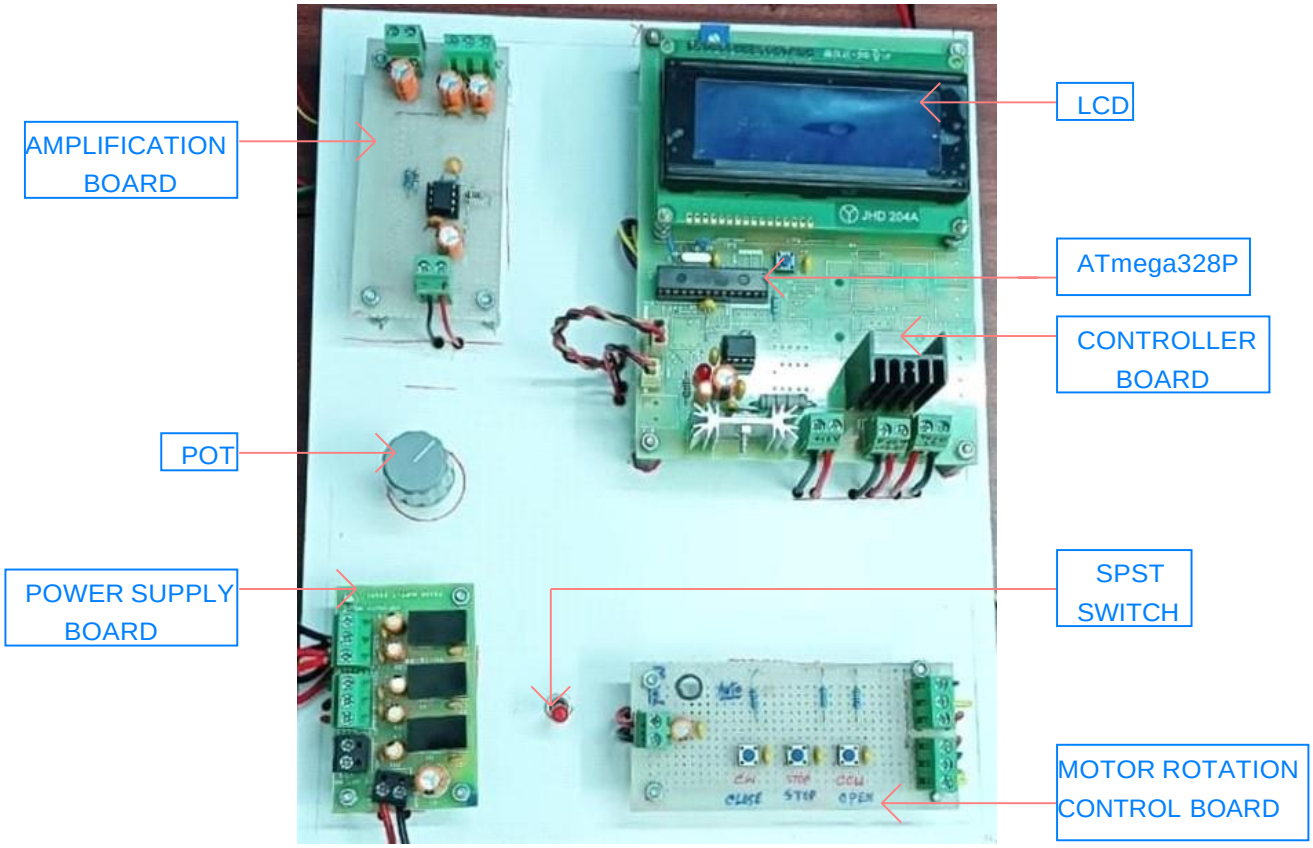

Fig.4.29 Configuration of main circuit board

4.4.2 Software implementation of the system

The proposed system has been explained by an algorithm. This can be implemented step by step. The following steps are discussing below.

A. Step by step analysis of algorithm of the proposed system

Step1: Initialize the Analog and Digital pins of microcontroller ATmega328P.

Step2: Enable the microcontroller pins i.e., LCD display pin, motor rotation control pin, LEDs pin, Photo detector pin and Set illuminance pin.

Step3: Set the illuminance (Es) between 0 lx to 300 lx by the use of potentiometer (10k).

Step4: Photo Detector (PD) detects the light level at that condition and the amplified signal is converted into Digital value using ADC.

Step5: Convert the PD digital value into illuminance value by the equation which is used as Measured Illuminance (Em).

Step6: Compare between Set Illuminance (Es) and Measured Illuminance (Em). This is denoted by absolute error (Er).

Step7: When Er > 0, the blinds is opening. If the desired illuminance is achieved, the lights as OFF condition. When the blinds are completely open and error is still greater than zero, then the duty of the PWM signal for LED will be increased and contribute the illuminance until the required illuminance is achieved.

Step8: When Er < 0, the blinds is closing. When the blinds are completely close and error is still less than zero, then the duty of the PWM signal for LED will be decreased. This process will be stop if the required illuminance is achieved.

Step9: when the Error is zero, no change in PWM and blinds condition.

The detailed flowchart of the software implementation of the controller is given in Fig.4.30. The system is first turned on with supply of 12 V DC power supply which initializes the ports and ADC of microcontroller as well as the LCD is turned on. The LCD is interfaced with the microcontroller and programmed to display the percentage of the duty cycle of LEDs. The percentage of the duty cycle has been converted into 8-bit digital value. The Set Illuminance values have been given from the graph between PD digital and measured illuminance (CL- 70F). The illuminance value is set by the user by varying the potentiometer as per requirement which is displayed on the LCD. Then PD reads the illuminance value on the working plane. The PD output signal has been modified by the use of amplifier circuit. The amplified PD Analog signal is converted into 8-bit Digital value. The Measured Illuminance has been considered with proper scaling. The error has been occurred between them. When the error less than zero and if the blinds are closed, the duty of the PWM signal is reduced by 1%. If the blinds are not closed then close the blinds by step wise. When the error is greater than zero and if the blinds are fully opened, the duty of the PWM signal is increased by 1%. Again, the condition is not maintained then opened the blinds by step wise. If the error is equal to zero then the duty has not been changed of the PWM signal. Again, the error is greater than zero then no change of PWM and no change of the blinds position. If the condition is not fulfilled then the process will be continued.

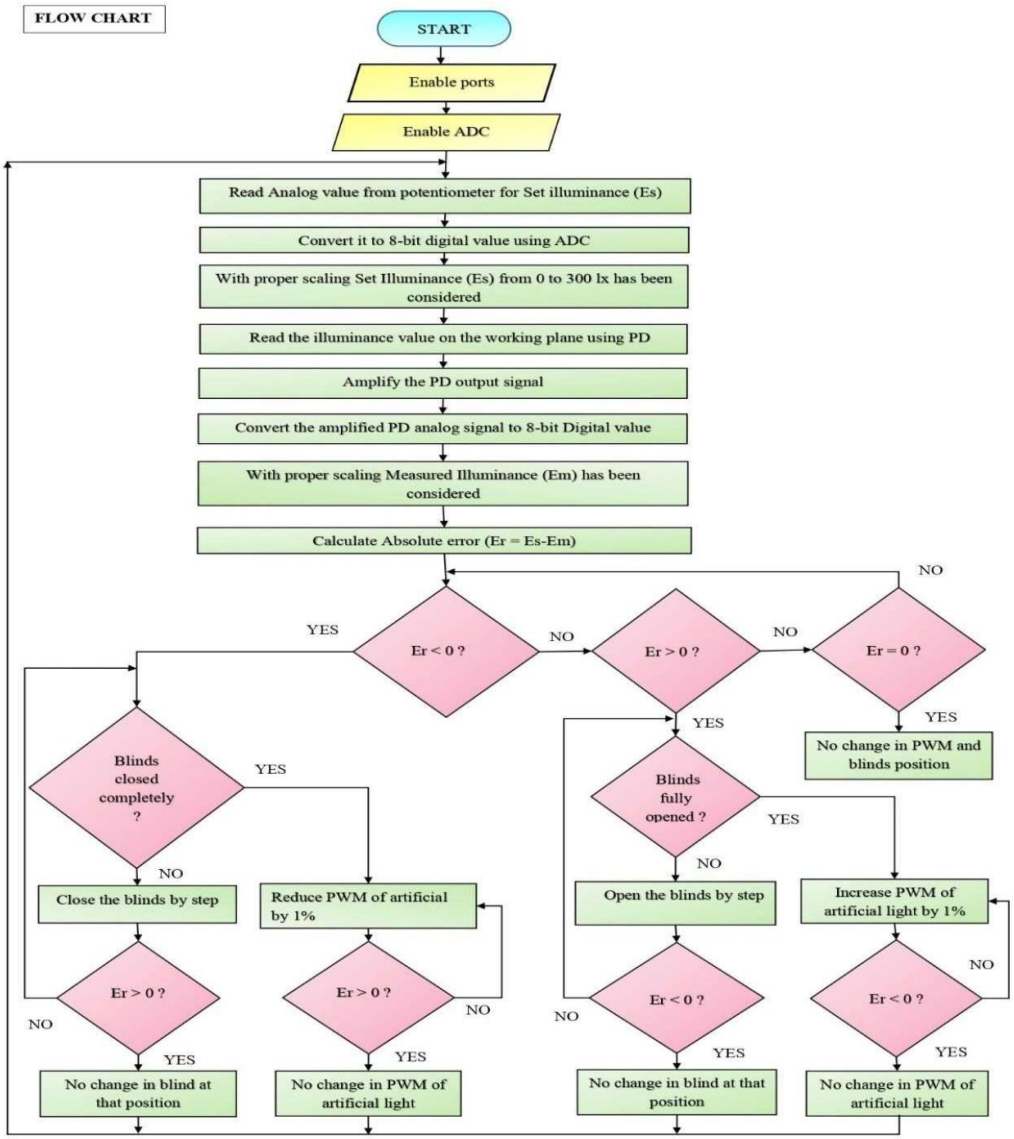

Fig.4.30 Flowchart of the software implementation of the program

4.5 Proposed artificial daylight using solar cell and MPPT controller

For the purpose of concept–proving we have chosen a laboratory space (length 6.2m *breadth 4.1m) with two windows on the northern side. The space will have six dimmable LED luminaires, four wall mounted and two ceiling mounted sensors that measure the work plane illuminance in an indirect way. Additionally, one of the walls will have an “Artificial Daylight (AD)”. The AD will consist of a roof-mounted solar panel, a microcontroller- (MCU) based LED driver and LED panel. The system will not have any battery storage. The MCU unit will employ a maximum power point tracking (MPPT) algorithm so that maximum power available

from the solar panel can be used for lighting [63]-[70]. It is foreseen that this concept can be utilized in spaces where adirect entrance of daylight through windows is not available.

4.5.1 Boost converter developed in the laboratory

As per the previous discussion, we know that a boost converter is a converter that boosts the voltage on the output side. The voltage enhancement process is based on the manipulation of the duty cycle. The duty cycle is the ratio of "the total time when the switch is closed (T_{on}) in a cycle" to the "total time required to complete the cycle (T)" i.e.

$$D = T_{on}/ T$$

Now, this D (= T_{on}/T) can be controlled by a signal from a current mode SMPS controller IC UC3843.The PWM output from the UC3843 chip manipulates the duty cycle by changing the ON Time of the base current of the MOSFET(switch) of a boost converter . The details of the UC3843 is describedin the APPENDIX chapter. The UC3843 is an 8 pin chip, on which pin 6 is the output voltage pin, which generates a variable PWM voltage up to 2.53 dc volts with respect to the ground pin (pin 5) and delivers the base current of the MOSFET (switch). The details of the duty cycle tester circuit are shown in fig 4.31.

A. Duty cycle tester circuit using UC3843

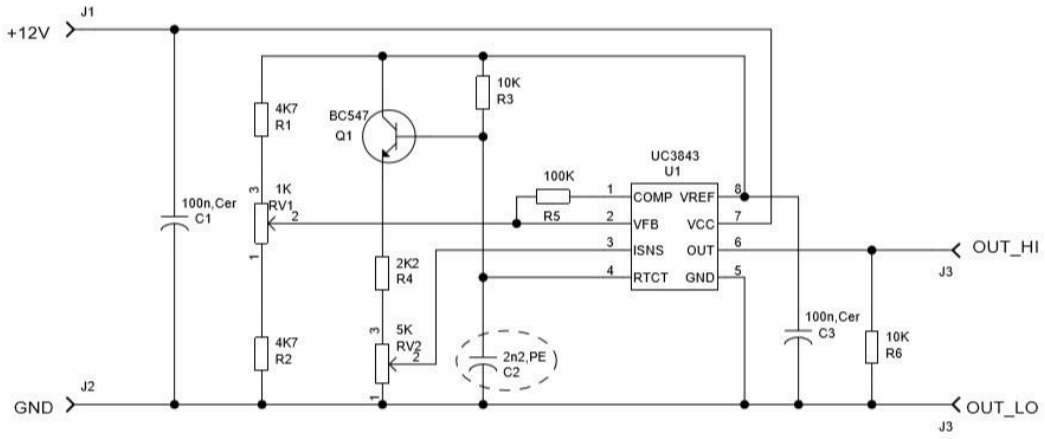

Fig 4.31 Duty cycle tester circuit diagram using UC3843

Fig 4.31 shows a tester circuit for duty cycle manipulation using the UC3843 output. The output remains in the high state (up to 2.53 volt) for a certain time called T_{on} and in the low state (0 volts) for the remaining time of called T_{off}. The total time for a cycle T is the sum of T_{on} and T_{off} .

$$\mathbf{T = Ton + Toff}$$

The circuit has an input voltage of 12 volts from the supply. The chip UC3843 generates a PWM output signal based on the input signal in the pin 2. The input signal in the pin 2 is controlled by two POTs RV_1 and RV_2. By

manipulating these two pots we can manipulate the ON Time of the output signal which will manipulate the duty cycle. Generally, RV_2 is kept constant because, after a certain point it becomes saturated.

In practical the RV_1 has a screw on top that can rotate in the clockwiseand anticlockwise direction. So, by rotating the screw on the pot RV_1 we can change ON Time of the output signal and that will change the duty cycle of the PWM output of the circuit.

Fig 4.32 shows the laboratory developed duty cycle tester circuit and fig 4.33 shows the PWM output of the circuit in an oscilloscope screen with a dutycycle of **65%.**

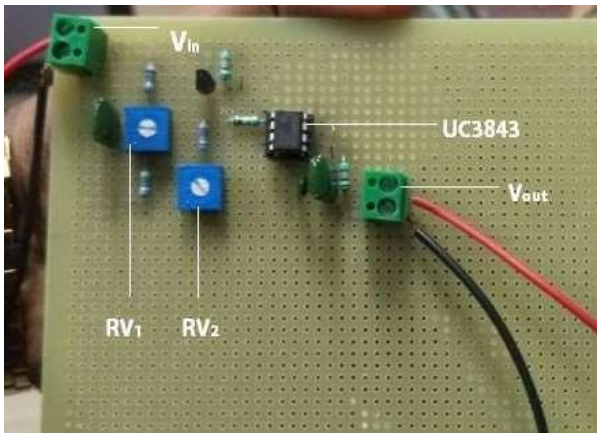

Fig 4.32 UC3843 tester board developed in the laboratory

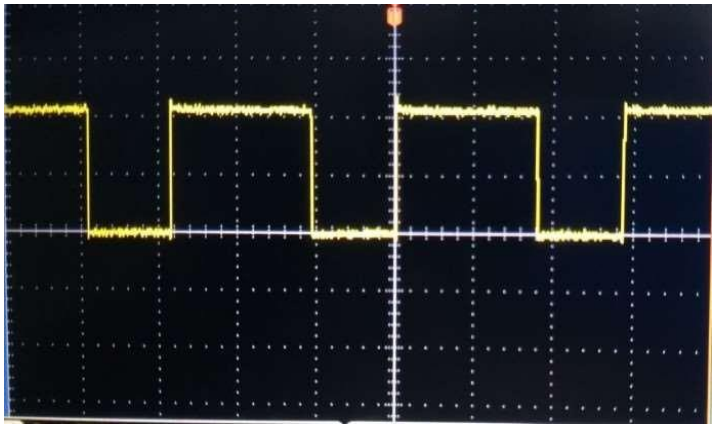

Fig 4.33 PWM Output voltage of the circuit developed in the laboratory

B. Inductance measurement circuit

In the boost converter inductance measurement is an important parameter that determines the output voltage of the converter. So, a circuit is developed in the laboratory to measure the inductance of the inductor, that will be used in the actual boost converter.

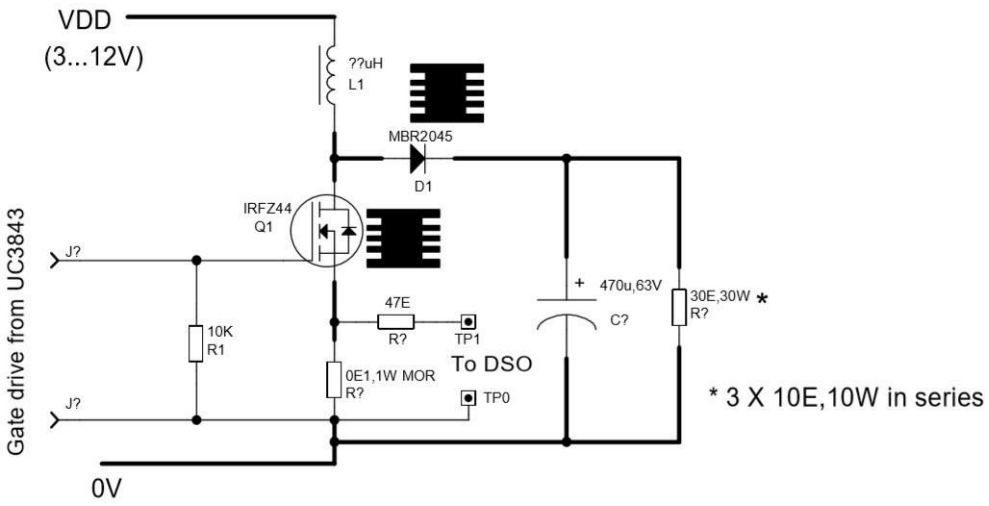

Fig 4.34 Inductance measurement circuit

Fig 4.34 shows the inductance measurement circuit. In this circuit, the duty cycleis controlled by the input gate signal of a MOSFET "IRFZ44", which is shownin the diagram as Q1. The MOSFET remains on during the positive gate signal (T_{on}) and remains off during no gate signal (T_{off}). The gate drive signal of the MOSFET Q1 comes from the PWM output of the UC3843. When the PWM signal reaches the gate of the MOSFET, it starts conducting and the currentflows from the supply positive to negative via the inductor, MOSFET, and one 0.1-ohm resistor. The current through the inductor does not change abruptly, soit takes time to store the energy. At the moment, when the gate signal is lost, the inductor current does not change abruptly again to zero. The current then startsto flow from supply to the load via the inductor and a rectifier. The rectifier is used to ripple out any ac component generated from the circuit or input and the capacitor across the load works as a filter. The rectifier used in the circuit is "MBR2045". The details of the MBR2045 and IRFZ44 is discussed in the APPENDIX. The boosting operation takes place as per previous expressions.

The testing of the circuit should never be done without connecting a load. If it is switched on without connecting a load, the full voltage will appear across the capacitor and it can burst out and damage the whole circuit. The load used here is three 10-ohm 10-watt resistors connecting in series giving a total of 30- ohm resistance bank.

Calculations:

$$\mathbf{V = L\ (dI/dT)}$$

Where, V = Input voltage, L = Measured Inductance, dI = (I_1-I_0) = Change incurrent, dT = T_{on}

Now,

V = 12V, dT = 15 micro-sec, I_0 = 0.4 A, I_1 = 4.8 A,

We get,

$$12 = L \times [(4.8-0.4)/ (15X10^{-6})]$$

So,

$$L = 40.9\ \mu H$$

Results:

Inductance value measurement from the boost converterInput voltage = 12 v

Frequency = 33 kHz

Resistance = 30 ohm

Inductor Turns = 14

Gap in the core = 1.2mm

C. Boost converter circuit with feed back control

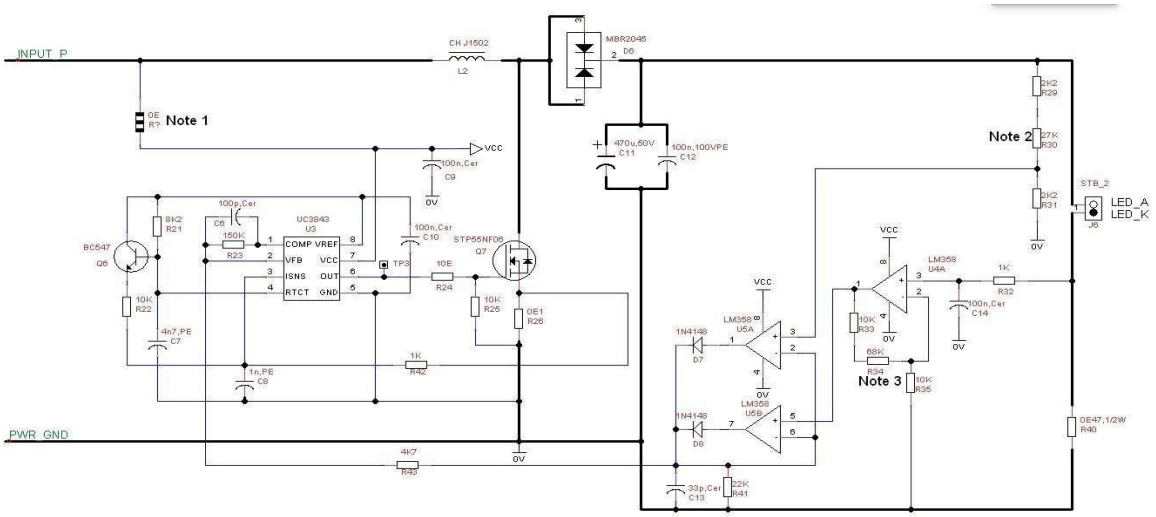

Fig 4.35 Full boost converter circuit with feedback control

Fig 4.35 shows the boost converter circuit with feedback control. The UC3843 chip requires an analog input signal in the PIN 2 to operate. In the tester circuit, the signal was manipulated by a POT but in an actual circuit, the control needsto be automatic. This analogue signal can be generated through a feedback circuit. The circuit in the right part of fig 4.35 shows two operational amplifiers that check the error and generates the feedback signal for the boost operation. It takes the voltage and current data from the load side and compares the error and sends the error feedback signal to the PIN 2 of UC3843.

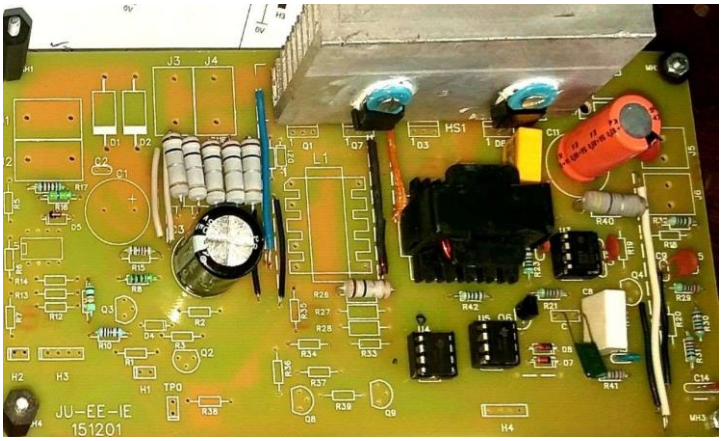

Fig 4.36 Laboratory-developed boost converter circuit

Fig. 4.36 shows the laboratory developed boost converter circuit. This circuit works as a boost converter. But it can be modified for MPPT. For MPPT asignal from the microcontroller "**e0**" can be attached to the feedback circuit and the output manipulates the duty cycle. The circuit with microcontroller input is shown in the fig 4.39.

4.5.2 Boost converter circuit with microcontroller input for MPPT control

The simplified block diagram of the artificial daylight is given below Fig. 4.37

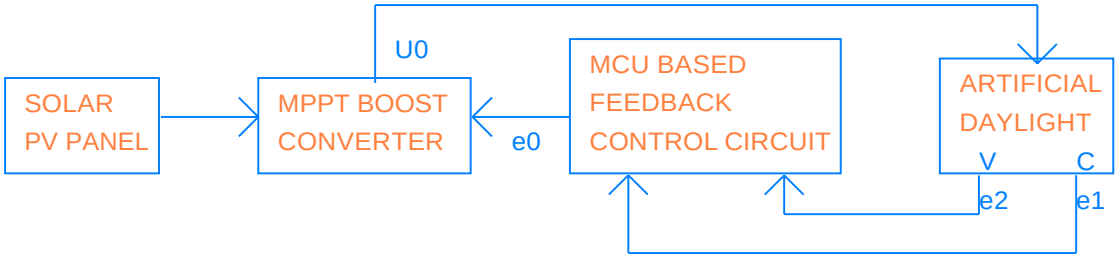

Fig. 4.37 Block diagram of the Artificial Daylight with MPPT boost converter

The circuit shown in fig 4.38 is the laboratory developed boost converter circuit for MPPT control. In this circuit, the switching operation conducts by the MOSFET Q1. The gate pulse comes from the UC3843 generated PWM output. The control signal of the UC3843 comes from the microcontroller-controlled feedback system. The

microcontroller takes the voltage and current data from both the input and load side of the converter circuit. Then the microcontroller processes an algorithm and decides the optimum duty cycle for the maximum power point of that state and sends a PWM signal "**e3**" to the feedback control circuit. The feedback control circuit then generates an analog signal "**e0**" and sends it to the PIN 2 "**VFB**" pin of the UC3843 to manipulate the ON Time of the output signal and control the duty cycle

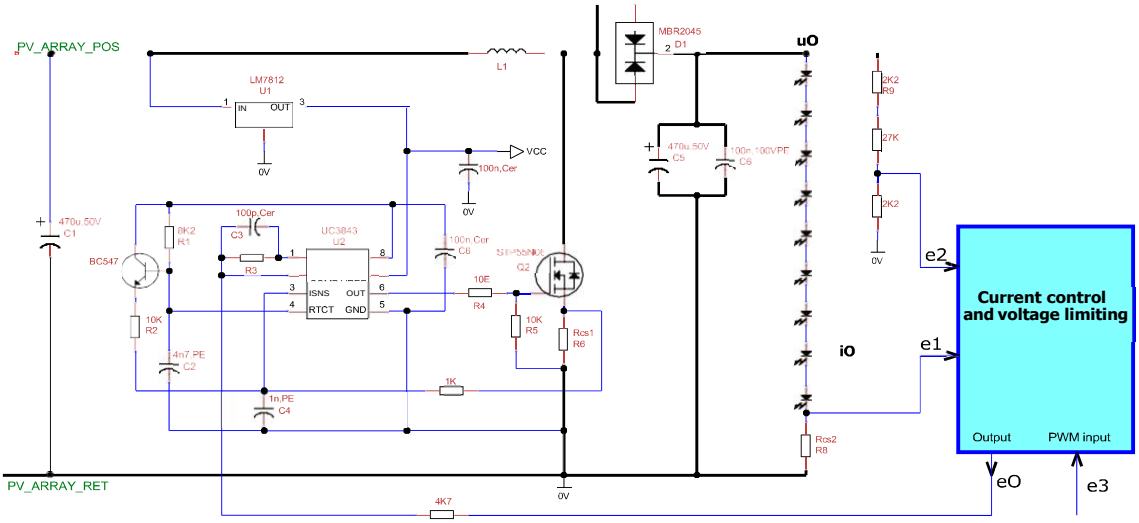

Fig. 4.38 Laboratory developed a boost converter circuit

In fig 4.38, the feedback control circuit is shown as a block named "Current control and voltage limiting circuit". Actual arrangement is similar to that shown in the Fig. 4.39

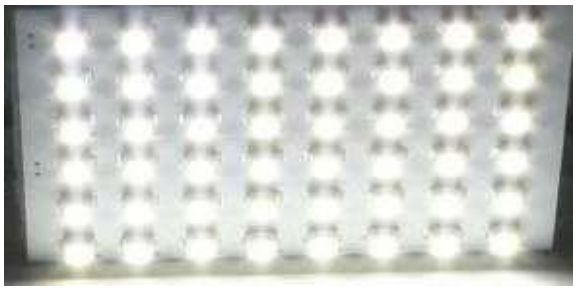

Fig. 4.39 A luminaire of Artificial Daylight

A. Feedback control circuit with microcontroller input

Fig 4.40 shows the feedback control circuit with microcontroller input. There are two signals **e1** and **e2** coming from the output side. **e2**is the voltage signal and **e1** is the current signal. The microcontroller generates a PWM signal. This signal is fed to the PIN 3 of the op-amp after passing througha filter circuit. The current signal **e1** also fed to the PIN 3 of the op-amp. The output of the circuit is an analog signal **e0** which is fed to the PIN 2 of the UC3843 for controlling the ON Time of the output voltage and it controls the duty signal.

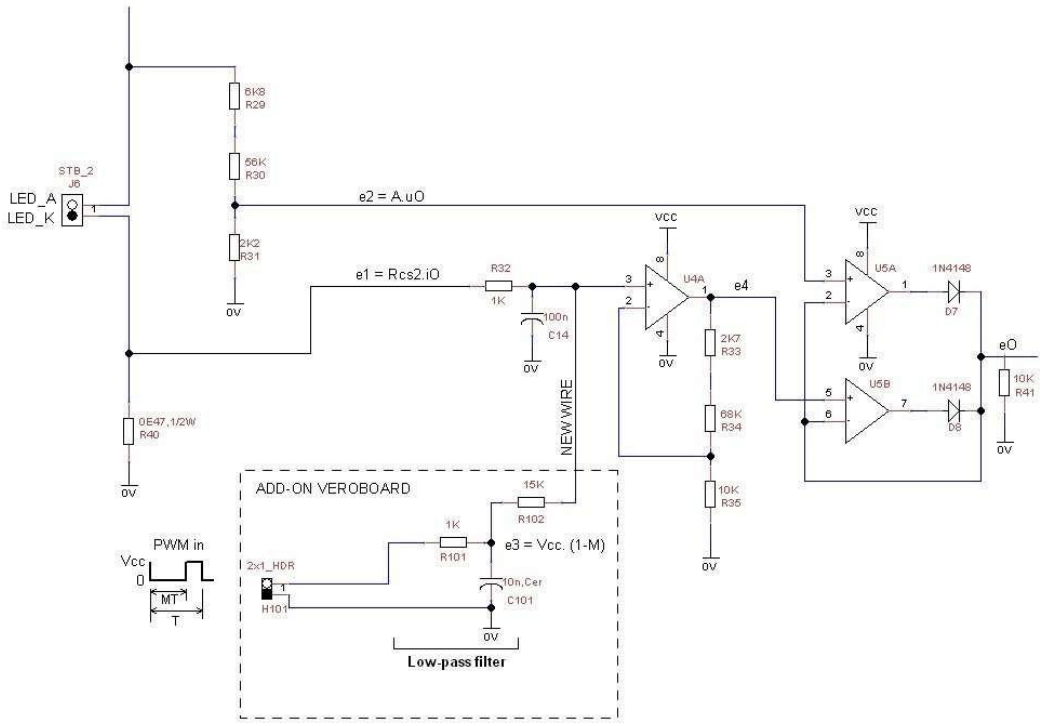

Fig 4.40 Feedback control with microcontroller input

4.5.3 Microcontroller unit development (MCU) board

Figure 4.41 displays the MCU development board's circuit diagram. The ATMega32A chip on the PCB has 40 PINs. A crystal operating at 16 MHz controls this device. Thus, 16000000 instructions can be executed by the microcontroller every second. The PINs 12 and 13, XTAL2 and XTAL1, respectively, are connected to the crystal. A 22 pf capacitor in the PIN11 (GND PIN) grounds each end of the crystal pin.

The microcontroller may be fully programmed using software, and the HEX code produced by the software can be physically programmed onto the microcontroller using a separate programmer called ISP HEADER (8 pins). For programming purposes, the microcontroller's PINs 1–8 are connected to the 8-pin ISP HEADER via the PC.

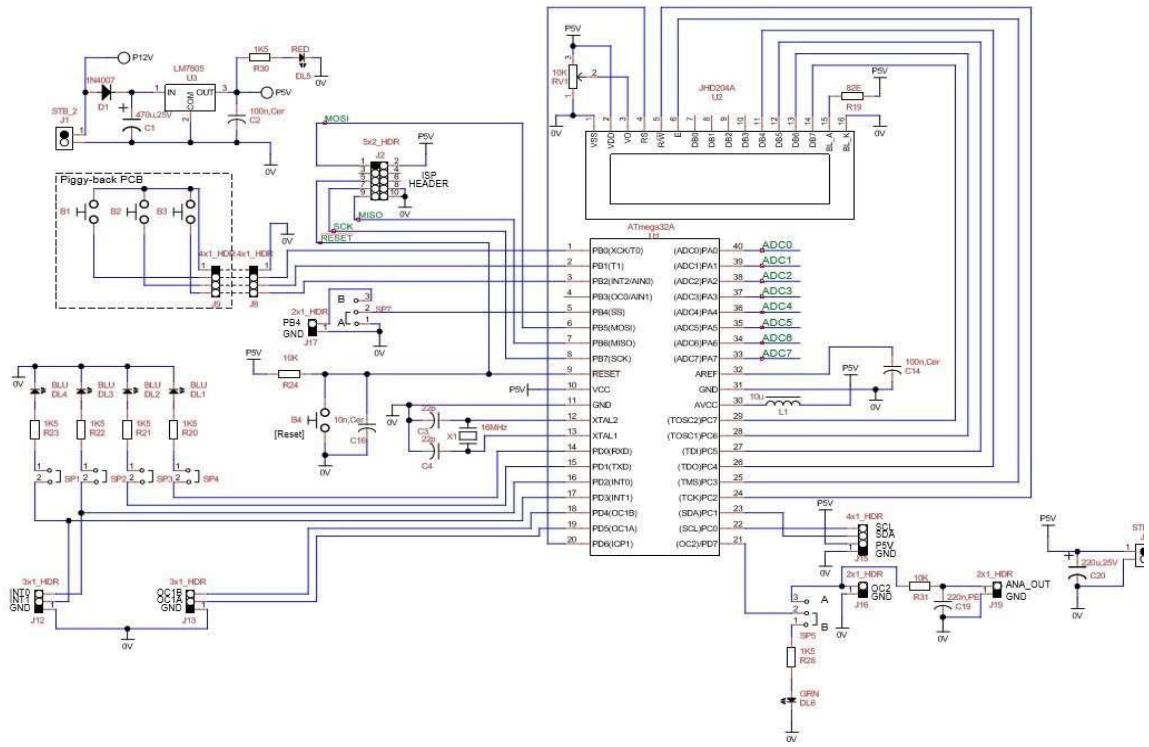

Fig. 4.41 Circuit of the MCU development board

The software used to write the program for this project was AVR Studio 5.1. Through the use of PROGISP software and an ISP HEADER programmer from a PC, the built and produced hex file from the software was burned to the microcontroller. With the PROGISP software, this programmer may easily write a new memory and flash the old one.

Eight ADC channels on the development board are linked to the microcontroller's PINs 33–40. In order to receive data from the source, such as the sensors, the PV module, certain ADC channels are needed. Although the board contains more ADC channels for future growth.The 16X2 LCD panel on the development board displays illuminance level, voltage and current as well as other system status information. The microcontroller and this LCD are linked by PINs 24-29 and 20.

The MCU reads the data it receives from the ADC channel, assembles the program according to its internal instructions, and outputs a PWM signal Fig. 4.42

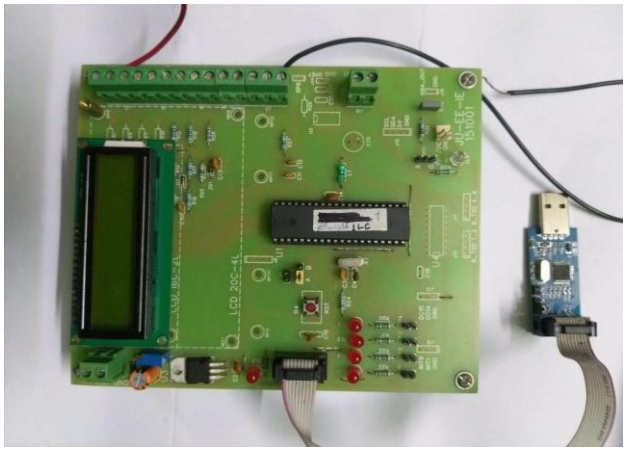

Fig 4.42 Laboratory developed MCU board with ISP header

4.5.4 Circuit for data transfer from the PV module to ADC

The ADC channel reads either voltage or current data. Fig 4.43 shows the circuit used for the ADC channel to intake data from the PV module. From the PV positive the voltage goes to a voltage divider channel and directly goes to the ADC1 channel of the development board.

The current passing through the circuit to the ADC channel is very lowand the ADC cannot read the data properly. So, there is an amplification process that amplifies the current which is enough for the ADC channel to read, andthen it goes to the ADC3 channel. There are five 0.1-ohm resistors connected in parallel to amplify the current.

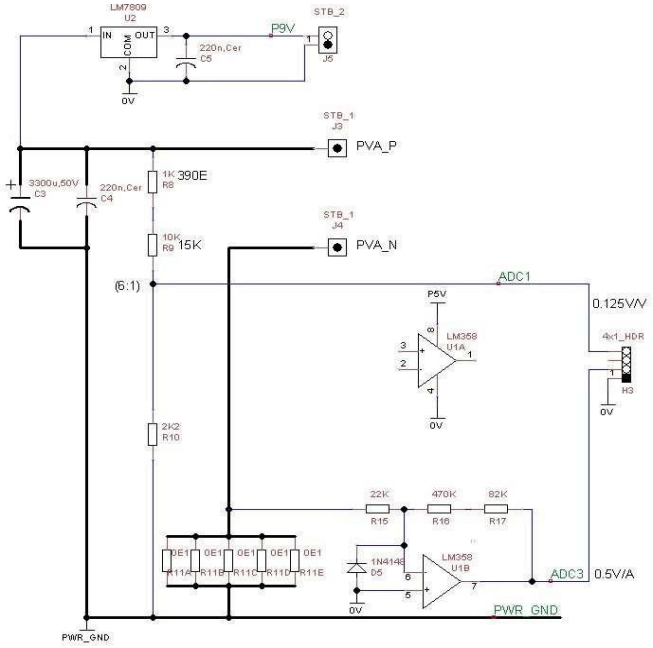

Fig 4.43 Circuit for data transfer from PV module to ADC

4.5.5 Methodology for MPPT

There are several methods available for MPPT that were discussed in chapter 2, but here we used a combination of hill climbing and incremental conductance method to find the maximum power point.

A. Formulation:

Let us assume, for a PV module

input voltage is = V, input current = I, and input power is = P.Now,

$$\frac{dP}{dV} = \frac{d}{dV}(VI) = I + V\frac{dI}{dV} \tag{4.39}$$

for, V not equal to 0,

$$\frac{1}{V}\frac{dP}{dV} = \frac{I}{V} + \frac{dI}{dV} \tag{4.40}$$

both $\frac{I}{V}$ and $\frac{dI}{dV}$ are conductance's, if we define the former as static conductanceG_s and the letter as the dynamic conductance G_d wet get,

for, V not equal to 0,

$$\frac{1}{V}\frac{dP}{dV} = G_S + G_d$$

In other words,

$$\frac{dP}{dV} > 0 \text{ , } G_S + G_d > 0$$

$$\frac{dP}{dV} = 0 \text{ , } G_S + G_d = 0$$

$$\frac{dP}{dV} < 0 \text{ , } G_S + G_d < 0$$

In the entire range $0 < V < V_{oc}$, $G_S > 0$ and $G_S < 0$

So, for MPPT, the condition $G_S + G_d = 0$ is necessary. Fig 4.44 shows the basic condition for MPPT.

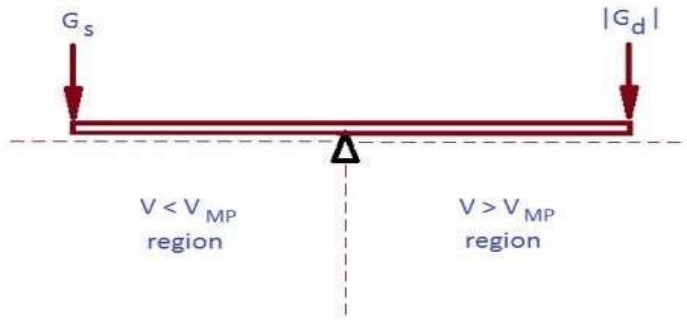

Fig 4.44 Basic condition for MPPT

B. Steps:

There are three conditions for maximum point tracking with this method is shown in table 4.2

Table 4.2 Condition of maximum point tracking

Condition	Required action
$G_S + G_d > 0$	**The voltage has to be increased**
$G_S + G_d = 0$	**The voltage has to keep unchanged**
$G_S + G_d < 0$	**The voltage has to be decreased**

C. Method of implementation:

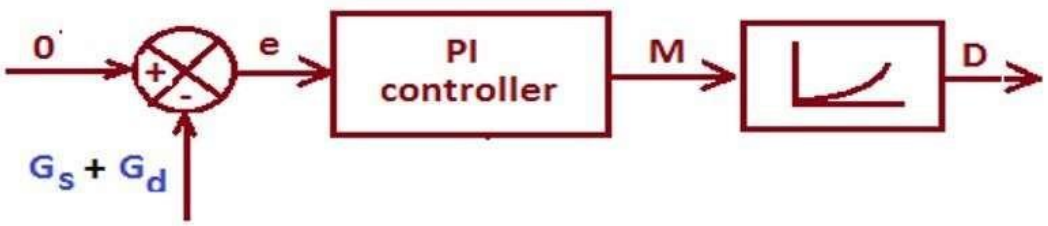

Fig 4.45 Method of implementation for MPPT

The method of implementation is the checking error signal from a PI controller.If there is an error from the PI controller as shown in fig. 4.45, i.e. $G_s + G_d$ is not equal to 0, then the voltage and system changes as per requirement.

D. Flowchart of the methodology used for MPPT

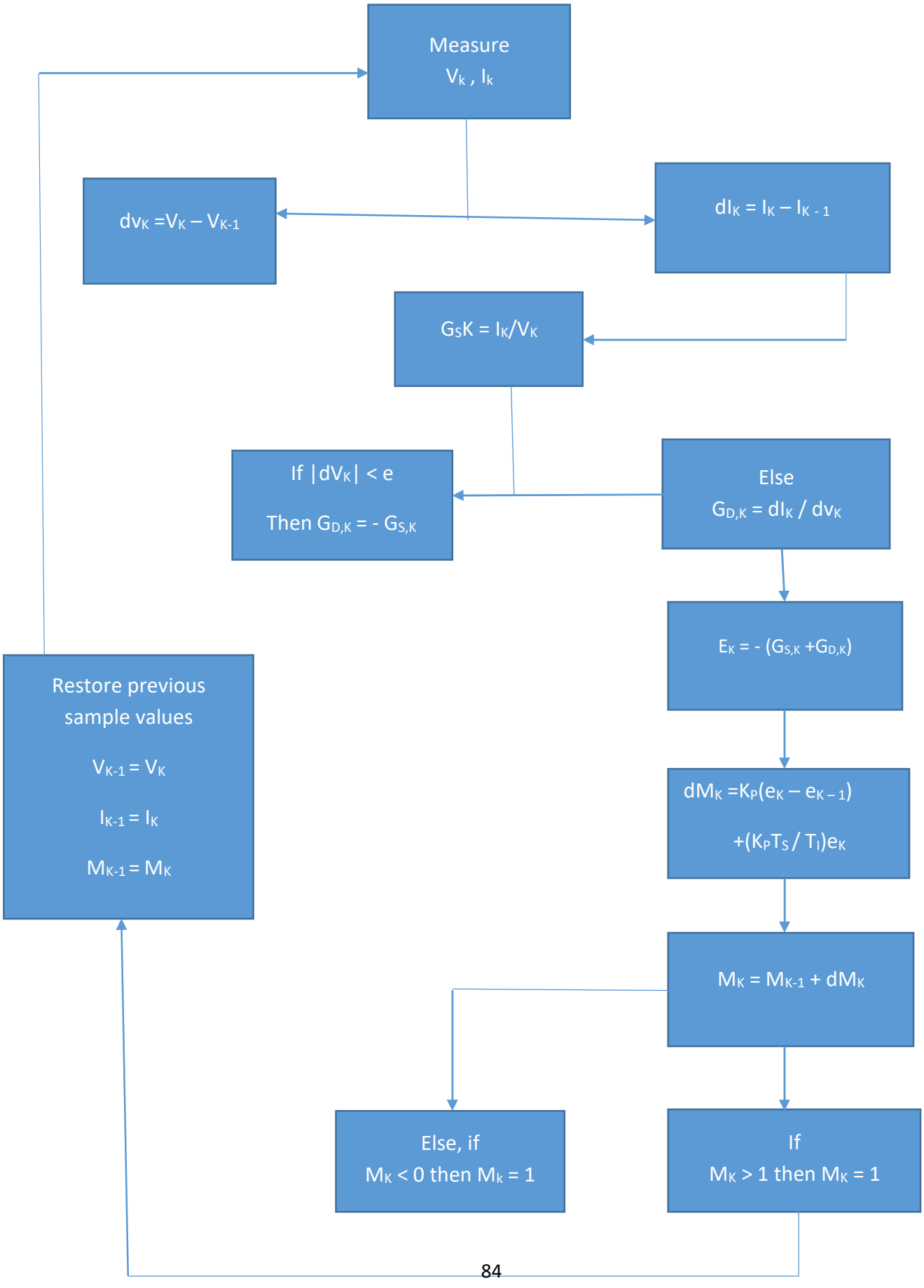

Fig. 4.46 Flowchart of the methodology used for MPPT

The MPPT program is displayed in the previously mentioned flowchart Fig. 4.46 and the necessary software coding has been completed to compile the MPPT process and burn it inside the MCU for execution.

E. Task chart for microcontroller

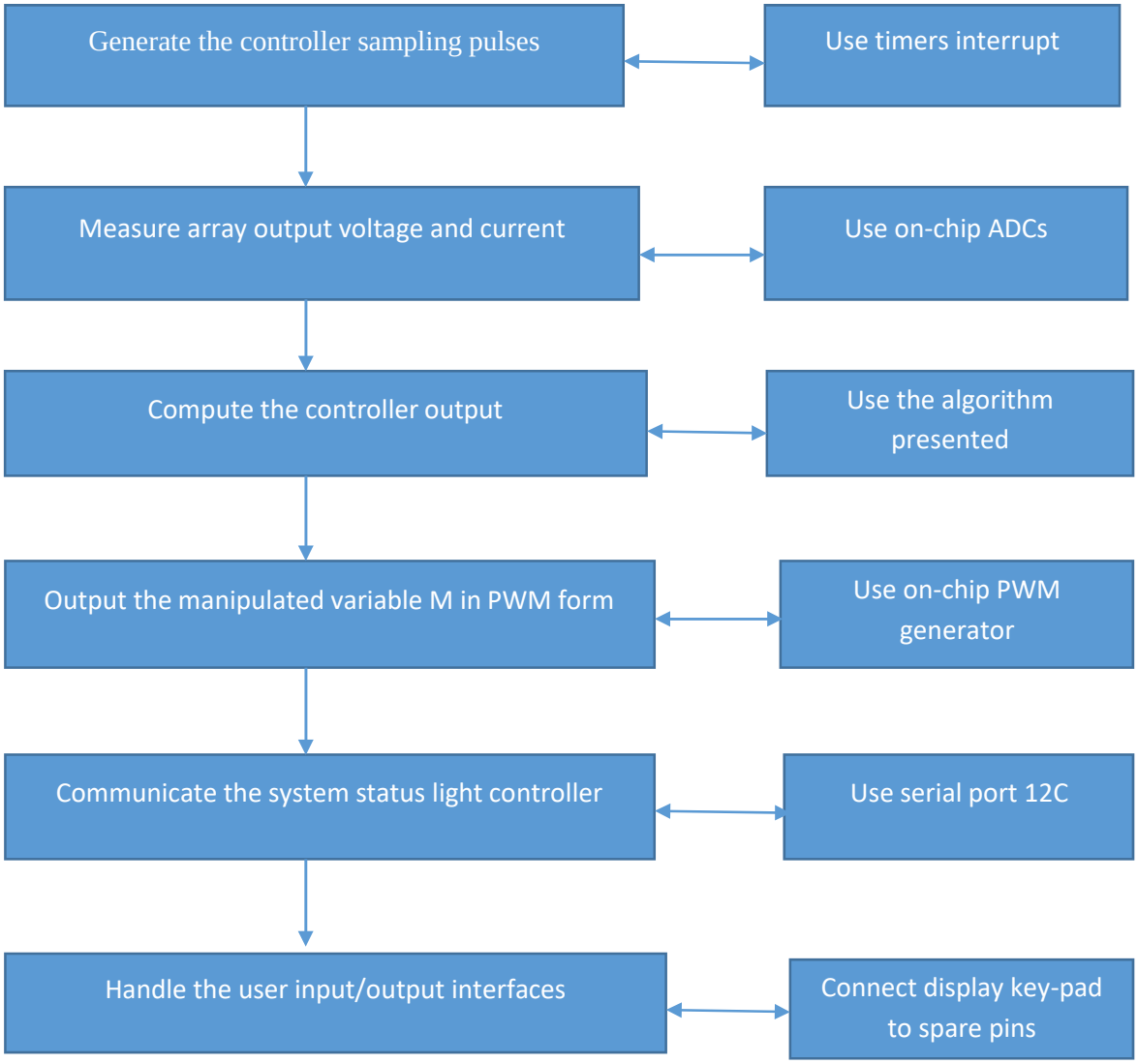

Fig. 4.47 Tasks for the microcontroller

The detailed work function task chart of the Artificial Day light system for achieving MPPT is displayed in the Figure 4.47. It outlines each segment's whole work process from start to finish as well as all system tasks in sequential order.

5. Experimental results and data analysis

5.1 Illuminance sensor data

A. Static Performance

Figure 5(a) plots the transmitter's ideal and actual output currents; the measured values correspond to E = 0, 5, 10, 25, 40, 70, and 100 lx. Since the inaccuracy is so tiny, the graph cannot be used to measure it precisely. This leads to the drawing of an Error vs. E graph in Figure 5(b). The greatest error magnitude is found to be less than 1% of the 16 mA span.

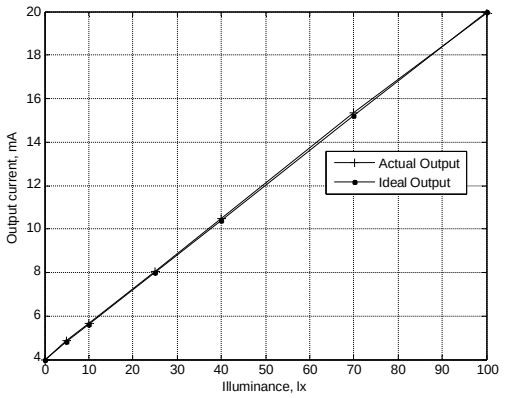

(a)

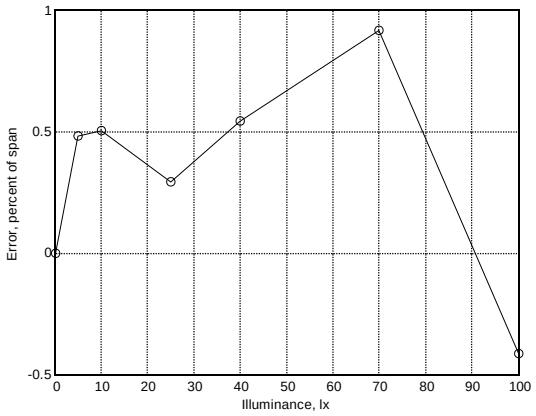

(b)

Fig. 5. (a) Actual and ideal output characteristics. (b) Error plot of the transmitter.

B. Dynamic Performance

To determine the time constant of the transmitter's first-order model, an experiment was conducted. It is necessary for the terminal current to go through a 100Ω resistor. A 10-bit A-to-D converter is used to transform the voltage drop that results into a number. A step increment in E from 0 to 100 lx is applied, and the output of the ADC is then saved for 800 ms at 20 ms intervals. A plot of the stored values with the step in E applied at 100 ms is shown in Fig. 5.1. The transmitter's time constant, or the length of time needed to reach 0.632 times the steady-state value, is approximately 40 ms given that the steady state ADC output is approximately 840.

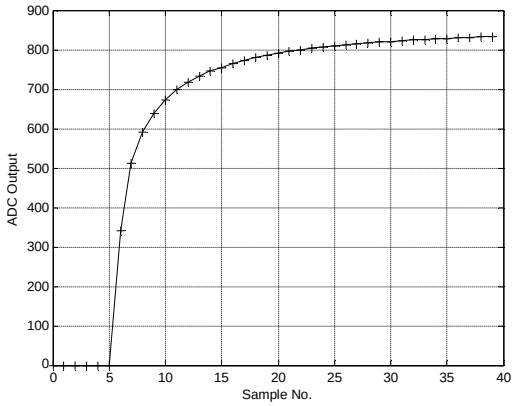

Fig. 5.1 Step response of the transmitter

5.2 LED Driver data

The proposed LED driver is tested in a lab setting using an 18W LED light source that receives an ac input voltage of 230V at a line frequency of 50 Hz which is shown in below Fig. 5.2
The experimental findings are covered in the section below.

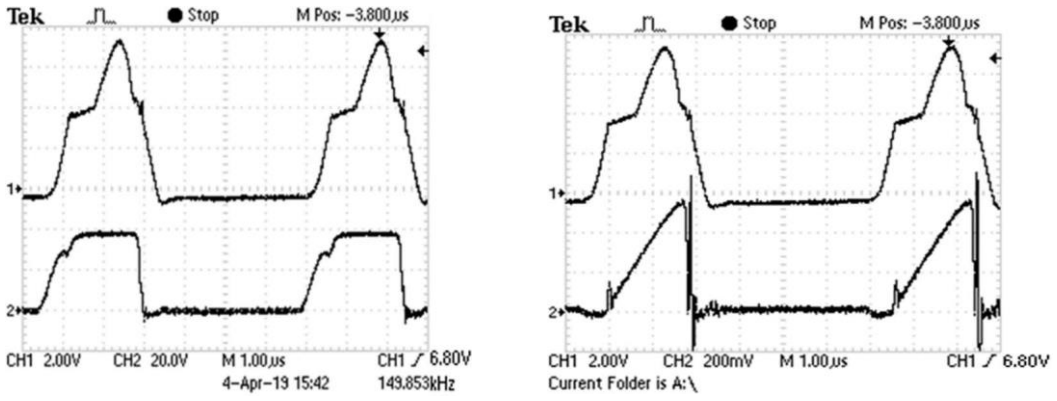

(a) (b)

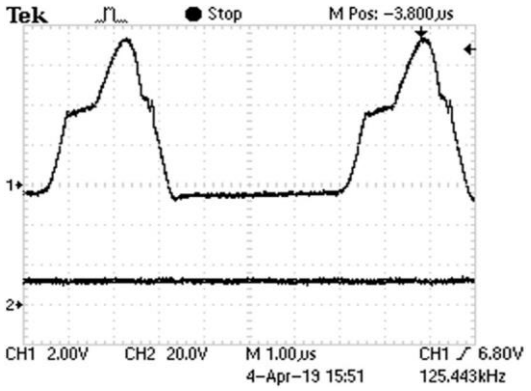

(c)

Fig. 5.2. Experimental waveforms of the proposed LED driver. (a) Gate to source voltage of Q_1 (CH1-2V/div), 4/T1 (CH2-20 V/div), time: 1µs/div. (b) Gate to source voltage of Q_1 (CH1-2V/div), S/Q1(CH2-200mV/div), time: 1µs/div. (c) Gate to source voltage of Q_1 (CH1-2V/div), 5/T1 (CH2-20V/div), time: 1µs/div.

The primary waveforms of the driver are depicted in Figs. 5.2(a) through 5.2(c), which are consistent with the theoretical theory.

When the LED is dimmed by PWM to 50% of its rated value, the output voltage and current waveforms are shown in Figures 5.3 and 5.4, respectively. The average output voltage fluctuates from 57V to 5V when the lamp current drops from 320mA to 0mA. The voltage and current of the lamp exhibit minute waves.

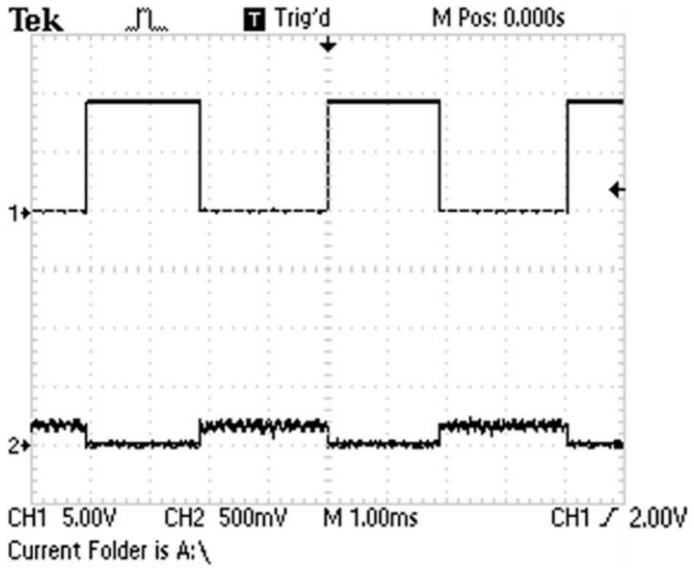

Fig. 5.3. PWM signal (CH1-5V/div), Output waveform of I_{LED} at 50% of the rated value (CH2-500 mV/div), time: 1 ms/div.

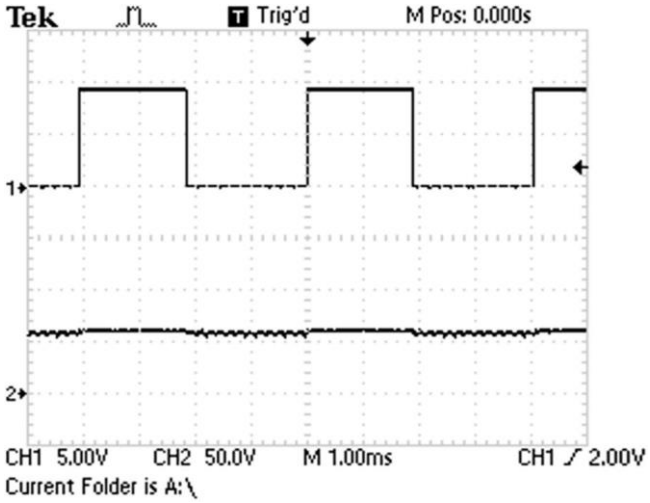

Fig. 5.4. PWM signal (CH1-5V/div), Output waveform of V_{LED} at 50% of the rated value (CH2-50V/div), time: 1 ms/div.

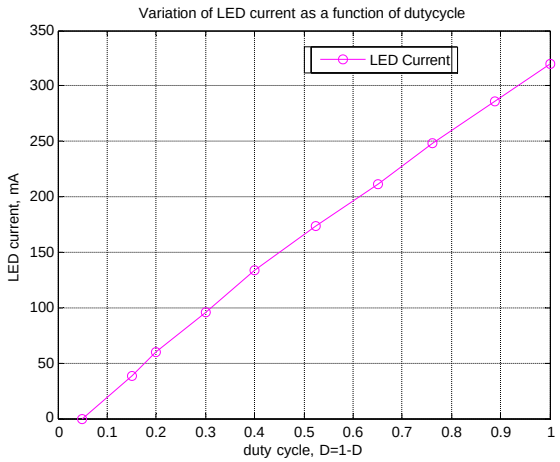

Fig. 5.5. Duty cycle versus LED current graph

Fig. 5.5 shows the variation of LED current with changing the duty cycle of PWM signal. The experimental graph depicts that increment in the LED average current is proportional to the increment in duty cycle, but the transfer characteristics is non-linear as it does not pass through the origin.

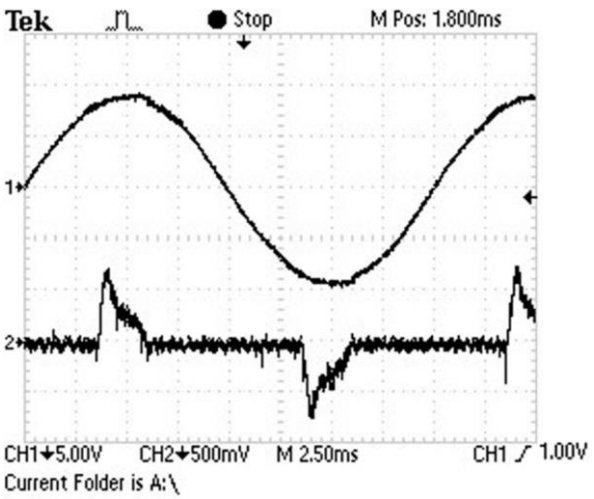

Fig. 5.6 Input AC voltage and current waveforms

The input AC voltage and current waveforms corresponding to D = 1 are show in Fig. 5.6. It is observed that the current waveform is far from sinusoidal. The current is in each half cycle flows in pulses, the base width of which about 2.5ms. This gives rise to a very poor power factor. However for such low power LED drivers there is no power factor restriction.

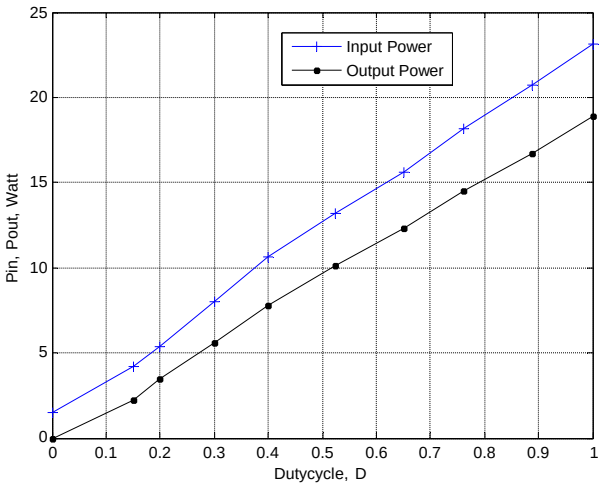

Fig. 5.7. Changes in input and output power (P_{in} and P_{out}) with duty cycle

The variations of input power and output power with duty cycle are shown in Fig. 5.7. The above graph shows that P_{out} increases linearly with duty cycle.

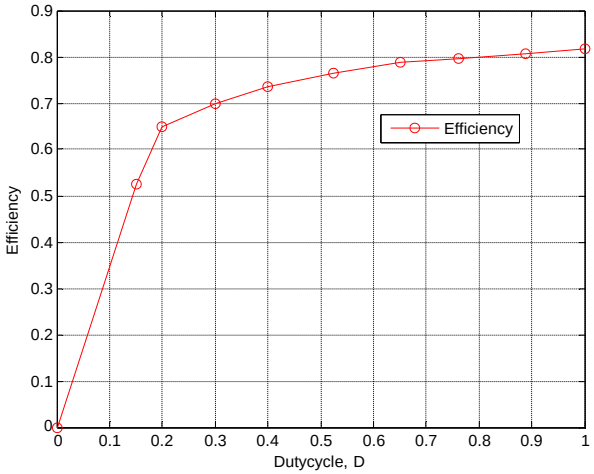

Fig. 5.8 Circuit efficiency with Duty cycle

Fig. 5.8, which depicts the driver's observed circuit efficiency with PWM dimming, shows. At the chosen lamp power, the circuit is 83% effective. It is significant to note that the experimental prototype can be modified to provide higher performance.

5.3 Window blinds data analysis

A. Formulation of Set Illuminance

The proposed control technique has been implemented with an LED luminaire and light sensor. Using the CRI illuminance meter CL-70F, measure the brightness of the LEDs at the working plane. Then The duty cycle is changed by a potentiometer from 1% to 100% with an

interval of 5%. The percentage of the duty cycle can be converted into an 8-bit digital value. The data table of duty cycle and measured illuminance is shown in Table 5.

Table 5 : Table of illuminance value for increasing duty cycle

Duty Digital (%)	Digital value of duty cycle	Measured Illuminance (lx) (CL-70F)
1	2	1.3
5	13	18.2
10	26	38.8
15	38	62.8
20	51	82.6
25	64	106.0
30	77	127.0
35	89	153.0
40	102	173.0
45	115	194.0
50	128	218.0
55	140	243.0
60	153	267.0
65	166	290.0
70	179	314.0
75	191	340.0
80	204	366.0
85	217	370.0
90	230	373.0
95	242	375.0
100	255	376.0

From Table 5, Illuminance values are obtained from 1.3 lx to 376.0 lx. The graph between the digital value of the duty cycle and measured illuminance is shown in Fig.5.9

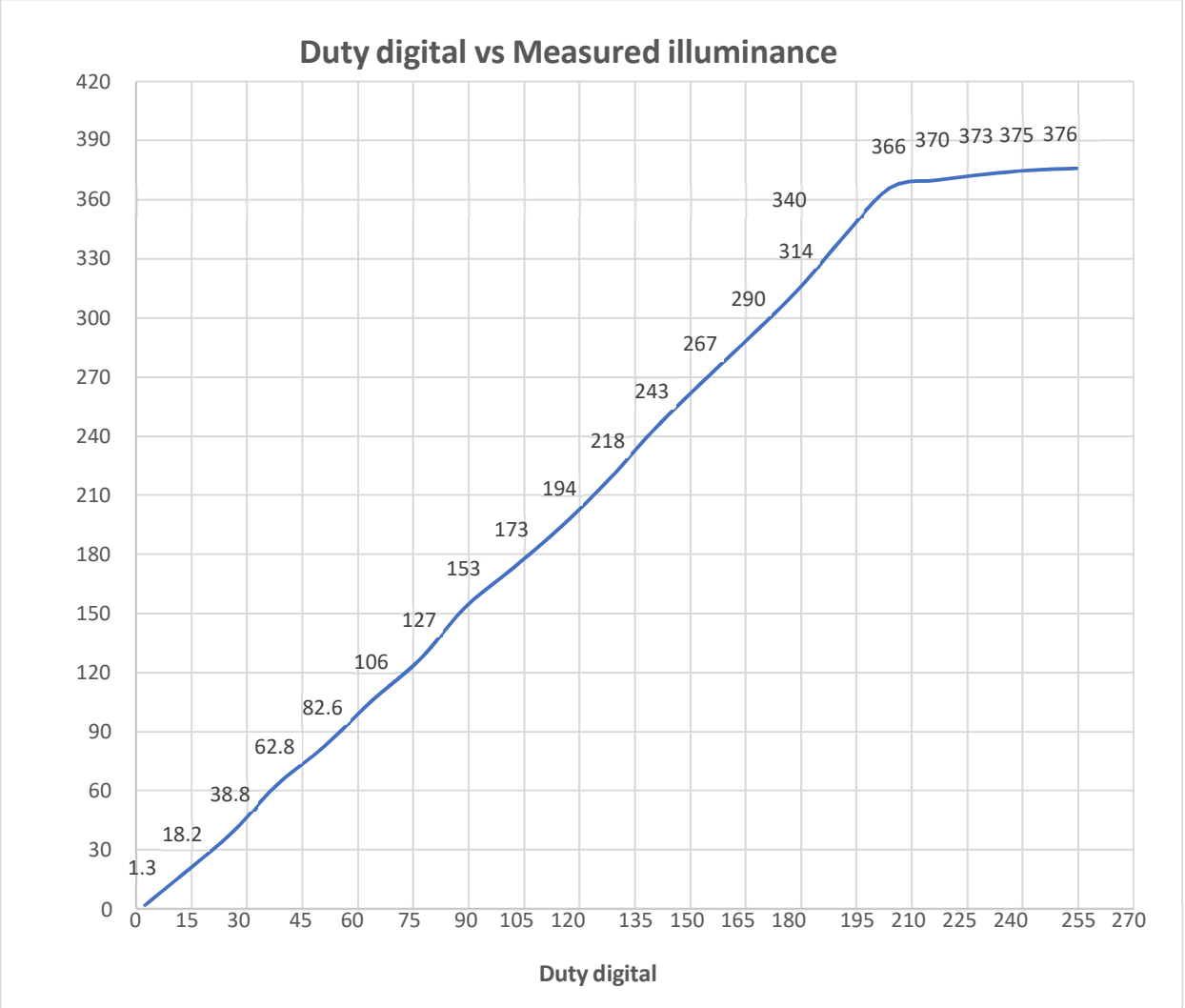

Fig.5.9: Duty digital vs Measured illuminance

The following graph is not linear characteristics. For this experiment, only linear region has been considered. In this case, measured illuminance will be used as a set illuminance. Set illuminance can be expressed mathematically.

Considering the points (5,18.2) and (204,366) The equation is

$$Y = 1.810303283\ X - 9.330406189 \quad (5)$$

Where, X= Duty digital value

Y= Measured illuminance in lx

Here, Y value represents as set illuminance (Es) in lx. The modified equation is

$$Es = 1.810303283\ X - 9.330406189 \quad (5.1)$$

B. Formulation of Measured Illuminance

Every close loop system requires a feedback path. In this close loop system, PD will be used as the feedback. Keeping the same condition of the room, the Set Illuminance value is varying from 0 lx to 300 lx using a knob with the interval of 10 lx. PD reads the Analog value and converted into digital value by the microcontroller. For an example, the Set Illuminance value is 200 lx then the PD output value is 26. The data table of Set Illuminance (Es), PD Analog value, PD digital value, and measured illuminance (CL-70F) are shown in Table 5.2.

The open loop system is shown in Fig. 5.10.

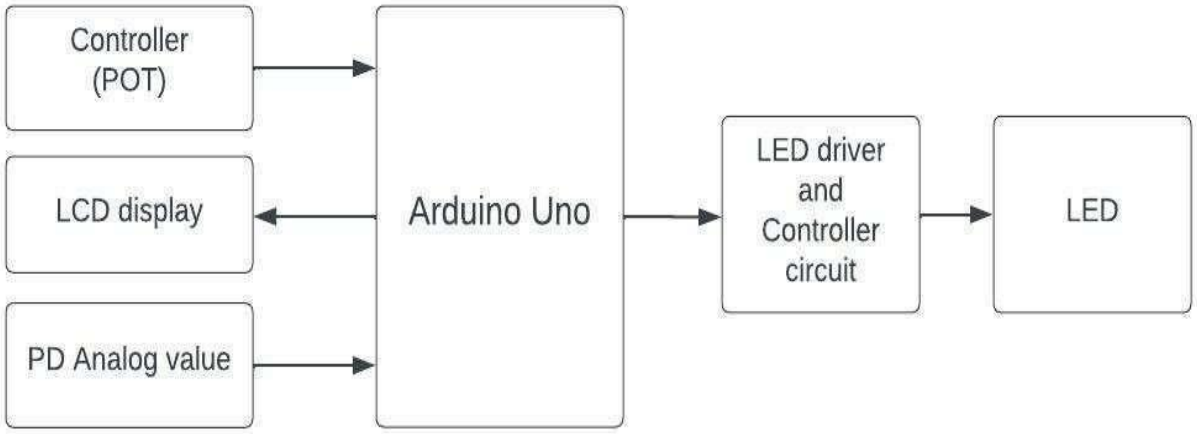

Fig.5.10 Block diagram of the open loop system

As shown in the diagram, PD output is connected to Analog pin A1 and Set Illuminance are connected to Analog pin A0 with the Arduino board. The LEDs is connected with the Arduino board of pin3. The Set Illuminance (Es) value and ADC value of PD are displayed on the LCD screen. Accordingly, changing the light intensity of LEDs with the change of Set Illuminance.

Table 5.1: Measured illuminance for increasing Set Illuminance

Set Illuminance (Es) (lx)	PD Analog value (mVolt)	PD digital	Measured Illuminance (lx) (CL-70F)
0	58.8	3	4.2
10	78.4	4	13.9
20	98.0	5	23.7
30	117.6	6	31.8
40	137.3	7	40.5
50	156.9	8	50.9
60	176.5	9	59.3
70	196.1	10	69.8
80	215.7	11	78.4
90	235.3	12	87.2
100	274.5	14	97.7
110	294.1	15	107.0
120	313.7	16	117.0
130	333.3	17	126.0
140	353.0	18	136.0
150	392.2	20	148.0
160	411.8	21	157.0
170	431.4	22	168.0
180	451.0	23	174.0
190	490.2	25	186.0
200	509.9	26	196.0
210	529.4	27	206.0
220	568.6	29	216.0
230	588.2	30	226.0
240	607.8	31	237.0
250	627.5	32	247.0
260	666.7	34	257.0
270	686.3	35	267.0
280	705.9	36	277.0
290	725.5	37	288.0
300	745.1	38	298.0

From the Table 5.1, a graph has been drawn between Set Illuminance (Es) and PD digital value. The graph is showing in Fig.5.11.

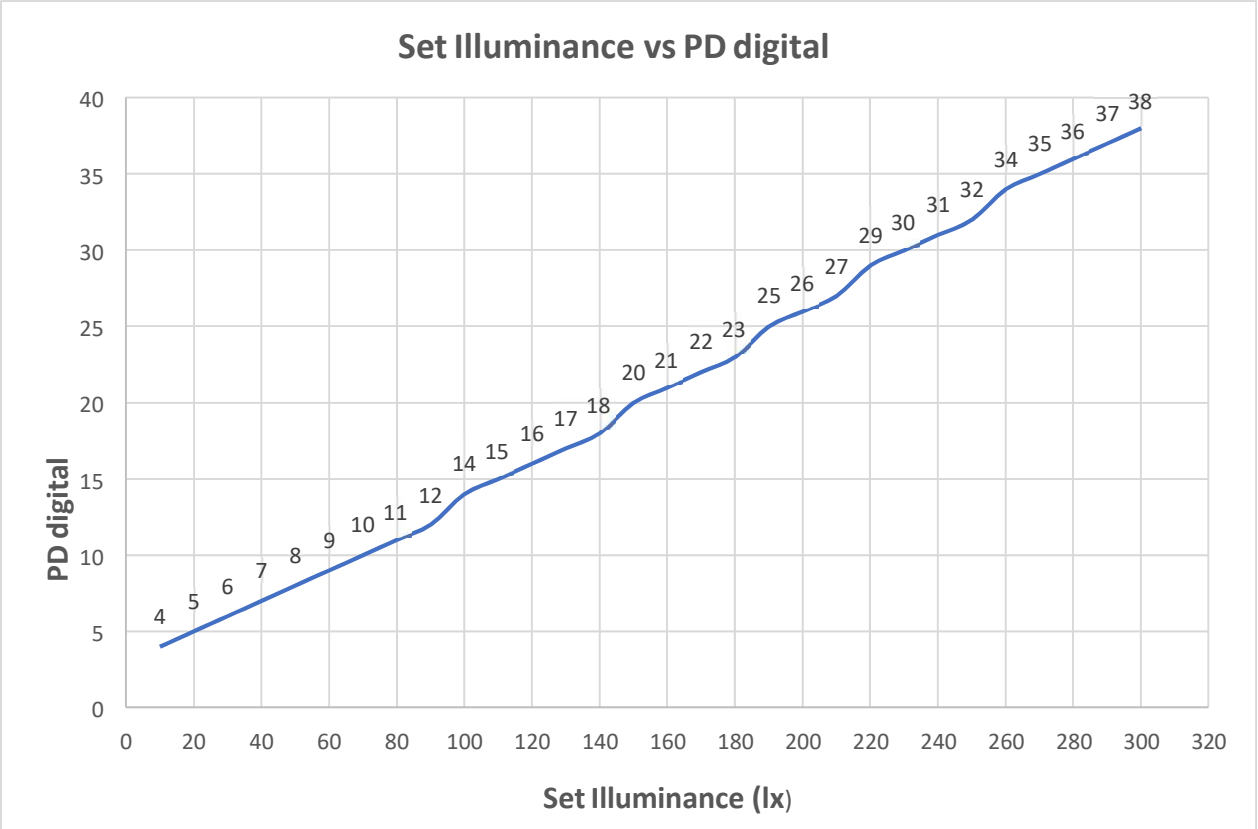

Fig.5.11 Set Illuminance (lx) vs PD digital

An equation has been developed by using this graph. In this case Set Illuminance using as Measured Illuminance (Em).

Considering the points (10, 4) and (300, 37)

The equation is

$$y = 0.12097886\,x + 1.848275862 \quad (5.2)$$

$$\text{or, } x = 8.265906953\,y - 15.277676299 \quad (5.3)$$

Where, x= Set Illuminance in lx, y = PD digital

The modified equation is

$$Em = 8.265906953\,x - 15.277676299 \quad (5.4)$$

C. Analysis of the system

In this section, the experimental results have been presented to evaluate the performance of the proposed system. The illuminance value has been set by the user between 0 lx to 300 lx. Now the Photo Detector reads the Analog value on the working plane and this value can be converted into digital value by the 8-bit microcontroller. The digital value of Measured Illuminance is changed into lx value with the help of Eq.5. The comparison between Set Illuminance (Es) and Measured Illuminance (Em) is denoted by Error

(Er). With varying the Set Illuminance (Es) value by the interval of 10 lx, the obtained measured Illuminance and error is shown in Table 5.2**.**

Table 5.2: The data table of measurement illuminance

Set Illuminance (Es) (lx)	PD digital	Measured Illuminance (Em) through PD (lx)	Measured illuminance (CL-70F) (lx)	Error (Er) (Es-Em)
0	2	1	4.2	-1
10	3	9	13.9	1
20	4	7	23.7	13
30	5	26	31.8	4
40	6	34	40.5	6
50	7	42	50.9	8
60	8	50	59.3	10
70	9	59	69.8	11
80	10	67	78.4	13
90	11	75	87.2	15
100	12	83	97.7	17
110	13	92	107.0	18
120	15	108	117.0	12
130	16	116	126.0	14
140	17	125	136.0	15
150	19	133	148.0	17
160	20	150	157.0	10
170	21	158	168.0	12
180	22	166	174.0	14
190	23	174	186.0	16
200	24	183	196.0	17
210	26	199	206.0	11
220	27	207	216.0	13
230	28	216	226.0	14
240	29	224	237.0	16
250	31	240	247.0	10
260	32	249	257.0	11
270	33	257	267.0	23
280	35	274	277.0	6
290	36	282	288.0	8
300	37	290	298.0	10

If Er > 0; the duty cycle of the LED is increased,

Er < 0; the duty cycle of the LED is decreased,

Er = 0; no change of the duty cycle.

The variation of Error with changing Set Illuminance (Es) is shown in Fig.5.12 (a) and Fig.5.12 (b).

For Without feedback, the error value is obtained from -1 to 23.

For With feedback, the error value is obtained from -5 to 5.

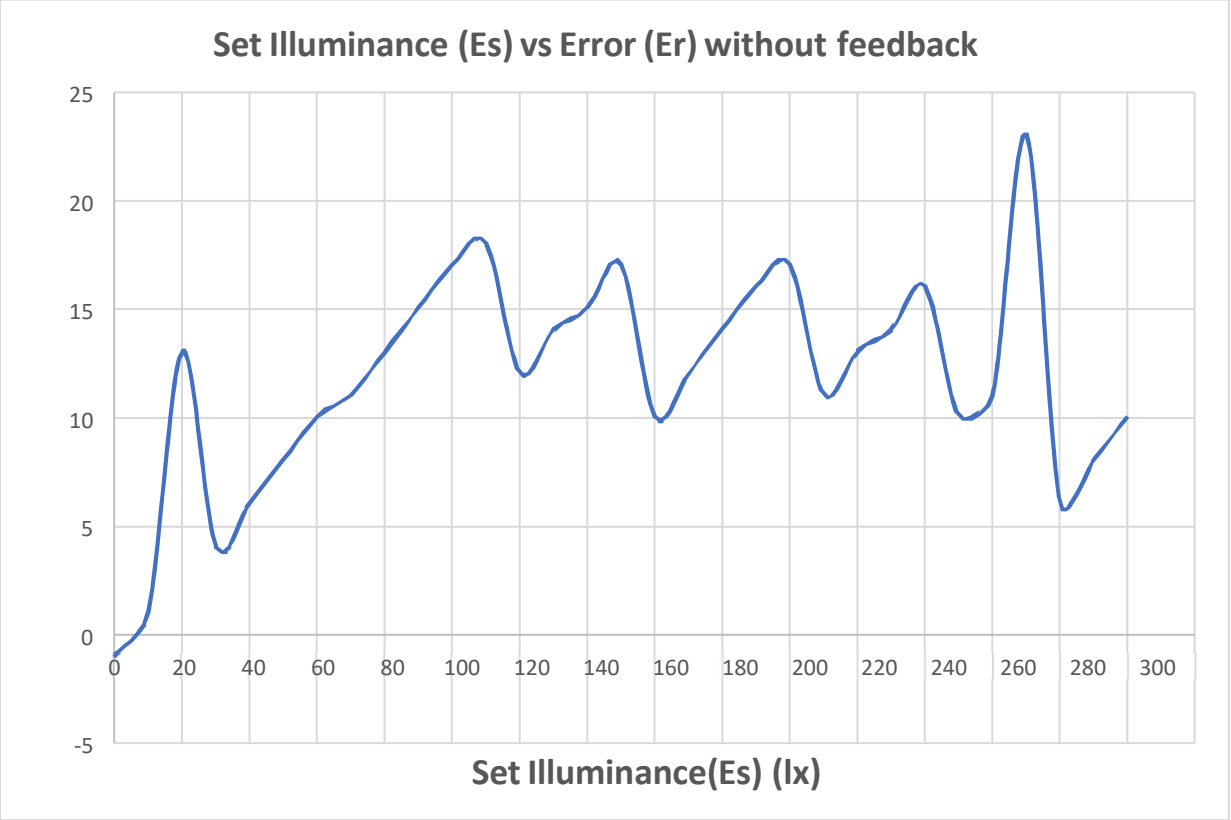

Fig.5.12 (a) Variation of Error with changing Set Illuminance without feedback

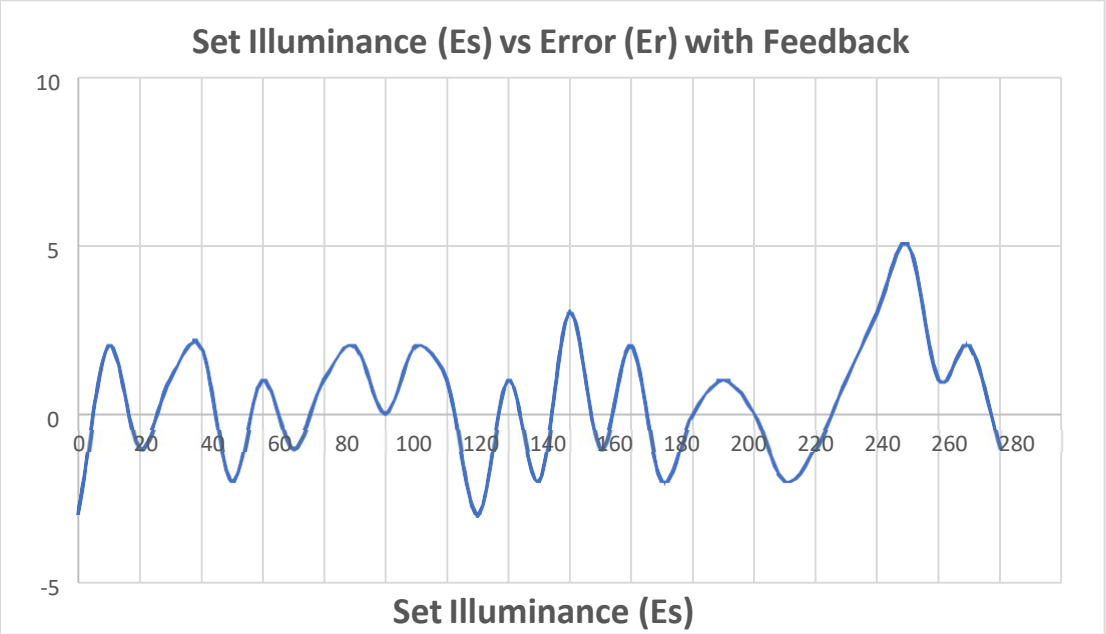

Fig.5.12 (b) Variation of Error with changing Set Illuminance with feedback

5.4 The results of Artificial daylights

A. The solar Photovoltaic (PV) module Data

The solar PV module data available from the solar panel is described below in table 5.3

Sky Type: - **Clear Sky** Date**: 22.04.2019** Time**: 01.30 PM**

Table 5.3: The solar Photovoltaic (PV) module Data

Current(A)	Voltage (Volt)	Power(watt)
3.13	0	0
3.046	1.661	5.059406
3.012	07.84	23.61408
2.806	14.04	**39.39624**
2.530	15.50	39.215
2.100	16.65	34.965
1.514	17.68	26.76752
1.198	18.14	21.73172
0.923	18.51	17.08473
0.718	18.75	13.4625
0.602	18.90	11.3778
0.489	19.04	9.31056
0.408	19.14	7.80912
0.327	19.22	6.28494
0.282	19.28	5.43696
0.248	19.31	4.78888
0.223	19.33	4.31059
0.203	19.36	3.93008
0.188	19.39	3.64532
0	19.56	0

Open Circuit Voltage: **19.56 V;** Maximum power available**: 39.39 watt**

Short Circuit Current: **3.13 A**

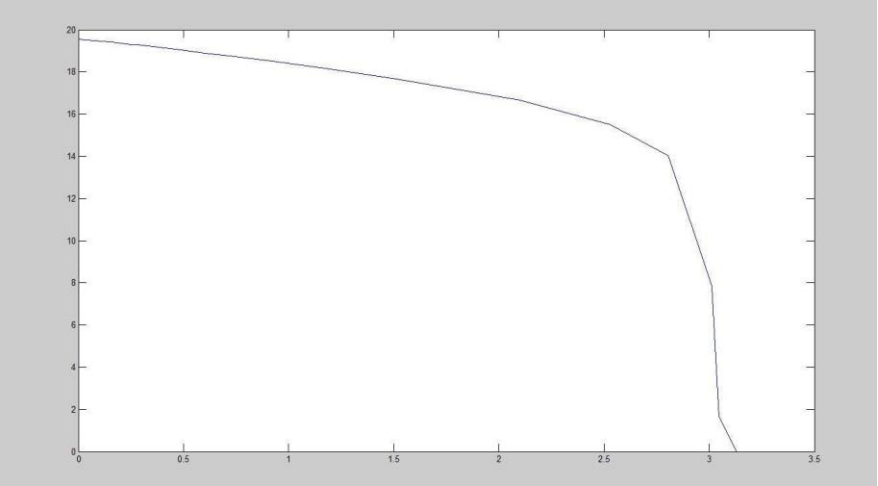

Fig. 5.13 V-I Characteristics

This characteristic graph in fig. 5.13 shows the maximum power availablefrom the module is **39.39 watts** which is enough to drive a led panel.

B. Chip On Board (COB) LED Panel data

There are six LEDs connected in a series to form a led panel. The power consumption characteristics of the panel are given below. The power was supplied to the LED panel via a 1-ohm resistance.

The LEDs can be arranged either as a total series connection or as two parallel forms of connection, each consisting of three LEDs in series. The whole panel could be covered with a diffuser to reduce direct glare and to have a uniform light distribution.

At starting (t =0)

Case I

Total Voltage – 63.18 V
Total Current – 0.7 A

Voltage drop across 1-ohm resistance – 0.698 V
Voltage across each LED

LED 1	LED 2	LED 3	LED 4	LED 5	LED 6
10.94v	10.10v	10.00v	10.07v	10.06v	10.64v

Wire drop = (Supply voltage – total drop across LEDs – drop across 1-ohmresistance) = 0.671v

Case II

Total Voltage – 49.67 V
Total Current – 0.1 A

The voltage drop across 1-ohm resistance – 0.102 V
Voltage across each LED

LED 1	LED 2	LED 3	LED 4	LED 5	LED 6
8.42v	8.22v	7.97v	8.21v	8.17v	8.40v

Wire drop = (Supply voltage – total drop across LEDs – drop across 1-ohmresistance) = 0.178 V

After 40 mins (t = 40)

Total Voltage – 62.22 V

Total Current – 0.7 A

Voltage drop across 1-ohm resistance – 0.701 V

Voltage across each LED

LED 1	LED 2	LED 3	LED 4	LED 5	LED 6
10.83v	9.95v	9.86v	9.92v	9.91v	10.51v

Wire drop = (Supply voltage – total drop across LEDs – drop across 1-ohmresistance) = 0.539

Case II

Total Voltage – 48.99 V
Total Current – 0.1 A

The voltage drop across 1-ohm resistance – 0.101 V

Voltage across each LED

LED 1	LED 2	LED 3	LED 4	LED 5	LED 6
8.33v	8.12v	7.90v	8.12v	8.09v	8.31v

Wire drop = (Supply voltage – total drop across LEDs – drop across 1-ohmresistance) = 0.019 V

For 0.7 A,

Measured voltage drop is (- 0.01v) per 40 sec.

Calculated voltage drop is (- 0.016v) per 40 sec or 0.024 per min.

So, it can be concluded that the LED panel is working fine.

C. Temperature data of the COB LEDs

Table 5.4 Temperature data of the COB LEDs

TIME	SINK -1 TEMPERATURE OF LED 1,3,5 (degree centigrade)	SINK -2 TEMPERATURE OF LED 2,4,6 (degree centigrade)
0 MIN	33.8	33.0
15 MIN	58.4	57.1
30 MIN	61.4	65.4
45 MIN	62.4	66.0
60 MIN	68.8	68.9

D. Photometric Data

Table 5.5 Photometric Data

Content	**Data**
No. of Grid Points	128 x 128
Height of Calculation Surface	0.76 meters
E_{av}	**474 LUX**
E_{min}	81 LUX
E_{max}	1017 LUX
U_0	0.171

6. Conclusion and future scopes

Conclusion:

This work will offer a working, cost-effective and indigenous sunlight harvesting system consisting of the hardware and software platforms. Working on these platforms (as opposed to computer simulation) people will be able to do experiment on the various hardware subsystems (e.g., sensors, digital and analog control systems and lamp drivers) and software algorithms for optimal or near-optimal utilization of available sunlight. The energy saving on lighting is expected to be at the tune of 20-40%.

The sensor presented in this study can be applied in scenarios where indirect placement (on a wall or ceiling) and two-wire connectivity are the main needs[11]. The final requirement stems from the fact that the necessary sensor is typically not able to be mounted directly on the work plane. This kind of sensor is being employed in an integrated feedback lighting system in this study, which combines artificial dimmable LED lights with natural daylight. At predetermined points-of-control (POC) on the job, this daylight harvesting control approach provides a significant electrical energy savings and uniformity of illumination.

An efficient and low cost approach to the self-oscillating fly back converter for LED lighting system has been presented. The driver uses feedback control with a P controller to achieve current regulation and PWM dimming by processing some of the converting power, which results in good efficiency. To avoid color shift while operating on the dimming feature, PWM control can be used. A laboratory circuit is demonstrated for an 18W LED lamp and the presented experimental results are satisfactory.

This is a closed-loop lighting control system that can adapt to both artificial and daylight lighting. Motorized blinds and dimmable LED sources with closed loop illuminance control have enhanced the proposed system. To maximize working plane illumination and block direct daylight, an automated vertical blind is operated in tandem with controllable LED lighting. In the prototype the blinds are operated with a servo motor. Energy savings and the amount of illumination at the working plane are well-balanced by the suggested method.

-Solar energy might be extremely important in supplying the growing need for electrical energy. Many buildings in the developing countries lack interior natural light. These locations within those buildings are suitable for the installation of this system. It will also lessen the building's load, which will advance the structure toward being a green building. A large solar panel can light up more lights and can illuminate several rooms according to its rated capacity. The artificial daylight consist of a roof mounted solar panel, a microcontroller based MPPT boost converter and LED panel. Without any battery storage the MCU unit will employ a maximum power point tracking (MPPT) algorithm. So that maximum power will be available from the solar panel for lighting purpose. This concept can be utilized in spaces where a direct entrance of daylight through windows is not available.

There are certain possible disadvantages to a solo solar photovoltaic system, such as the inability to generate enough electricity to directly illuminate artificial lighting on cloudy days. On some days, the system may be unable to handle the workload. As a backup supply,

conventional power might be utilized to address this issue. It is possible to light up the luminaires with a building's conventional power even at night, when there is no sunlight. It is possible to create a hybrid controller that can manage conventional and solar electricity simultaneously and switch sources on its own as necessary. Through the use of its intelligent technology, it will maximize the use of solar power and decrease the consumption of conventional power. The cost of installation will be higher if this controller is utilized in a standalone system because days of autonomy are needed to supply the load on cloudy days and nights.

Future scopes:

In future this cost effective system may be applicable in our laboratory space (length 6.2m * breadth 4.1m) with two windows on the northern side. Six dimmable LED luminaires will be installed in the area; two ceiling-mounted sensors and four wall-mounted sensors will be used to assess the work plane's indirect illumination. Later on, wireless sensors for this use might be taken into consideration.

A simplified block diagram of the proposed system is shown below Fig. 6

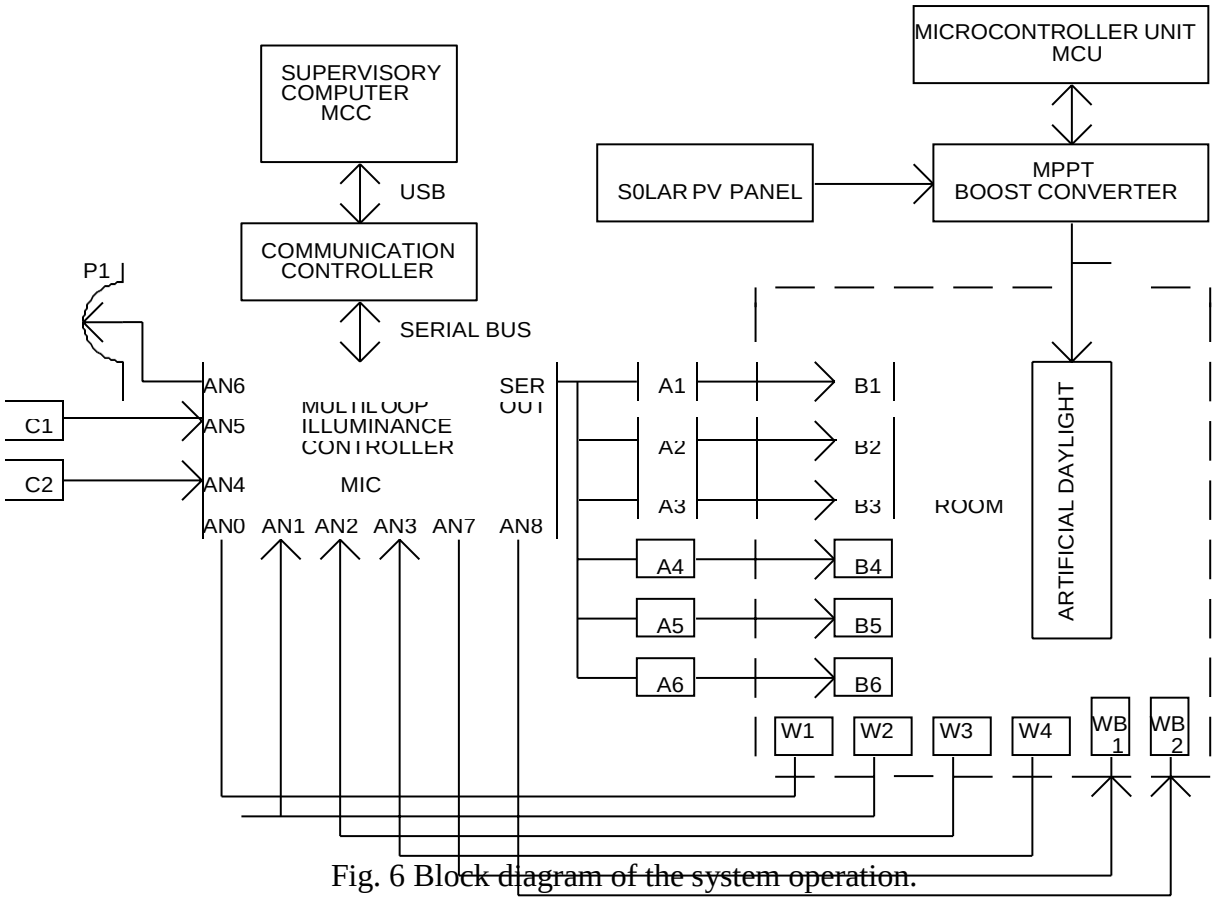

Fig. 6 Block diagram of the system operation.

Legends:

PI : Illuminance level setting POT
C1, C2: Ceiling-mounted sensors
W1-----W4: Wall-mounted sensors
WB1,WB2: Window blinds
A1------A6: Serial-in, PWM-out processors
B1----- B6: PWM-dimmable LED array
AN0..... AN8: Analog to digital converter channels (ADC)
Main Control Computer (MCC) (Supervisory Computer)
Multiloop Illuminance Controller (MIC)
MPPT Boost Converter
Microcontroller Unit (MCU)

All of the incoming environmental variables, such as the amount of light coming from the daylight outside the room, the amount of light coming from the lamp inside the room, and ultimately the user input, are collected by the indirect illuminance sensor and controller. The controller is in charge of analyzing all inputs and coming up with the best way to light the space while using the least amount of energy.

The MIC manages the all sensors data and adjusts the PWM-dimmable LED luminaries' light output. The MCC serves as the human-machine interface and supervises the MIC. In this instance, a laptop computer will serve as the MCC. A common serial interface, like USB or RS232C, will be used for communication between the MIC and MCC.

Roadmap of the further works:

(i) Experimental evaluation between illuminances at points of interest (POI) and illuminance sensor outputs.

(ii) Determination of a suitable transformation for conversion of sensor output to illuminance at POIs.

(iii) Development and implementation of a P-I-D-like nonlinear controller for computing the duty cycles of the LED drivers.

(iv) Development of the communication software between the MIC, its slaves and the Master controller

(v) Development of the graphic user interfaces for the MCC.

(vi) Stability studies of the system.

References

[1] G. R. N. Anca D. Galasiu, Cristian Suvagau, Daniel M. Sander,"Energy saving lighting control systems for open-plan offices: a field Study," Leukos, vol. 4, pp. 7-29, July 2007.

[2] "IEEE Recommended Practice for Energy Conservation and Cost Effective Planning in Industrial Facilities," IEEE Std 739-1984, p 0_2, 1984

.

[3] J. B. Arthur H. Rosenfeld, Karen Douglas, "Daylight Harvesting Made Simple," California Energy Commission's Public Interest Energy Research (PIER).2008

[4] European Council, Directive 2002/91/EC of the European parliament and of the council of 16 December 2002 on the energy performance of buildings, Official Journal of the European Communities. 2002.

[5] D. Caicedo and A. Pandharipande, "Distributed illumination control with local sensing and actuations in networked lighting systems," IEEE Sensors J., vol. 13, no. 3, pp. 1092-1104, Mar. 2013.

[6] S. Tanaka, M. Miki, T. Hiroyasu, M. Yoshikata, "An evolutional optimization algorithm to provide individual illuminance in workplaces", *Proc. IEEE Int. Conf. Syst. Man Cybern.*, pp. 941-947, Oct. 2009.

[7] N. van de Meugheuvel, A. Pandharipande, D. Caicedo, P. M. J. van den Hof, "Distributed lighting control with daylight and occupancy adaptation", *Energy Buildings*, vol. 75, pp. 321-329, Jun. 2014.

[8] A. Pandharipande, D. Caicedo, "Smart indoor lighting systems with luminaire-based sensing: A review of lighting control approaches", *Energy Buildings*, vol. 104, pp. 369-377, Oct. 2015.

[9] D. Caicedo, A. Pandharipande, F. M. J. Willems, "Light sensor calibration and dimming sequence design in distributed lighting control systems", *Proc. IEEE 11th Int. Conf. Netw. Sens. Control (ICNSC)*, pp. 344-349, Apr. 2014.

[10] D. Caicedo, A. Pandharipande, F. M. J. Willems, "Illumination gain estimation and tracking in a distributed lighting control system", *Proc. IEEE Multi-Conf. Syst. Control (MSC)*, pp. 1650-1655, Oct. 2014.

[11] M. Dyble, N. Narendran, A. Bierman and T Klein, "Impact of dimming white LEDs: Cromaticity shifts to different dimming methods", Fifth International Conference on Solid State Lighting, pp. 291-299, 2005.

[12] E. M. S. Junior, "Estudo de Novas Estruturas de Reatores Eletrônicos para LEDs de Iluminação", Tese de Doutorado, UFSC, Florianopolis/SC, Brasil, 2007.

[13] https://www.electronics-tutorials.ws/io/io_4.html.

[14] J.B. Arthur H. Rosenfeld, Karen Douglas, “Daylight Harvesting Made Simple,” California Energy Commission’s Public Interest Energy Research (PIER). 2008.

[15] G. R. N. Anca D. Galasiu, Cristian Suvagau , Daniel M. Sander, “Energy saving lighting control systems for open-plan offices: a field study,” Leukos, vol. 4, pp. 7-29, July 2007.

[16] “IEEE Recommended Practice for Energy Conservation and Cost-Effective Planning in Industrial Facilities,” IEEE Std 739-1984, p. 0_2, 1984.

[17] Bela G. Liptak, Instrument Engineers Handbook. Boca Raton, London, New York, Washington: D.C., CRC Press, 4th Edition, 2003.

[18] John G. Webstar, The Measurement, Instrumentation And Sensors Hand book. N.W., Boca Raton: CRC Press, and IEEE Press, 1999.

[19] Carlos A. dos Reis Filho, “An integrated 4-20 mA two-wire transmitter with intrinsic temperatures sensing capability”, IEEE Trans. Solid-State Circuits, Aug.1989. V24, #4, pp. 1136-1142.

[20] Murata Power Solutions, DMS Application Note 20: 4-20 mA Current Loop Primes. [Online]. Available: www.murata-ps.com/support.

[21] S. Li, A. Pandharipande, Daylight sensing LED lighting system, IEEE sensors journal May 1, 2016. V16, #9, pp.3216-3223.

[22] A. Pandharipande, S. Li, Light-harvesting wireless sensors for indoor lighting control, IEEE sensor journal December 2013. V13, #12, pp.4599-4606.

[23] A. Pandharipande, D. Caicedo, Smart indoor lighting systems with luminaire-based sensing: A review of lighting control approaches, *Energy Buildings* (Oct. 2015). V104, pp 369-377.

[24] D. Caicedo, A. Pandharipande, F. M. J. Willems, Light sensor calibration and dimming sequence design in distributed lighting control systems, *Proc. IEEE 11th Int. Conf. Netw. Sens. Control (ICNSC)*, Apr. 2014. pp. 344-349.

[25] D. Caicedo, A. Pandharipande, F. M. J. Willems, Illumination gain estimation and tracking in a distributed lighting control system, *Proc. IEEE Multi-Conf. Syst. Control (MSC)*, Oct. 2014. pp 1650-1655.

[26] Gaspare Boscarino, Mehrdad Moallem, Daylighting control and simulation for LED based energy-efficient lighting systems, IEEE transsactions on industrial informatics, February 2016. V12, #1, pp.301-308.

[27] Karl W. Boer, Cadmium sulfide enhances solar cell efficiency, Energy conversion and management, Elsevier, 2011. 52, pp. 426-430.

[28] BPW34 datasheet, Vishay Semiconductors. [Online]. Available: www.vishay.com/doc?91000.PDF

[29] Carlos A. dos Reis Filho, “An integrated 4-20 mA two-wire transmitter with intrinsic temperatures sensing capability”, IEEE Trans. Solid-State Circuits, Aug.1989. V24, #4, pp. 1136-1142.

[30] TEMT6200FX01 datasheet, Vishay Semiconductors.[Online].Available: www.vishay.com/doc?91000.

[31] Plastic coated CdS photocells. [Online]. Available: www.selcoproducts.com

[32] PGM CDS Photo resisters, version 2010. [Online]. Available: www.token.com/tw

[33] A. S. Sedra and K. C. Smith, Microelectronic Circuit, New York: Oxford University press,1998.

[34] Sergio Franco, Design with operational amplifiers and analog integrated circuits. NY, USA: McGraw-Hill Education, 2015.

[35] Toumazou, C., Lidgey, F. J. and Haigh, D. G., (EDS), Analogue IC design: the current-mode approach. London: IEE, Peter Peregrinus Ltd, April 1990.

[36] P. Dietz, W. Yerazunis, D. Leigh, Very low-cost sensing and communication using bidirectional LEDs, *Proc. 5th Int. Conf. Ubiquitous Comput,* Oct. 2003. pp. 175-191.

[37] A. Pandharipande, S. Li, Illumination and light sensing for daylight adaptation with an LED array: Proof-of-principle, *Proc. 39th Annu. Conf. IEEE Ind. Electron. Soc. (IECON)*, Nov. 2013. pp. 6081-6086.

[38] M. G. Villalva, J. R. Gazoli, E. R. Filho, Modeling and circuit-based simulation of photovoltaic arrays, *Proc. Power Electron. Conf. (COBEP)*, 2009. pp. 1244-1254.

[39] M. Esteki, S. A. Khajehoddin, A. Safaee and Y. Li, "LED Systems Applications and LED Driver Topologies: A Review," in *IEEE Access*, vol. 11, 2023 pp. 38324-38358.

[40] D. A. Steigerwald, J. C. Bhat, D. Collins et al., "Illumination with solid state lighting technology", *IEEE Journal of Selected Topics in Quantum Electronics*, vol. 8, no. 2, Mar. 2002. pp. 310-320.

[41] H. J. Chiu, Y. K. Lo, J. T. Chen, S. J. Cheng, C. Y. Lin, and S. C. Mou, “A high-efficiency dimmable led driver for low-power lighting application,” *IEEE Trans. Ind. Electron.*, vol. 57, no. 2, Feb. 2010. pp. 735–743.

[42] Şanal, E., Dost, P., Sourkounis, C.: ‘LCL-filter design for a battery charger based on buck converter (DCDC converter)’. IEEE Int. Conf. Renewable Energy Research and Applications (ICRERA), Birmingham, UK, pp. 617–621. 2016.

[43] R. Malik, K. K. Ray and S. Mazumdar, "Wide-Range, Open-Loop, CCT and Illuminance Control of an LED Lamp Using Two-Component Color Blending," in *IEEE Transactions on Power Electronics*, vol. 33, no. 11, 2018, pp. 9803-9818.

[44] D. Gacio, J. M. Alonso, A. J. Calleja, J. Garcia, and M. Rico-Secades, "A universal-input single-stage high-power-factor power supply for HBLEDs based on integrated buck-flyback converter," *IEEE Trans. Ind.Electron.*, vol. 58, no. 2, Feb. 2011. pp. 589–599.

[45] R. Malik, K. K. Ray, and S. Mazumdar, "A Low-Cost, Wide-Range, CCT-Tunable, Variable-Illuminance LED Lighting System", *LEUKOS*, VOL. 16, NO. 2, 157–176, 2020.

[46] Y. C. Li and C. L. Chen, "A novel single-stage high-power-factor AC-to-DC LED driving circuit with leakage inductance energy recycling," *IEEE Trans. Ind. Electron.*, vol. 59, no. 2, Feb. 2012, pp. 793–802.

[47] R. Malik, S. Mondal, N. K. Saha and S. Bhunia, "A CCT Tunable Daylight-Integrated LED Lighting System for the Improvement of Health and Well-Being of Human Beings," *2023 IEEE Sustainable Smart Lighting World Conference & Expo (LS18)*, Mumbai, India, 2023, pp. 1-5.

[48] He, D., Xiong, Z., Lei, Z., et al.: 'Design optimisation of self-powered gate driver for ultra-fast DC solid-state circuit breakers using SiC JFETs', *IET Power Electron.*, 2017, 10, (15), pp. 2149–2156.

[49] S. Beczkowski and S. Munk-Nielsen, "LED spectral and power characteristics under hybrid PWM/AM dimming strategy," in *Proc. IEEE ECCE*, 2010,pp. 731-735.

[50] Irving Brian T. and Jovanović Milan M. Analysis and Design of Self-Oscillating Flyback Converter. APEC Seventeenth Annual. Con. IEEE, 2002, V2, pp. 897–903.

[51] M. Dyble, N. Narendran, A. Bierman, and T. Klein, "Impact of dimming white LEDs: Chromaticity shifts due to different dimming methods," in Proc. SPIE, vol. 5941, pp. 291–299, Aug. 2005.

[52] R. Malik, and S. Mazumdar, "Development of CCT Tunable LED Lighting System using Red-Blue-White LED", *Light & Engineering*, vol- 25, no-4, pp. 99-108, 2017.

[53] J. Okumura, Y. Kozawa, Y. Umeda and H. Habuchi, "Hybrid PWM/DPAM Dimming Control for Digital Color Shift Keying Using RGB-LED Array," in *IEEE Journal on Selected Areas in Communications*, vol. 36, no. 1, 2018, pp. 45-52.

[54] Bullough JD, Hickcox K Sweater, Klein TR, NarendranN. Effects of flicker characteristics from solid-state lighting on detection, acceptability and comfort. Lighting Res Technol, 2011. V43, #2, pp. 337–348

[55] 2015. Atmel ATmega32A [DATASHEET]. <http://www.atmel.com/images/atmel-8155–8-bit microcontroller-avr-atmega32a_datasheet.pdf > Accessed 2015 December 11.

[56] S. Xu, Q. Shen, C. Wang et al., "A digital control scheme for PSR flyback converter in CCM and DCM", *IEEE Trans. Power Electron.*, vol. 8, no. 3, pp. 2837-2849, Sep. 2020.

[57] Y.-Y. Li and Z-M. Zhu, "A constant current control scheme for primary-side controlled flyback controller operating in DCM and CCM", *IEEE Trans. Power Electron.*, vol. 35, no. 9, pp. 9462-9470, Feb. 2020.

[58] C. Wang, D.-Y. Sun, W.-H. Gu and S. Gui, "Digital voltage sampling scheme for primary-side regulation flyback converter in CCM and DCM modes", *IEEE Trans. Circuits Syst. I Reg. Papers*, 2022.

[59] M.-G. Chen, S. Xu, L.-L. Huang et al., "A novel digital control method of primary-side regulated flyback with active clamping technique", *IEEE Trans. Circuits Syst. I Reg. Papers*, vol. 68, pp. 950-962, Feb. 2021.

[60] F.-C. Syu, S.-C. Yeh, Y.-C. Chang, J.-Y. Lin, Y.-C. Hsieh, H.-J. Chiu et al., "Design and implementation of 1 MHz active-clamped resonant flyback converter", *Proc. Annual Canf. IEEE Ind. Electron. Society*, pp. 4438-4442, Dec. 2017.

[61] S.-H. Yang, S.-H T.-H. Tsai, H. Chen et al., "High accuracy knee voltage detection for primary-side control in flyback battery charger", *IEEE Trans. Circuits Syst. I Reg. Papers*, vol. 64, no. 4, pp. 1003-1012, Apr. 2017.

[62] C. Wang, S. Xu, X.-P. Kou, S.-L. Lu and W.-F. Sun, "A simple average current control with time-length equality for primary - side regulation flyback converter with constant output current control", *in Proc. Int. Journal of Circuit Theory and Applications*, vol. 46, pp. 2477-2496, Jul. 2018.

[63] Y. Olzhabay, A. Ng and I.A. Ukaegbu, "Perovskite PV energy harvesting system for uninterrupted IoT device applications", *Energies*, vol. 14, no. 23, pp. 7946, 2021.

[64] D. Venkatramanan and V. John, "Dynamic modeling and analysis of buck converter-based solar PV charge controller for improved MPPT performance", *IEEE Transactions on Industry Applications*, vol. 55, no. 6, pp. 6234-6246, 2019.

[65] S. Kantareddy et al., "Perovskite PV- powered RFID: Enabling low-cost self-powered IoT sensors", *IEEE Sensors Journal*, vol. 20, no. 1, pp. 471-478, 2020.

[66] M. Ouremchi, S. El Mouzouade, K. El Khadiri, A. Tahiri and H. Qjidaa, "Integrated energy management converter based on maximum power point tracking for the photovoltaic solar system", *Int. J. Electr. Comput. Eng*, vol. 12, no. 2, pp. 1211-1222, 2022.

[67] M. Orabi, F. Hilmy, A. Shawky, J. A. Abu Qahouq, Hasaneen and E. Gomaa, "On-chip integrated power management MPPT controller utilizing cell-level architecture for PV solar system", *Sol. Energy*, vol. 117, pp. 10, 2015.

[68] F. Berrezzek, K. Khelil and T. Bouadjila, "Efficient MPPT scheme for a photovoltaic generator using neural network", *2020 1st International Conference on Communications*, pp. 503-507, 2020.

[69] A. Paras, U. Prasad and A. K. Choudhary, "Comparative Assessment of ANN-based MPPT Algorithm for Solar PV System", *2022 IEEE North Karnataka Subsection Flagship International Conference (NKCon)*, pp. 1-6, 2022.

[70] R. Anand, D. Swaroop and B. Kumar, "Global Maximum Power Point Tracking for PV Array under Partial Shading using Cuckoo Search", *2020 IEEE 9th Power India International Conference (PIICON)*, pp. 1-6, 2020.

Moutusi Bag.
9.12.2024